Technical Report **R 489**

HINGING IN STATICALLY AND DYNAMICALLY LOADED REINFORCED CONCRETE BEAMS

October 1966

NAVAL FACILITIES ENGINEERING COMMAND

U. S. NAVAL CIVIL ENGINEERING LABORATORY

Port Hueneme, California

HINGING IN STATICALLY AND DYNAMICALLY LOADED REINFORCED CONCRETE BEAMS

Technical Report R- 489

Y-F011-05-04-001

Type C

by

William J. Nordell, Ph.D.

ABSTRACT

The objective was to investigate the hinging mechanism in under-reinforced concrete beams subjected to static or dynamic loads. Two test series on simply supported beams with a 6-foot span length were conducted. In one series, 11 beams were subjected to two concentrated loads symmetrically placed 18 inches apart; the primary variable was the magnitude of the step load pulse (1.0 to 1.4 times the static yield load). In the other series, 15 beams were subjected to a concentrated load at midspan; the primary variables were the type of load (static or dynamic), the amount of tension reinforcement ($p = 0.9$, 1.3, and 2.0; $p'/p = 0.67$), and the size of the transverse reinforcement (1/8- and 1/4-inch round bars and No. 3 deformed bars).

Hinge development was similar in the statically and dynamically loaded beams and resulted from the formation and propagation of a yielded zone or zones in the tension reinforcement. Strain hardening of the tension reinforcement increased the static resistance above the yield value; the increase ranged from 5 to 60 percent.

Although decreasing the amount of tension reinforcement increased the deflection at certain stages, the ultimate rotation capacity was not significantly affected. In addition, the size of the transverse reinforcement had a negligible effect on the ultimate rotation capacity.

Strain hardening of the tension reinforcement and the ductility of confined concrete were considered in the analysis. Good correlation was obtained between the computed and experimental static load-deflection relationship as well as the static moment-rotation relationship for the centrally loaded beams. However, for the beams subjected to two loads, the deformation capacity beyond the crushing stage was not predicted.

The dynamic resistance was established using the computed static resistance and the measured strain rate at yield. The computed dynamic resistance and beam response were generally in reasonable agreement with the measured values.

CONTENTS

Page

APPENDIXES

INTRODUCTION

Hinge formation refers to the ability of some flexural members to rotate at sections of high moment with little or no change in the moment resistance of the section. The importance of the hinge mechanism in the design of indeterminate structures is evident in limit design of reinforced concrete and plastic design of steel. Both methods are based on the occurrence of a redistribution of moment at high loads, as a result of the formation of hinges at distinct locations.

Under the auspices of the European Concrete Committee, several investigations of hinging in reinforced concrete beams have been conducted at various laboratories. Reference 1 contains a summary of the results from some of these studies as well as results from other investigations of hinge formation in reinforced concrete. Based on these studies, the primary factors affecting hinge rotation are considered to be the depth of the compression zone, the maximum compressive strain of the concrete, and the amount of transverse reinforcement.[2,3,4] These factors, in turn, are influenced by other parameters such as the amount of tension and compression reinforcement, mechanical properties of the reinforcement, concrete strength, axial load, beam geometry, and moment gradient in the hinge zone.[2,3,4,5,6] Although considerable progress has been made in investigating the relationship between the various parameters, the mechanics of hinge formation is still not completely understood. Furthermore, all previous studies have been concerned with hinging under static loads. The effect of dynamic loads on hinge formation has received little attention.

The objective of this study is to obtain a better understanding of the hinge mechanism in reinforced concrete beams subjected to static and dynamic loads. The method used to achieve this objective consists of measuring the magnitude of the angle of hinge rotation and correlating resisting moment with the angle of deformation for beams subjected to dynamic loads. The results are intended to aid in the development of procedures for predicting the ultimate load capacity of reinforced concrete structures.

Phase I of this investigation[6] was concerned with the effects of compression reinforcement, load configuration, and type of load (static or dynamic) on the hinge mechanism.

In this report, Phase II, the results of two series of tests are presented. One series was conducted on beams with a uniform moment region to determine the effect of dynamic loads on hinge development. The primary variable was the magnitude of the dynamic load. Similar beams had been tested previously and it was found that under dynamic loads the hinge did not develop uniformly, as it did under static loads, prior to crushing of the concrete at the extreme compressive surface of the beam.[6] The present test series was conducted to investigate further the nonuniformity of hinging under dynamic loads.

In the second series of tests, hinging at beam-column connections was studied by means of tests on beams subjected to a single concentrated load at midspan. The primary variables were the amount of tension reinforcement and the size of the transverse reinforcement; both static and dynamic tests were conducted.

In all tests, the beams were under-reinforced so that yielding of the tension reinforcement occurred before the concrete in compression failed. Also, the beam dimensions and the ratio of the amount of compression reinforcement to that of the tension reinforcement were the same in all cases. Transverse reinforcement (closed stirrups) was provided to prohibit a shear failure.

The test results are presented first and discussed in relation to the development of hinge rotation in the beams. The static and dynamic test data are compared. Next, the analysis of the test results is presented, and then the computed and experimental data are compared. A list of symbols is provided following the main body of the report.

EXPERIMENTAL WORK

Two series of tests were conducted; one on beams subjected to two equal concentrated loads located 9 inches on each side of midspan, and the other on beams subjected to a single concentrated load at midspan. A sketch of the test beam is shown in Figure 1; the geometry is similar to that used previously.[6]

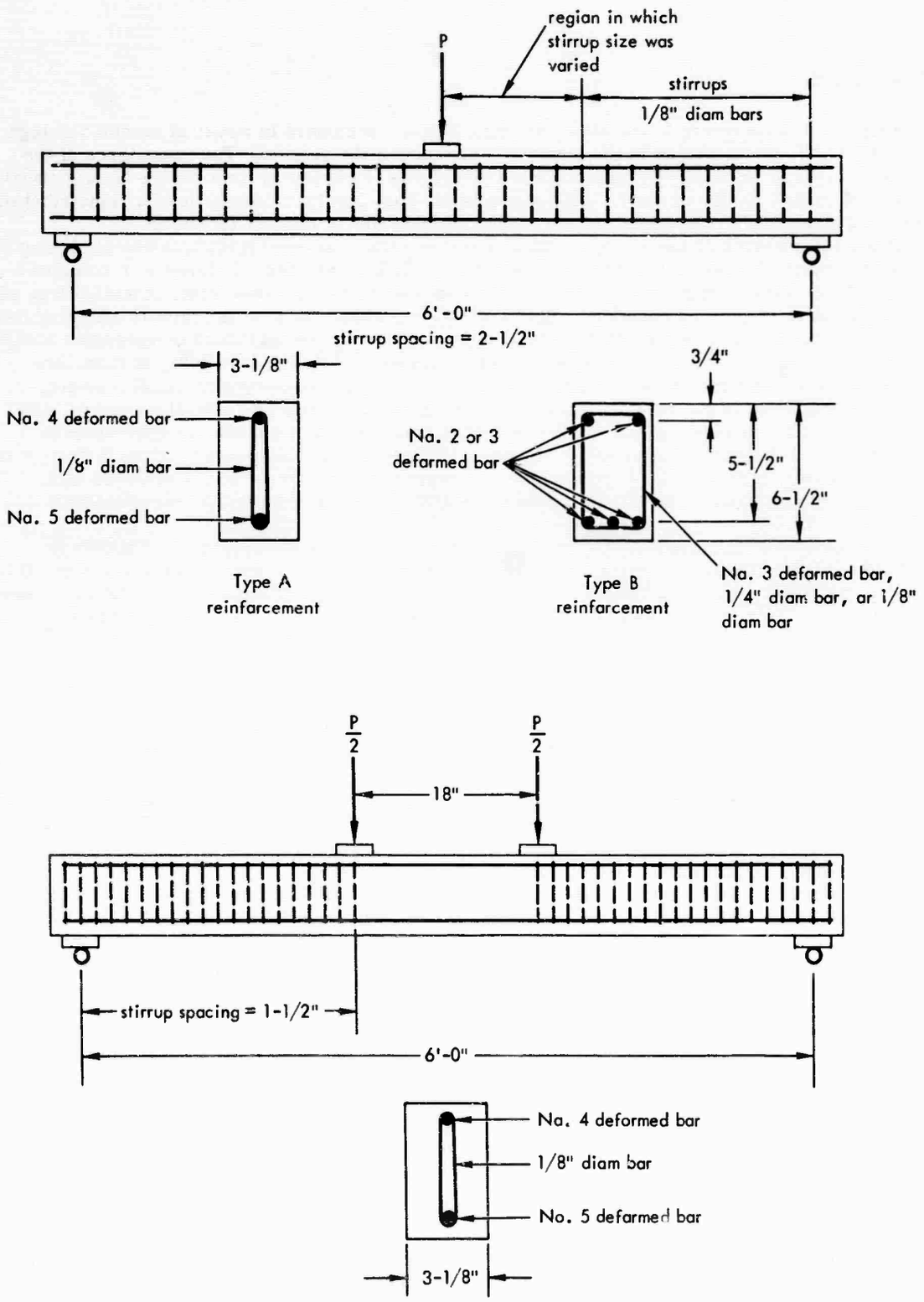

Figure 1. Beam description.

For the tests on beams subjected to two concentrated loads, the primary variable was the magnitude of the dynamic load which ranged from 1 to 1.4 times the static yield load. Eleven beams were tested in this series, and they were all reinforced with a No. 5 deformed bar in tension and a No. 4 deformed bar in compression. Three of the 11 beams were loaded statically and the remainder dynamically.

In the series of tests on beams loaded at midspan, six were tested statically and nine dynamically. The primary variables were the amount of tension reinforcement and the amount of transverse reinforcement. The Type B reinforcement arrangement was used in 14 of the beams and the Type A in one of the beams. Reinforcement arrangements similar to Type A were used in the earlier tests.[6] The percentages of tension steel reinforcement were 0.9, 1.3, and 1.9 percent. The ratio of the amount of compression to tension reinforcement was equal to 0.7 in all tests. The amount of transverse reinforcement was varied by changing the size of the stirrup bars in the center one-third of the beam. No. 3 deformed bars, 1/4- and 1/8-inch round bars, were used. The transverse reinforcement was varied only in those beams in which the percentage of tension reinforcement was 1.9 percent.

The yield strength of the reinforcement was approximately 50,000 psi except for the yield strengths of the No. 2 deformed bars and the 1/8-inch round bars (stirrups) which were 60,000 and 85,000 psi, respectively. The average concrete cylinder strength was 5,000 psi.

Dynamic loads were applied with the Naval Civil Engineering Laboratory (NCEL) 10,000-pound rapid load machine. The load was applied by a differential pressure acting on a piston connected to a load strut. Static loads were applied with a 20,000-pound hydraulic jack reacting against a steel test frame.

Measurements were taken of the applied load, reactions, deflections at midspan and the load points, strains in the tension and compression steel, and concrete strains on the top surface of the beam. In addition, rotations at various locations along the longitudinal axis were measured with devices which consisted of two linear potentiometers connected between two aluminum brackets which were secured to the beam at sections 6 inches apart. In some tests, the end rotations were measured with an angular differential transducer.

A complete discussion of the material properties, test equipment and procedure, and instrumentation is presented in Appendix A.

TEST RESULTS

The results from both series of tests are considered collectively except in the discussion of the effects of the test variables. The order of presentation is as follows: (1) static load-deflection behavior; (2) dynamic resistance-deflection behavior; (3) hinge formation under static and dynamic loads; and (4) effect of test variables.

Static Load-Deflection Behavior

Five stages were noted in the behavior of the statically loaded beams, and these stages are marked on the load-deflection diagrams in Figure 2. The first stage was that at which cracks developed in the concrete in tension (cracking stage, cr). Because cracking slightly decreased the stiffness of the beams, this stage is characterized on the load-deflection diagrams by a slight break in the slope of the curve. The cracks developed when the maximum moment reached 15 to 20 inch-kips.

The yield stage, y, is the one at which yielding begins in the tension reinforcement. Since the steel was an intermediate grade with a yield plateau, an abrupt and significant change in the slope of the load-deflection diagram occurred at this stage.

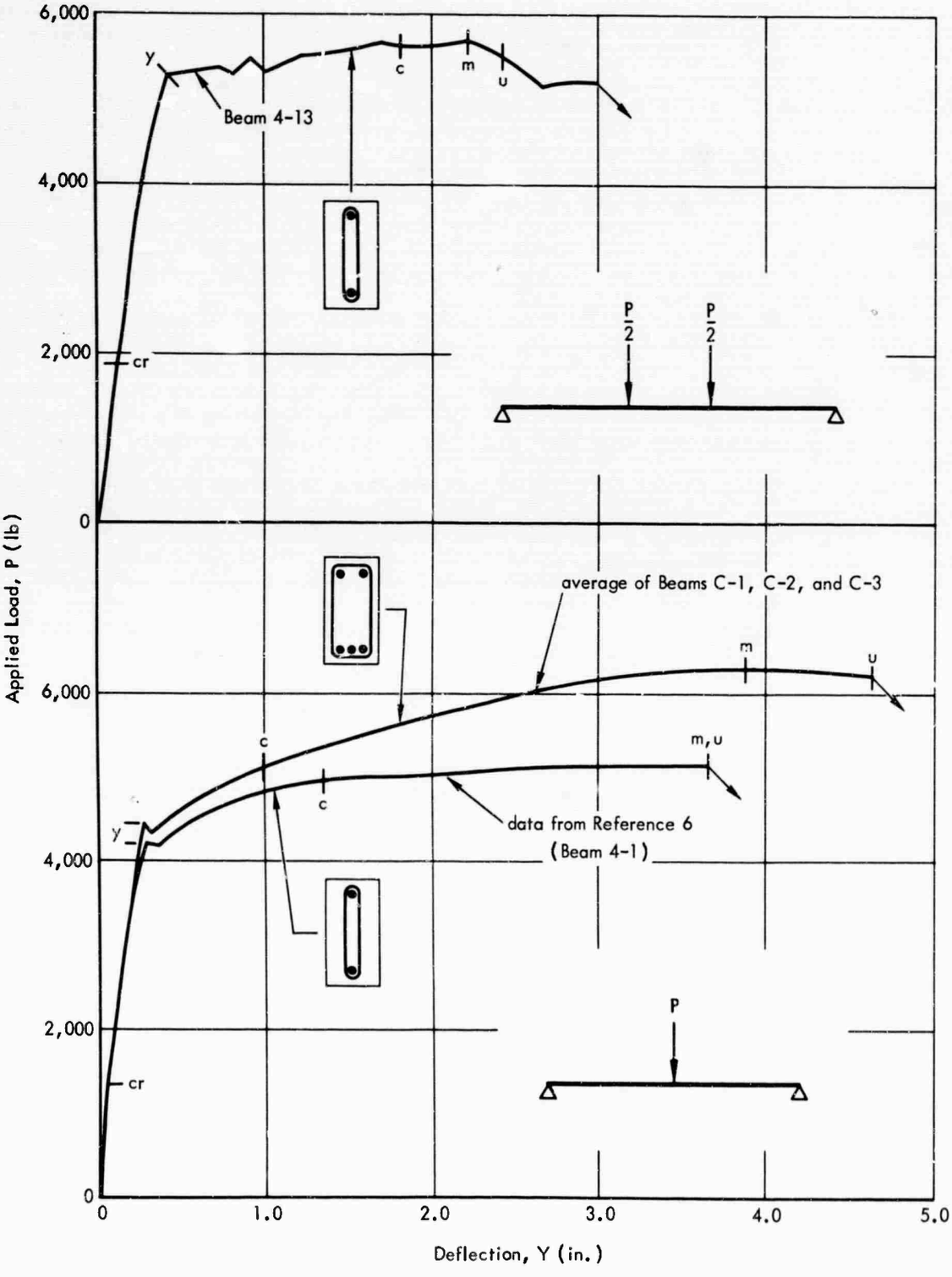

Figure 2. Static load versus deflection (p = 1.9 percent, p' = 1.3 percent).

The crushing stage, c, indicates the stage at which the concrete at the extreme surface of the compression zone started to fail. No manifestation of this stage was noted on the load-deflection diagrams, and as a result the crushing stage is difficult to establish exactly. Generally, this stage is defined by either visual inspection of flaking or cracking during the test, or by the reversal of the concrete strain gage readings. In the present study, visual observation of the onset of crushing during the dynamic tests was not possible, even with the aid of high-speed movies. Hence, for consistency in both the static and dynamic tests, the crushing stage was defined by the reversal of the concrete strain gage readings. A diagram of deflection versus concrete strain at midspan was used in this determination. Examples are shown in Figures 3 and 4; the deflections at crushing are marked, and for comparison the deflections at which spalling or flaking of the compressed concrete was first observed in the static tests are marked. Both values were about equal for the beams loaded at two points, but for the centrally loaded beams the values based on visual observations were as much as 40 percent greater than those based on the concrete strain gage data. Difference between the results obtained by the two methods has been noted by others.[4,5,6] The method used in this study provided a lower bound.

The point on the load-deflection diagram corresponding to maximum load is identified by m. In some cases, this stage and the ultimate stage, u, were coincident. The ultimate stage is defined in this report as the stage at which the load began to decrease rapidly with respect to deflection or that stage at which the resistance dropped below the yield resistance, whichever occurred first.

Photographs of a statically loaded beam from each test series are presented in Figures 5 and 6 to show the crack pattern, crack size, and general appearance of the beams at various stages. The applied loads, deflections, strains and rotation measurements are presented in Appendix B for the yield, crushing, maximum load, and ultimate stages.

Failure of the beams resulted from either (1) the fracture of the tension reinforcement, (2) buckling of the compression reinforcement, or (3) failure of the concrete in compression. The centrally loaded beams failed by either (1) or (2), whereas the beams subjected to two concentrated loads failed by either (2) or (3), usually (3). The mode of failure for each beam is given in Table B-4.

Dynamic Resistance-Deflection Behavior

Experimental measurements of the dynamic resistance were computed by using the acceleration and load data in the equation

$$Q_d = P - m_e \frac{d^2Y}{dt^2} \qquad (1)$$

In the computations the high-frequency vibrations were neglected. An equivalent mass of the beam equal to one-half the actual mass was used. For the beams subjected to two concentrated loads, an additional mass equal to one-half the actual mass of the distributing beam (which was approximately 10 percent of the beam mass) was assumed to be concentrated at each load point.

Typical resistance-deflection diagrams are shown in Figures 7 and 8, which also include static test data for comparison. The effect of strain rate on the beam resistance is apparent.

The beams usually were not loaded to collapse, but rather to a deflection equivalent to the maximum load deflection in the static tests. When a beam did collapse the collapse deflection was equal to or greater than the ultimate deflection of a corresponding beam tested statically. This result is in agreement with previous findings.[6,7]

The appearance of a dynamically loaded beam was similar to that of a corresponding beam loaded statically to a deflection equal to the maximum dynamic deflection. For the centrally loaded beams, crushing of the concrete under the load-bearing plate occurred in some dynamic tests, whereas it did not in the static tests. This crushing resulted from the impact of the load ram and the beam. A comparison of the appearance of those beams which collapsed under dynamic loads with that of the statically loaded beams after failure would not be meaningful because greater damage resulted in the dynamic tests. The beams loaded dynamically were forced beyond the actual collapse deflection and they usually struck the safety blocks; both circumstances caused additional damage not sustained in the static tests.

The dynamic test data are summarized in Appendix B. The values of deflection, strain, and rotation at the yield and crushing stages and at maximum deflection are listed.

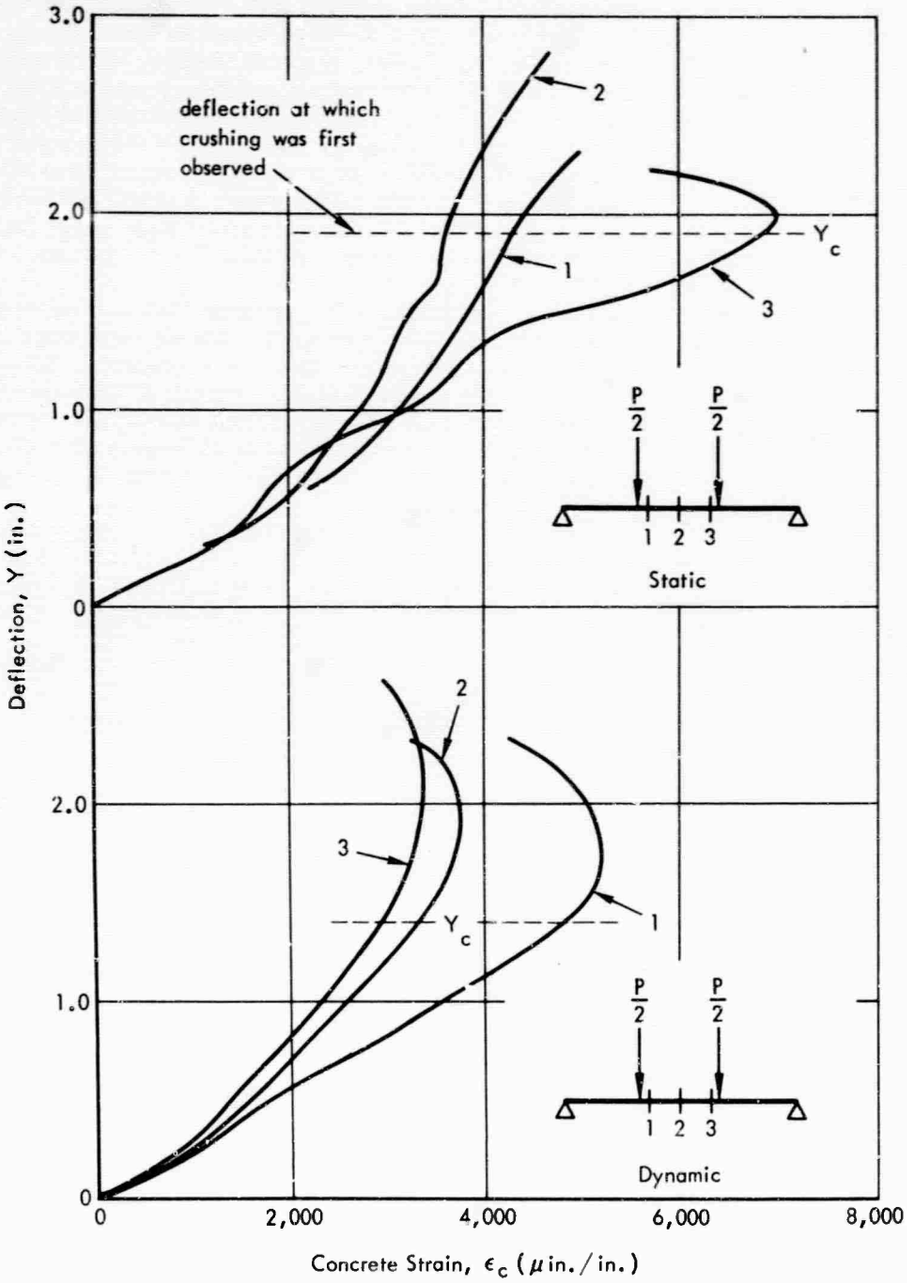

Note: Curves 1, 2, and 3 correspond to strain measurements at locations 1, 2, and 3, respectively.

Figure 3. Deflection versus concrete strain - beams loaded at two points.

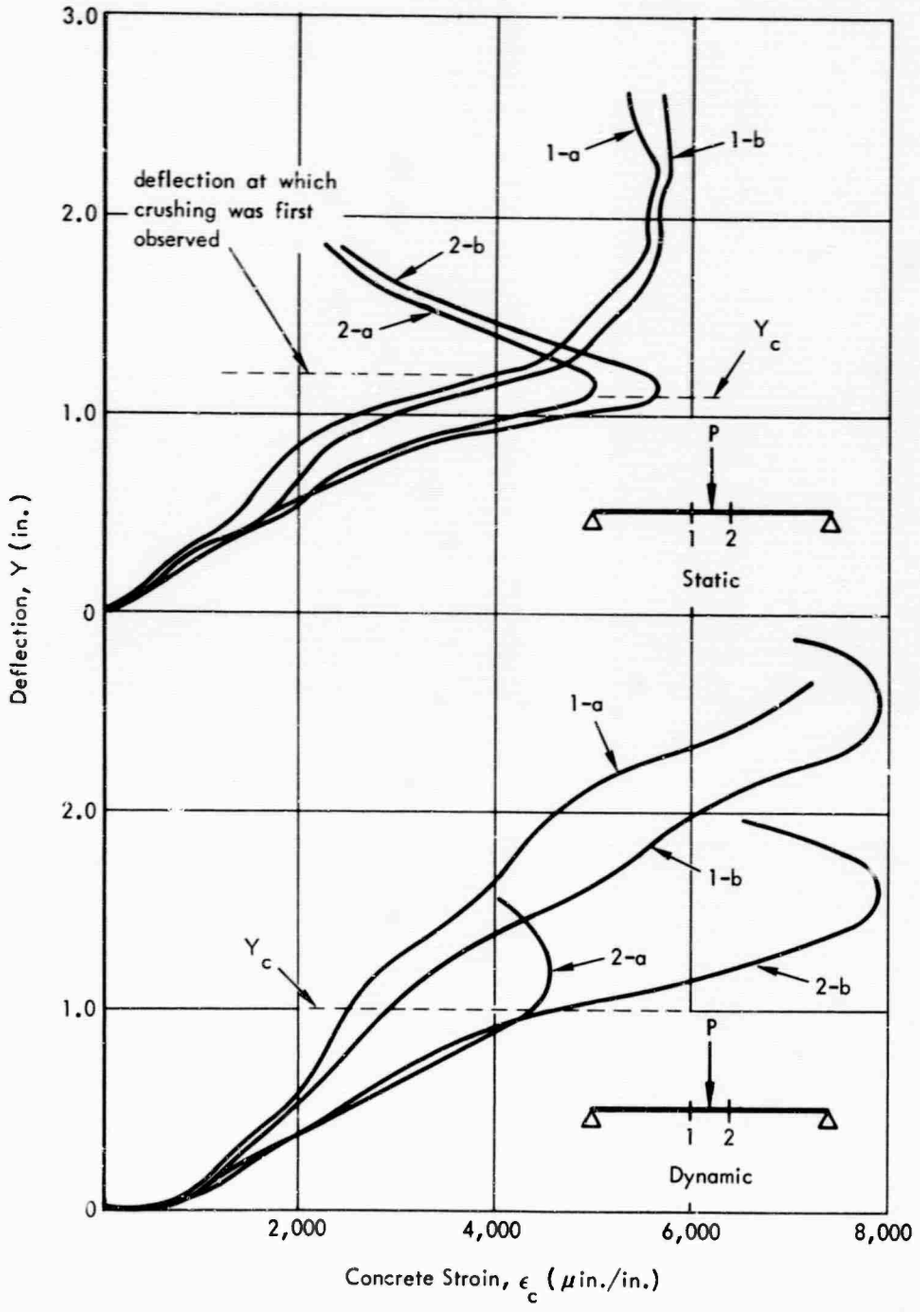

Note: Curves 1 and 2 correspond to strain meosurements at locations 1 and 2, respectively, with suffixes a and b indicating results of meosurements from two gages positioned 3/4 inch on each side of midwidth at locations 1 and 2.

Figure 4. Deflection versus concrete strain - centrally loaded beams.

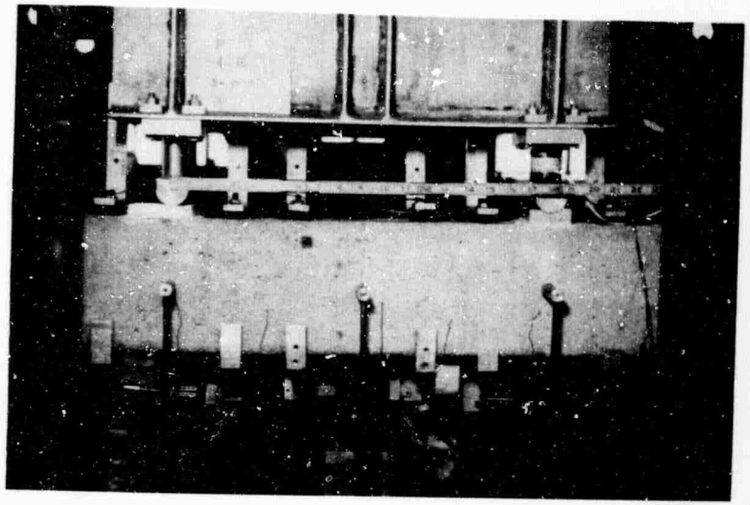

(a) Y = 0.10 in.

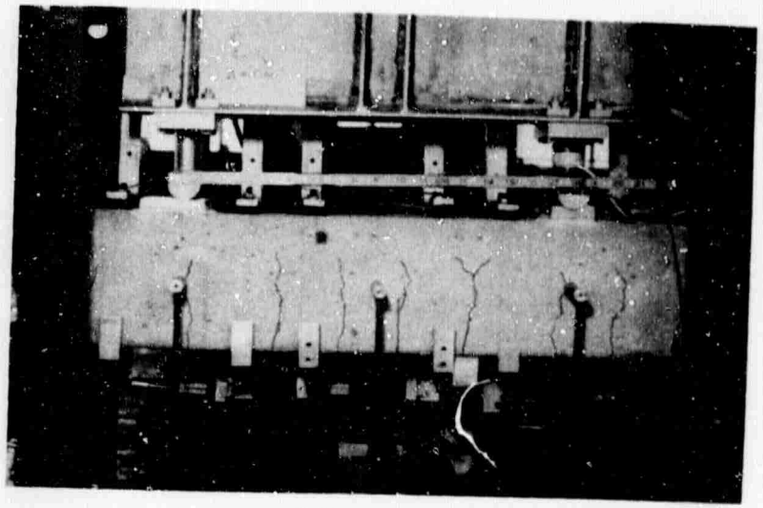

(b) Y = 0.50 in.

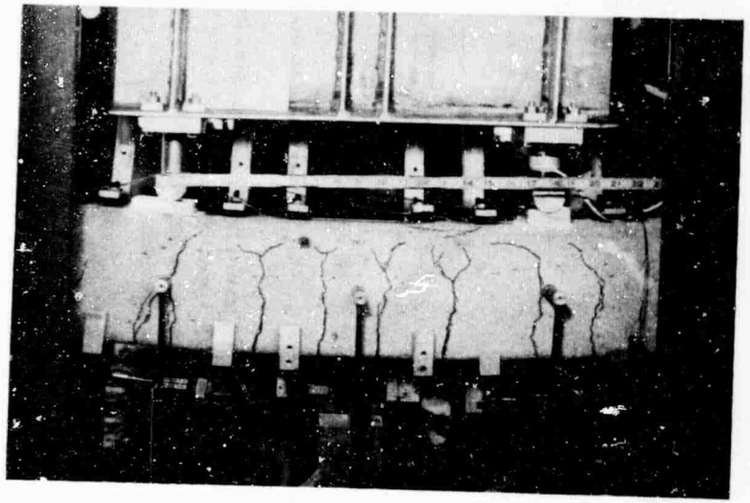

(c) Y = 2.00 in.

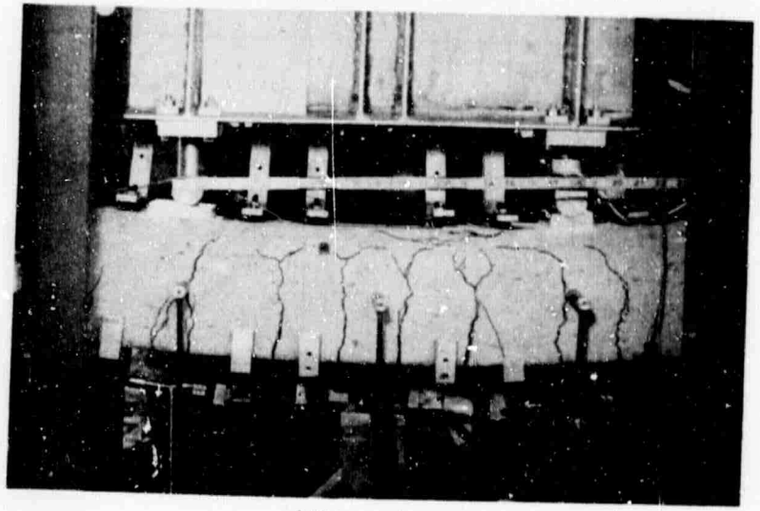

(d) Y = 2.40 in.

Figure 5. Photographs of Beam 4-13, statically loaded at two points, at various stages of behavior (Y_y = 0.34 in.; Y_c = 1.80 in.; Y_m = 2.24 in.; Y_u = 2.40 in.).

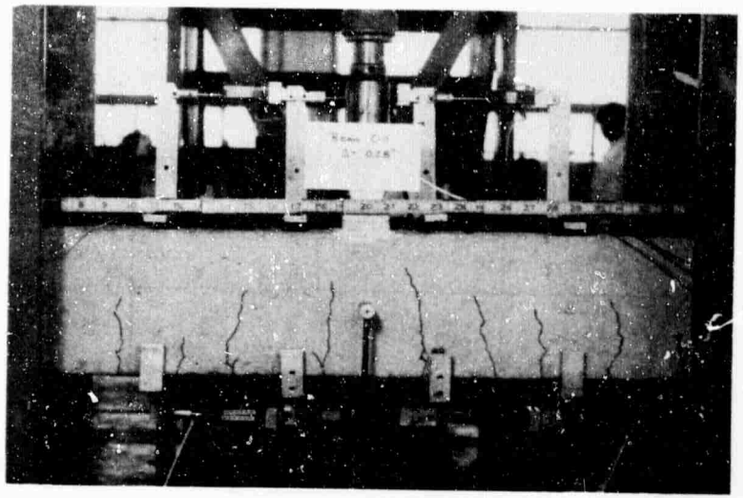

(a) Y = 0.28 in.

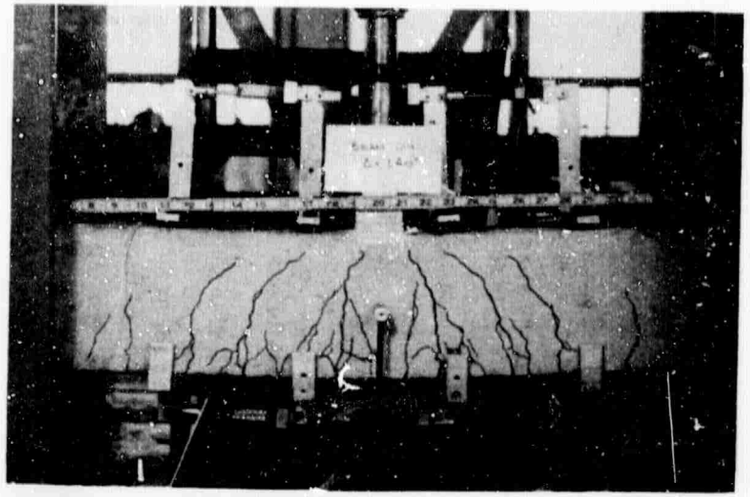

(b) Y = 1.40 in.

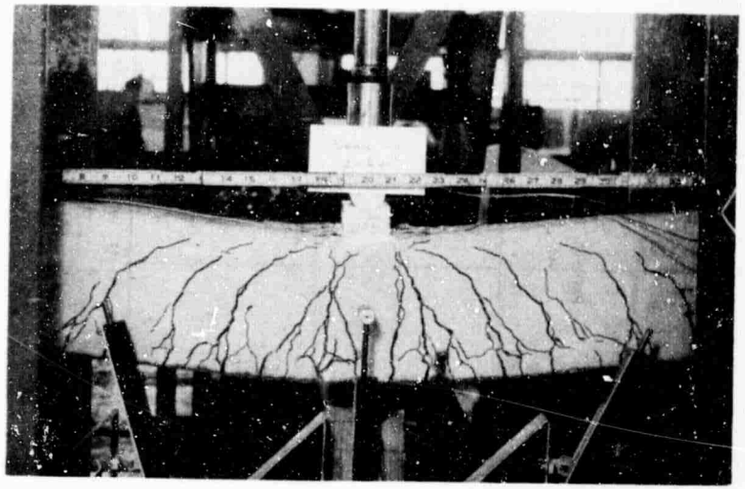

(c) Y = 4.00 in.

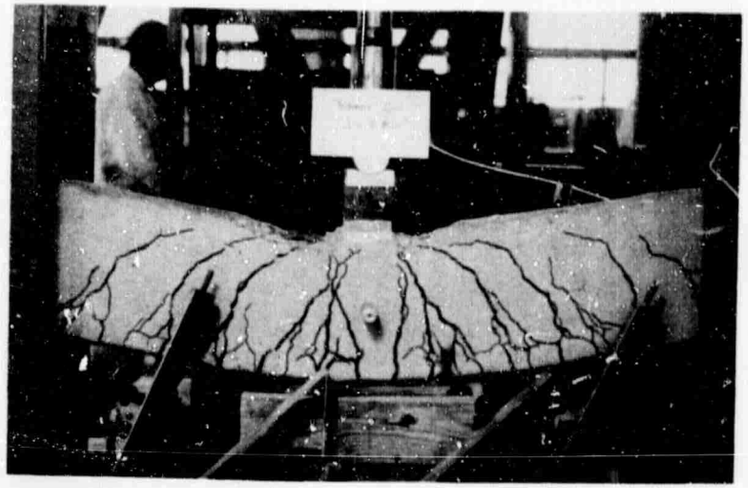

(d) Y = 5.80 in.

Figure 6. Photographs of Beam C-11, statically loaded at central point, at various stages of behavior (Y_y = 0.26 in.; Y_c = 1.20 in.; Y_m = 4.60 in.; Y_u = 5.80 in.).

Hinge Formation Under Static and Dynamic Loads

Hinge formation under static loads is discussed first and then the effect of dynamic loads.

At the yield stage the strain in the tension reinforcement at midspan increased abruptly from the yield value to a value corresponding to the upper limit of the yield range in the static tensile tests (approximately 1.5 percent strain). This is shown in Figure 9 for one of the beams loaded at two points. For these beams yielding did not propagate symmetrically about midspan. As shown in Figure 9, yielding occurred at sections 7 inches each side of midspan (within the maximum moment region) at different deflections.

The change in deflection was small as the strain increased through the yield range because the gage length of the strain gages was short (0.5 inch); although the strain increase was large, the total deformation was relatively small and had a negligible effect on the deflection of the beam. If a longer gage length had been used, the increase in strain would have been less abrupt.

These results indicate that hinging is in part a propagation of the yielded zone or zones throughout the maximum moment region. For the beams with a = 18 inches, there was a relatively long span subjected to maximum moment. Little additional load beyond the yield load was needed to propagate the yielded zones through the uniform moment region, but the propagation of the yielded zones resulted in a considerable change in the deflection of the beam. Thus, the load-deflection diagram (Figure 2) or the moment-rotation diagram (Figure 10) for these beams can be represented by an elastoplastic load-deformation relationship.

For the beams subjected to a concentrated load at midspan, the deflection did not increase much beyond the yield stage without a relatively significant increase in applied load (Figure 2), because there was no uniform moment region. The strain at midspan increased abruptly; however, due to the moment gradient adjacent to midspan, additional load was continually required to propagate the yielded zone. Thus, strain hardening of the tension reinforcement came into effect at or just beyond the yield stage. The moment-rotation diagram for these beams is similar to that shown in Figure 10.

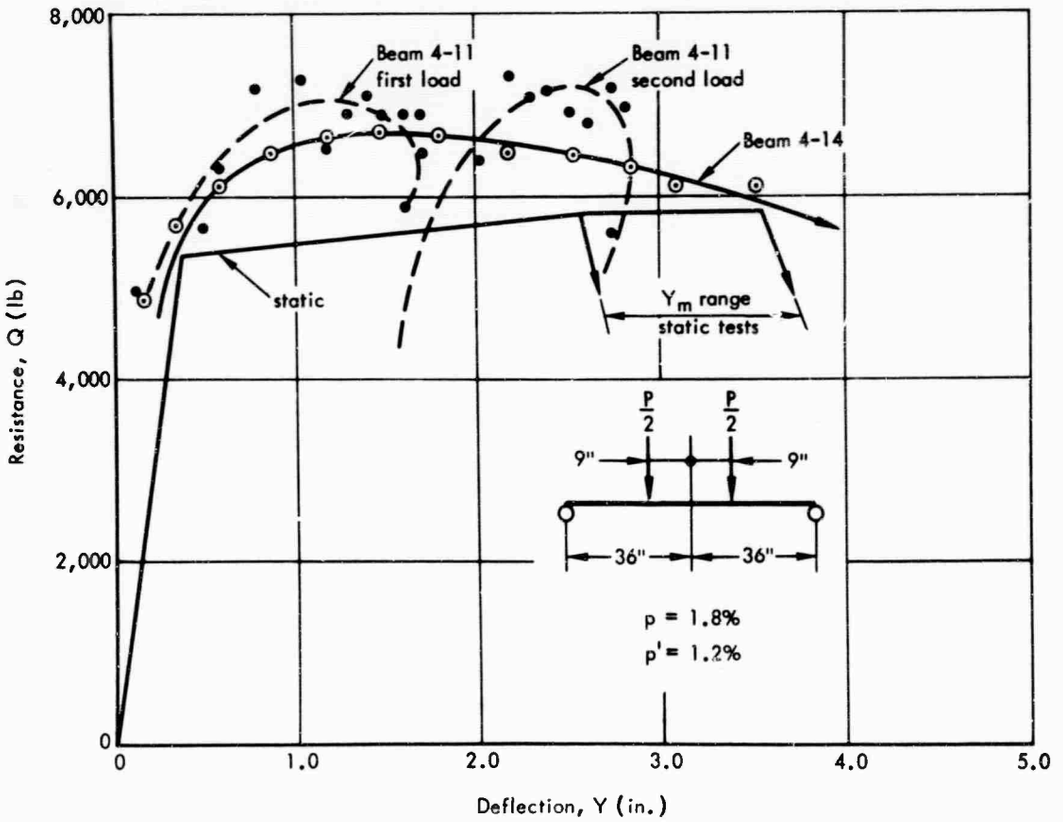

Figure 7. Dynamic resistance versus deflection - beams with uniform moment region.

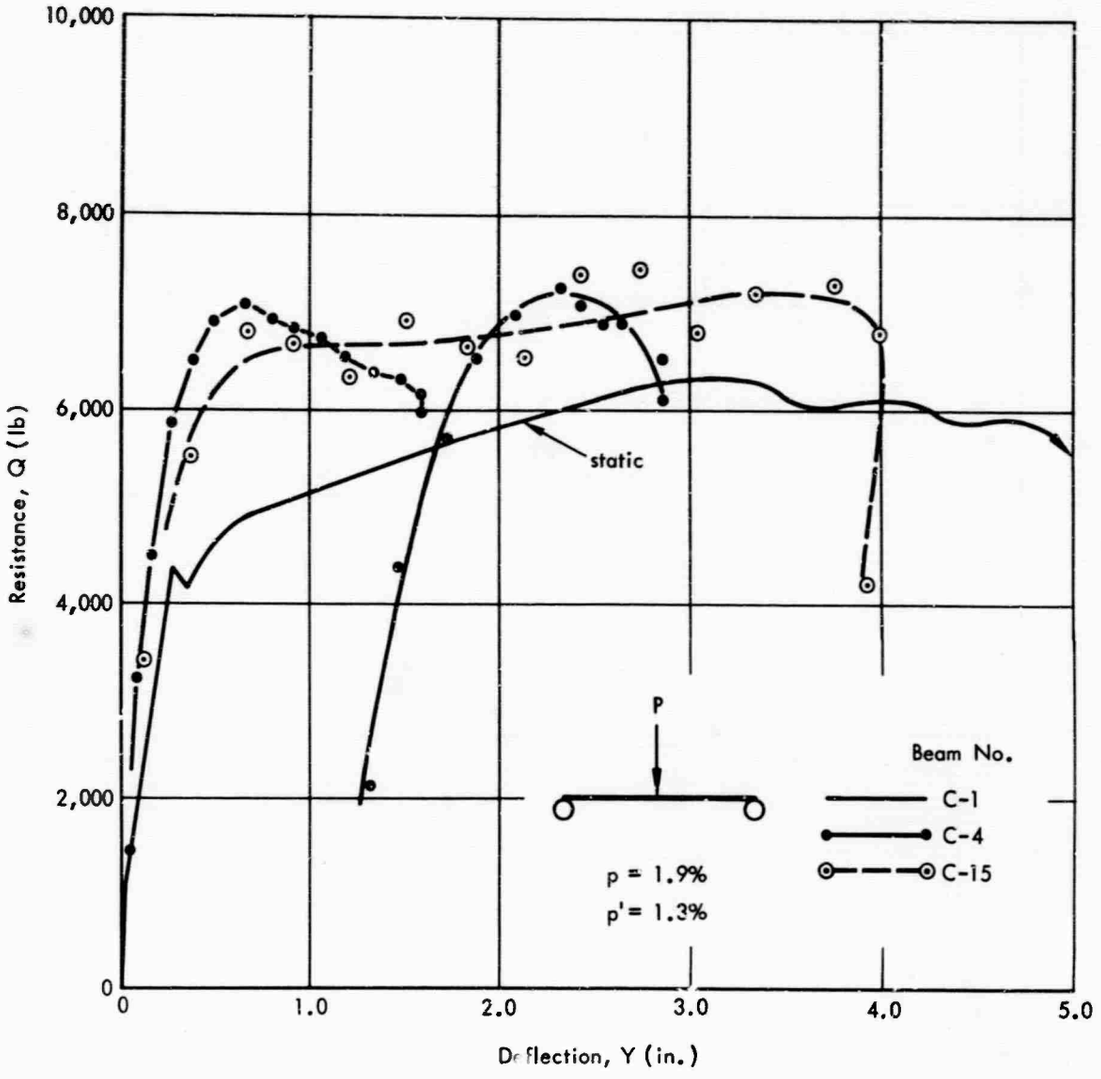

Figure 8. Dynamic resistance versus deflection - centrally loaded beams.

Actually, for either load configuration, the increase in resistance above the yield value was primarily a result of strain hardening of the tension steel. This is shown in Figure 11. The solid line represents the tensile stress-strain relationship for the reinforcement. The experimental data indicated by the other two lines represent the relationship between moment and tension steel strain at midspan for one beam from each test series.

Beyond the crushing stage, hinge rotation was usually confined to the section where crushing first developed. For the centrally loaded beams, hinge rotation was not noticeably affected by crushing because the hinge was essentially concentrated at one location, midspan. However, for the beams subjected to two loads, crushing could occur at any location in the uniform moment region. When crushing did occur at a section, the stiffness at that section decreased, thus causing subsequent deformations to result primarily from rotations at that section. However, near the ultimate stage, extensive horizontal cracking developed at the level of the compression reinforcement in the uniform moment region. This cracking propagated horizontally from the flexural cracks and sometimes resulted in the detachment of the top cover of concrete. The curvature distribution will be discussed further in the next section.

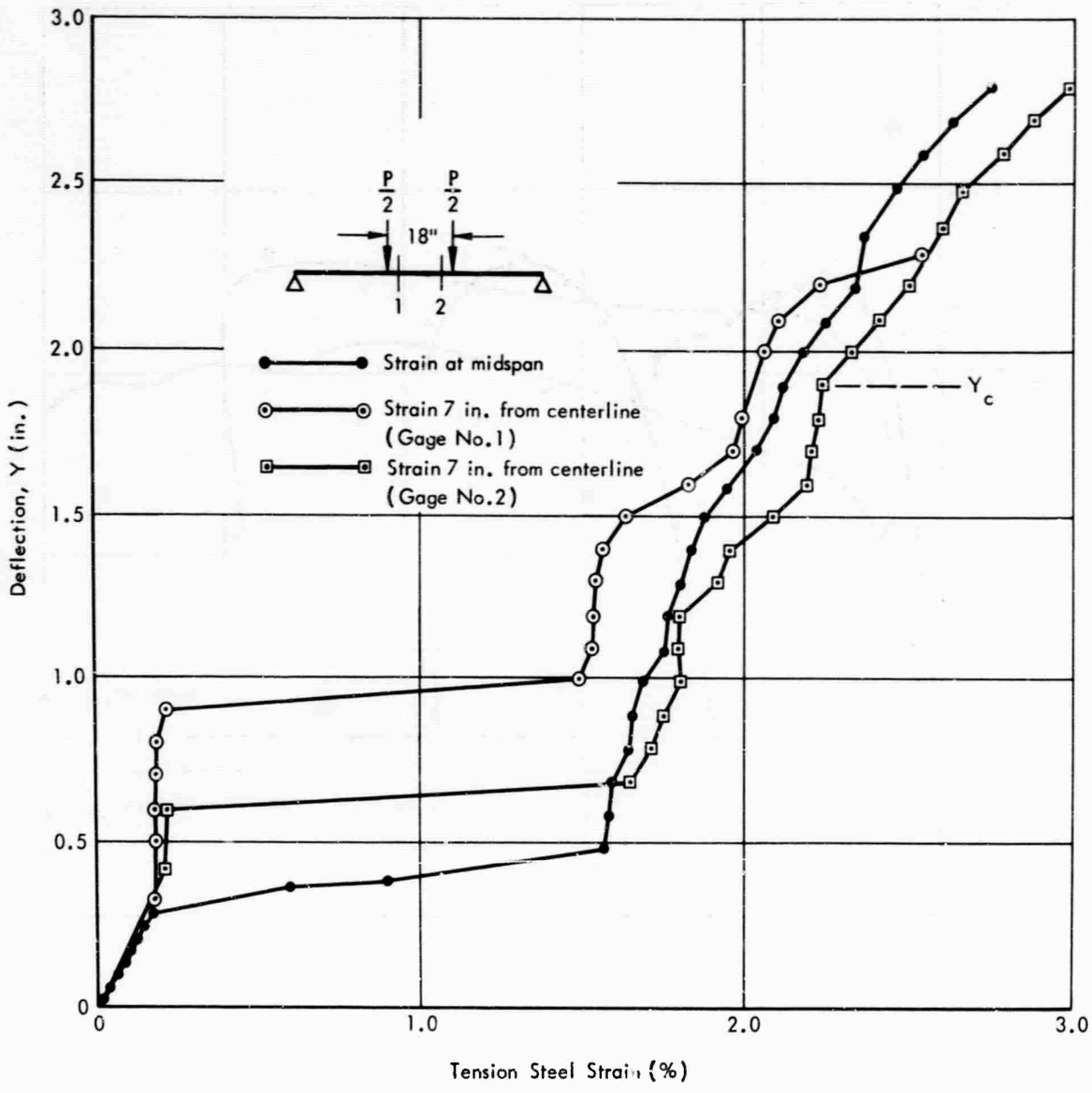

Figure 9. Deflection versus tension steel strain - static test, Beam 4-6.

The spread of the yielded zones was related to the moment gradient as shown in Figure 12. Permanent deformations occurred over that portion of the beam resisting a moment greater than the yield moment. Also, the magnitude of the permanent strain at a section was about proportional to the magnitude of the maximum moment beyond the yield moment, at that section.

In the dynamic tests, hinging developed in a manner similar to that observed in the static tests. However, as a result of the strain rate effect, the strain values at the limits of the yield range were greater than the static values (Figure 13).

For the beams loaded at midspan, the curvature distribution within the hinge zone was similar for the static and dynamic cases. At large deflections, the average curvatures at midspan in the dynamically loaded beams were slightly greater than those in the corresponding statically loaded beams, as shown in Figure 14. This difference was attributed to the crushing of the concrete under the load-bearing plate in the dynamic test; this crushing apparently slightly reduced the stiffness of the beam at midspan.

Hinge formation in beams subjected to two concentrated loads will be discussed in the next section.

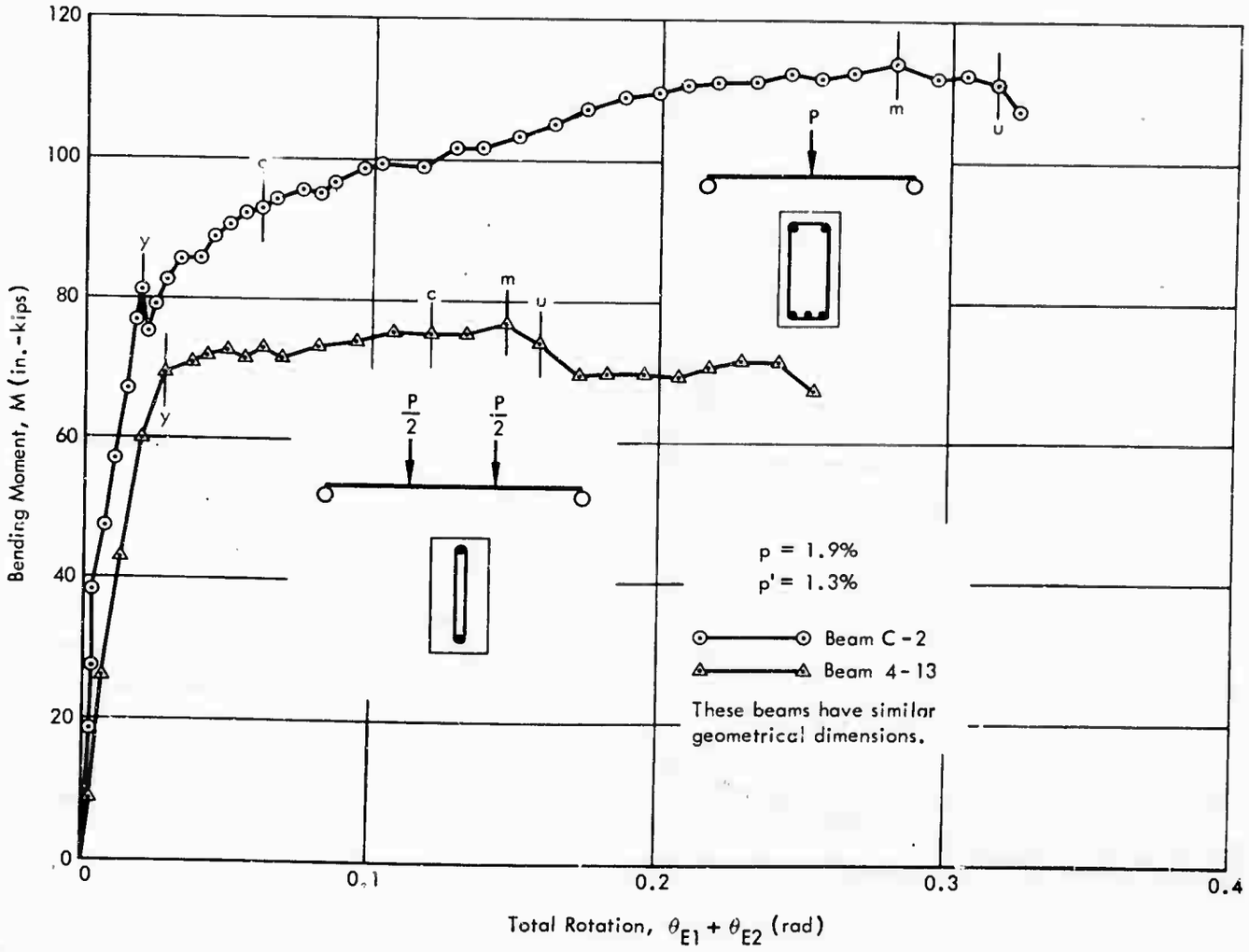

Figure 10. Static moment-rotation relationships.

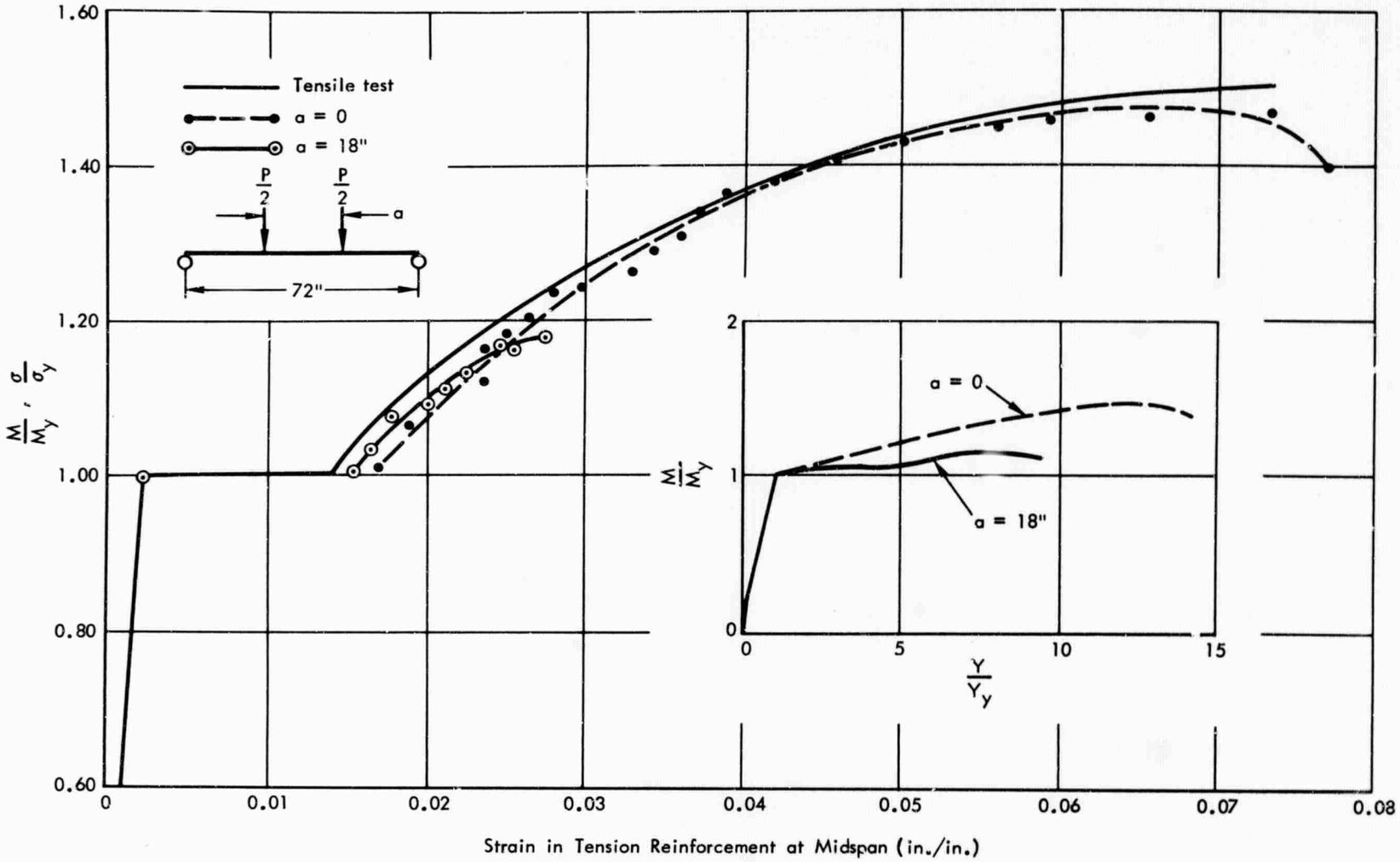

Figure 11. Moment-tension steel strain relationship.

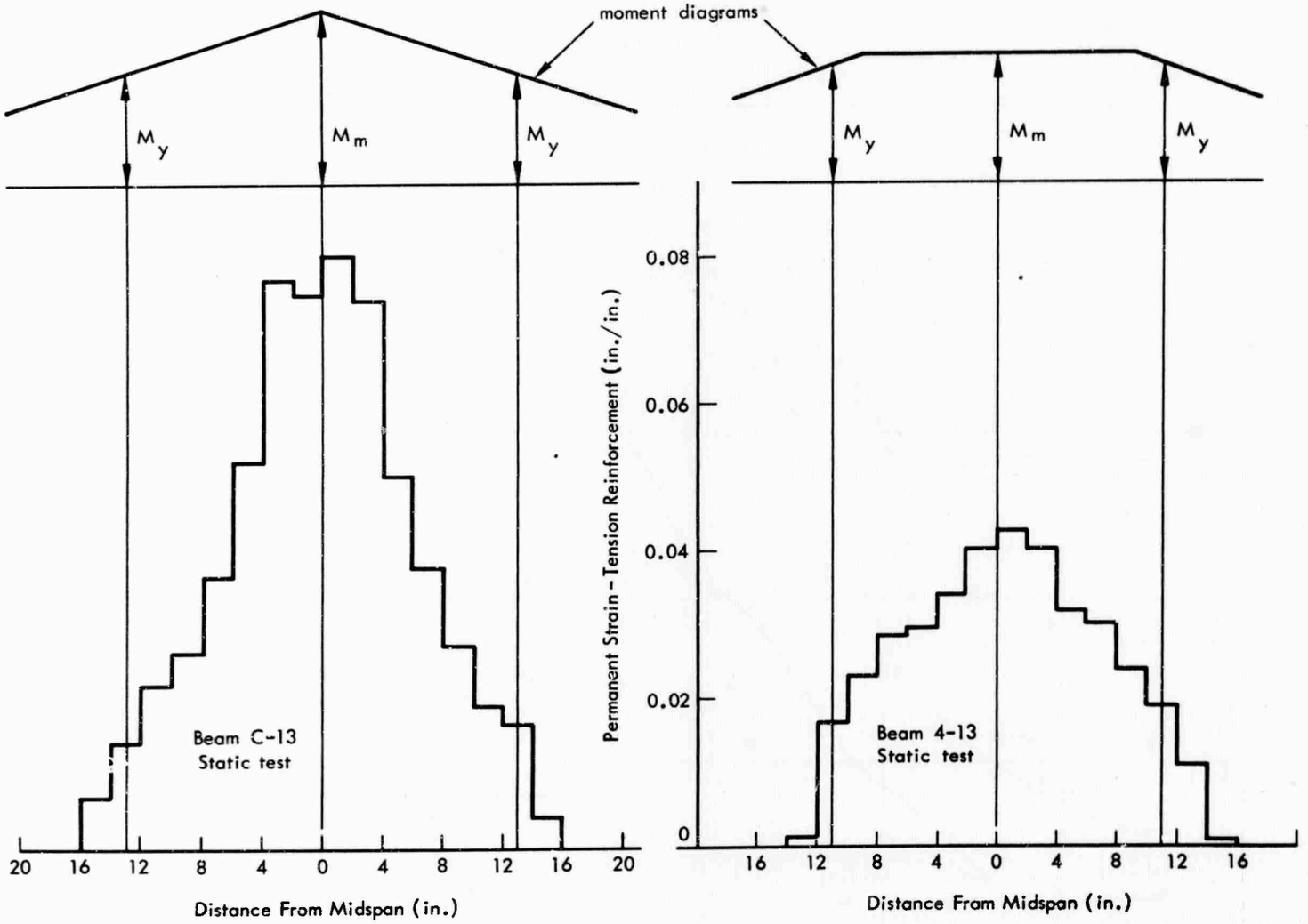

Figure 12. Yielded zone - tension reinforcement.

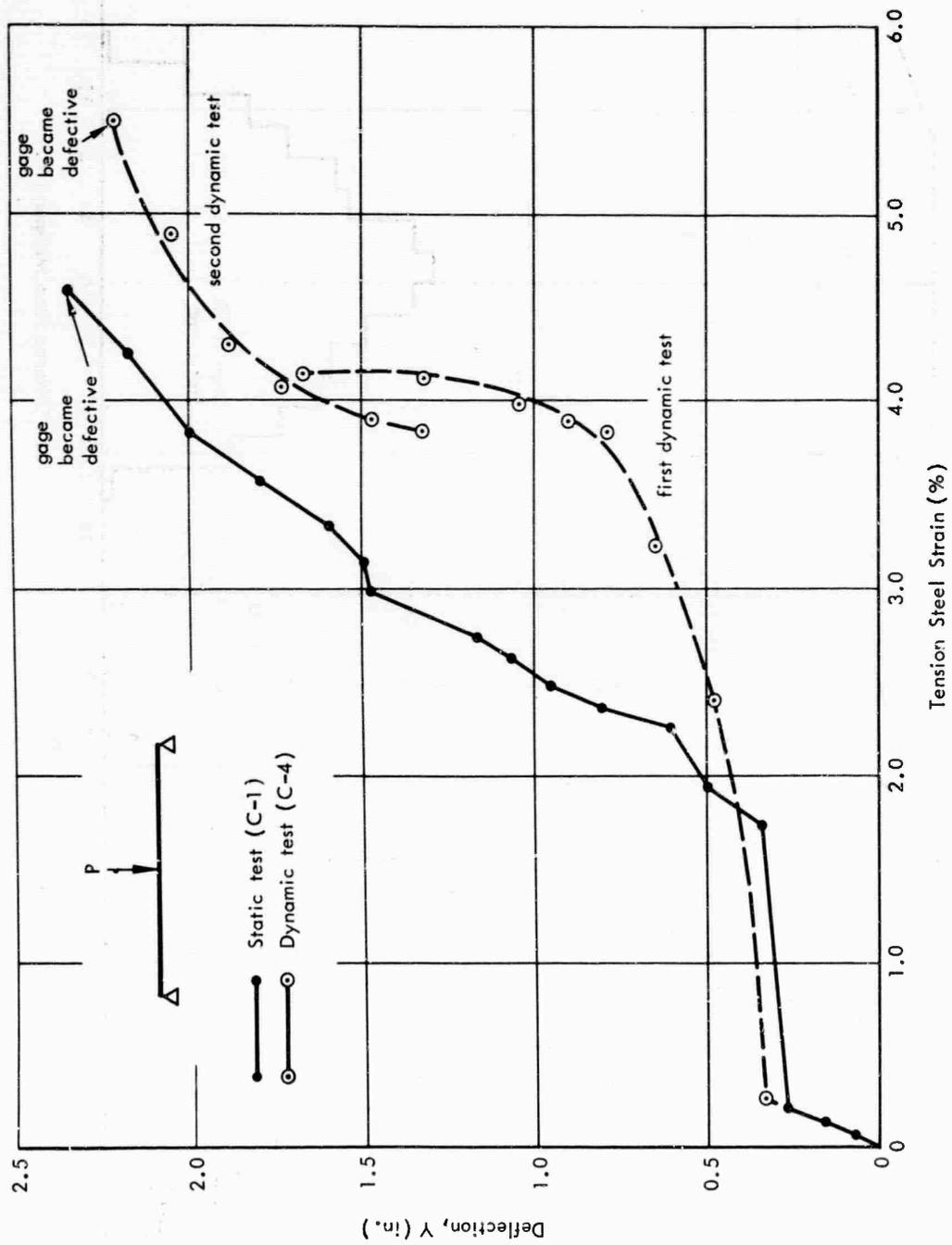

Figure 13. Tension steel strain - static versus dynamic.

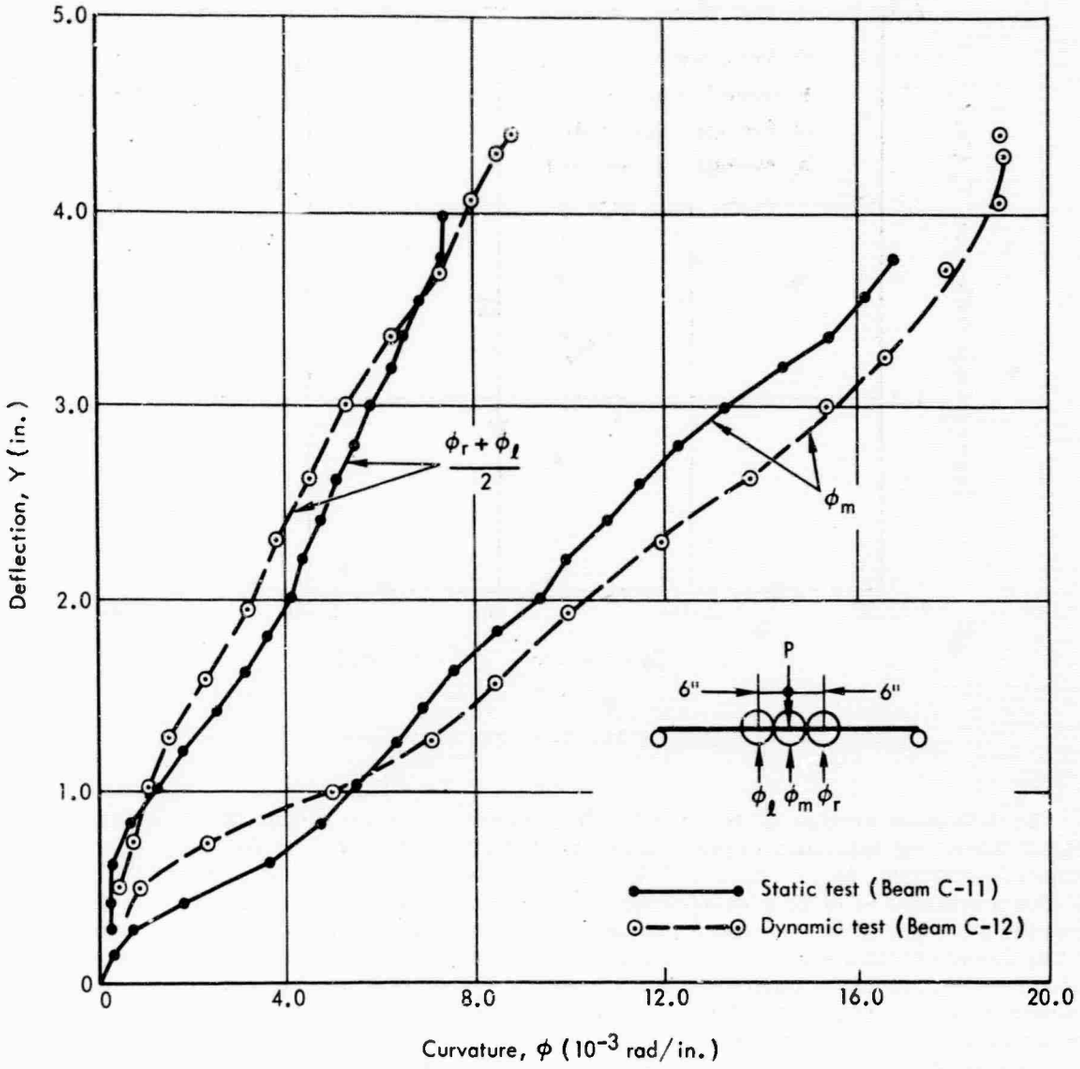

Figure 14. Curvature distribution - centrally loaded beams.

Effect of Test Variables

Beams Subjected to Two Concentrated Loads. In the corresponding Phase I beam tests, the crushing stage deflections in the dynamic tests were less than in the static tests.[6] This difference was attributed to an apparent concentration of hinge rotation in the dynamically loaded beams. However, the test results presented herein indicate that this concentration was not any more severe than that in the static tests.

In Figure 15, the deflection and concrete strain data are summarized for the beams subjected to two concentrated loads. Results from the Phase I tests are included in this figure. For the beams in which crushing occurred during the second or third dynamic test, the cumulative values of deflection and strain were used. As shown, the average concrete strain at midspan was equivalent for both the static and dynamic tests, but the deflections were not. The values of the critical concrete strain are within the range of previous test data.[8,9] The results in Figure 15 indicate the average dynamic crushing stage deflection to be 25 percent less than the average static value.

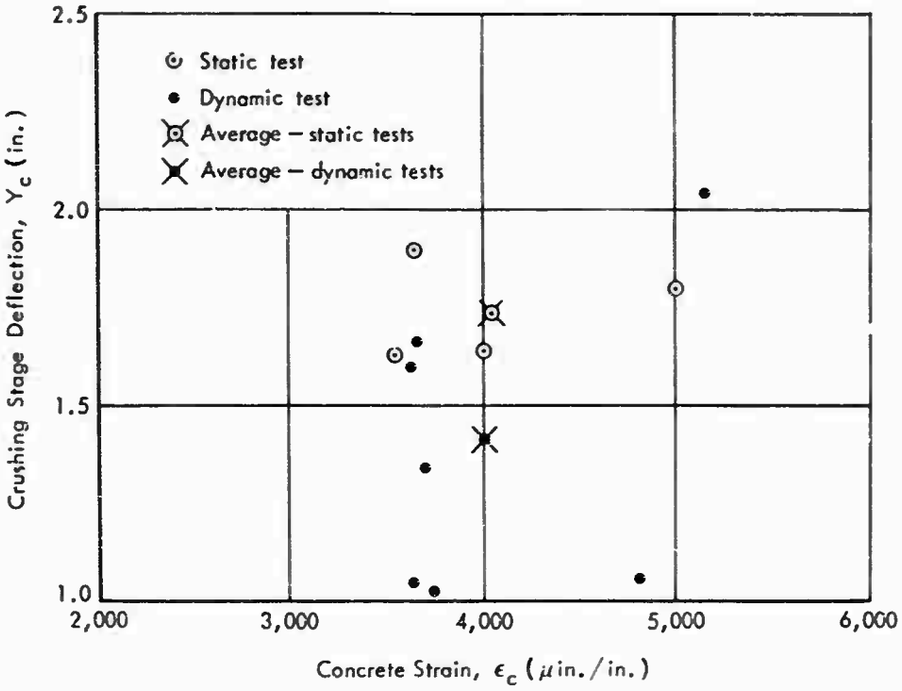

Figure 15. Crushing stage data.

To determine whether hinge formation at the crushing stage was similar under static and dynamic loads, the ratio of maximum measured curvature (ϕ_m, ϕ_r, or ϕ_ℓ) to the average measured curvature $(\phi_m + \phi_r + \phi_\ell)/3$ was computed from the crushing stage data. This ratio provides a measure of hinge concentration; a value of one indicates that the curvature at the middle and at the extremes of the maximum moment region are equal. The values of this ratio versus the corresponding crushing stage deflections are plotted in Figure 16. Based on these results, the premature crushing stage apparently is not a result of a concentration of rotation within the maximum moment region. For both the static and dynamic test results, the ratios of maximum to average rotation are within the same range (1.1 to 1.5), except for the two extreme values, one of which is a dynamic test result and the other a static test result.

Even though the onset of crushing occurred at a lower deflection in the dynamic tests than in in the static tests, no immediate effect on the resistance-deformation relationship was observed. This result is similar to that observed in the static tests.

Centrally Loaded Beams. The static load-deflection diagrams for the beams in which the tension reinforcement percentage was the primary variable are presented in Figure 17. The increase in the crushing stage deflection with decrease in q, and in these tests q - q', is known. Essentially, this increase results because decreasing the amount of tension reinforcement decreases the compression zone depth required to satisfy the equilibrium of internal forces for a given maximum fiber strain. Since curvature is inversely proportional to the depth of the compression zone, kd, the average curvature increases and results in a greater deflection.

These statements are also appropriate for the subsequent stages. As shown in Figure 17, the deflection at maximum load and at the ultimate stage increased as the amount of tension reinforcement decreased. However, at the ultimate stage, ductility of the tension reinforcement and stability of the compression reinforcement are important parameters which also must be considered. For example, Beam C-7 failed because the tension steel fractured; if the ductility of the tension steel had been less, the difference between ultimate deflections of Beams C-1 and C-7 would have been less and perhaps negligible considering the difference as a percentage of the ultimate deflection. Furthermore, for one set of conditions, two beams were tested; one (C-8) failed when the

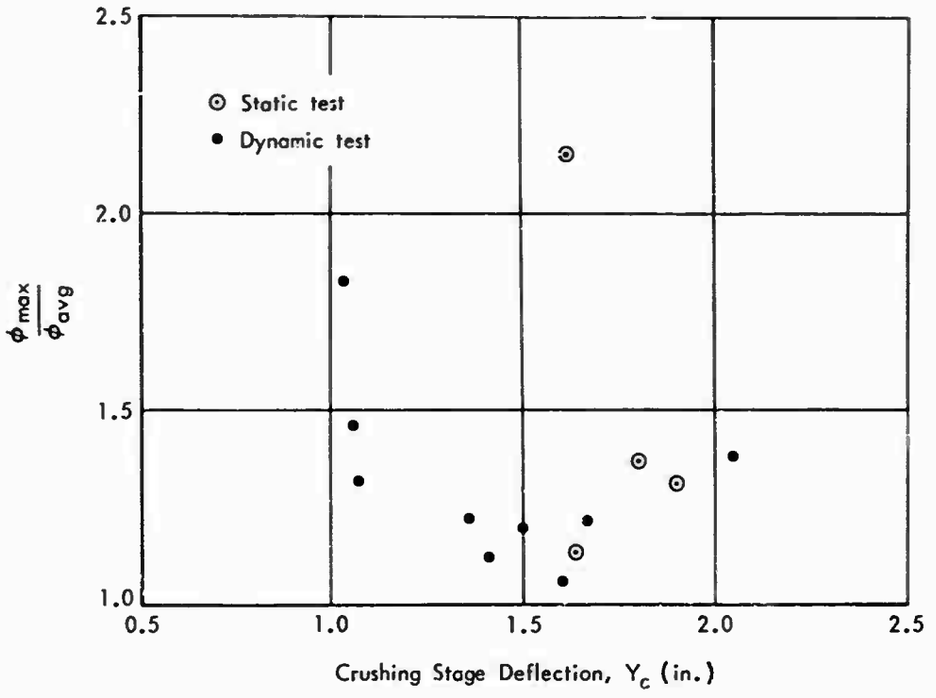

Figure 16. Curvature distribution at crushing stage.

tension reinforcement broke and the other (C-11) failed when the compression steel buckled. The difference in the ultimate deflections between these two beams is equivalent to the difference in the ultimate deflections of Beams C-1 and C-7. Therefore, the effect of the amount of tension reinforcement on rotation capacity is not completely defined by these results.

Based on the occurrence of tension steel failures in these tests, similar beams ($p'/p = 0.67$) with $p < 1$ percent will probably fail by fracture of the tension reinforcement, and beams with $p > 2$ percent will probably fail in a flexural compression mode. A transition zone would be between these limits. Moreover, in these beams, the ductility of the tension steel was being utilized completely, so that the addition of more compression reinforcement would have a negligible effect on the rotation capacity of the beams.

The effect of transverse reinforcement size on rotation capacity was negligible, as shown in Figure 18. The beam in which 1/8-inch round stirrups were used exhibited a lower maximum load and ultimate deflection, but the difference was small compared to the magnitude of the total deflection. Beam C-1 failed by buckling of the compression reinforcement, whereas the other two beams failed when the tension reinforcement broke. Since the ductility of the tension reinforcement was exhausted in two of the beams, a further increase in the amount of transverse reinforcement should have no effect on the rotation capacity of the beams.

The behavior of two beams with similar properties except for the size and arrangement of the reinforcement are compared in Figure 2. The results apparently indicate the effect of confined concrete. Both beams had well-tied compression reinforcement, but in one case the area of compressed concrete circumscribed by the transverse reinforcement was negligible. For this beam the load did not increase much beyond the value at the crushing stage. The deflection at ultimate load for this beam was 30 percent less than that for the other beam. The difference in maximum resistance was approximately 20 percent.

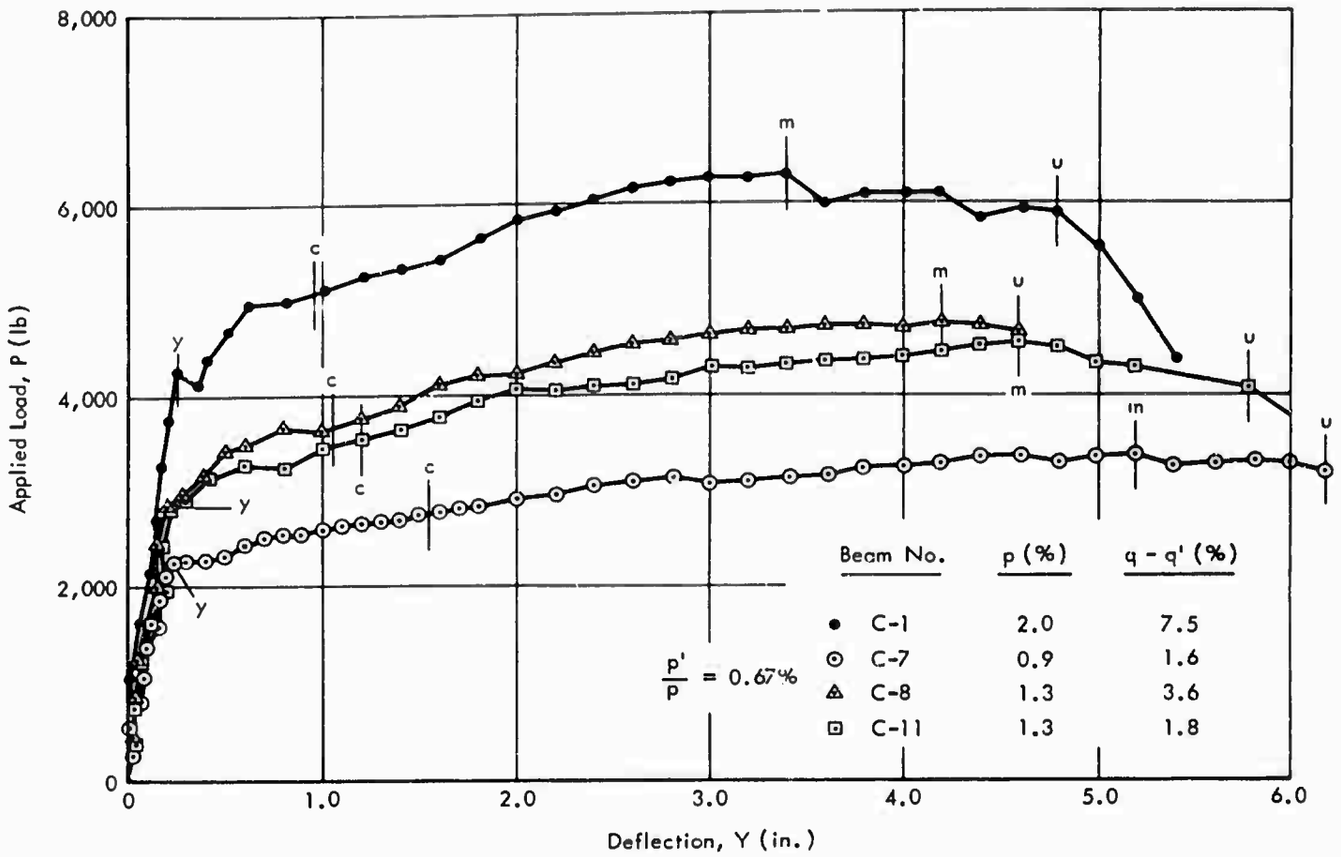

Figure 17. Effect of tension reinforcement.

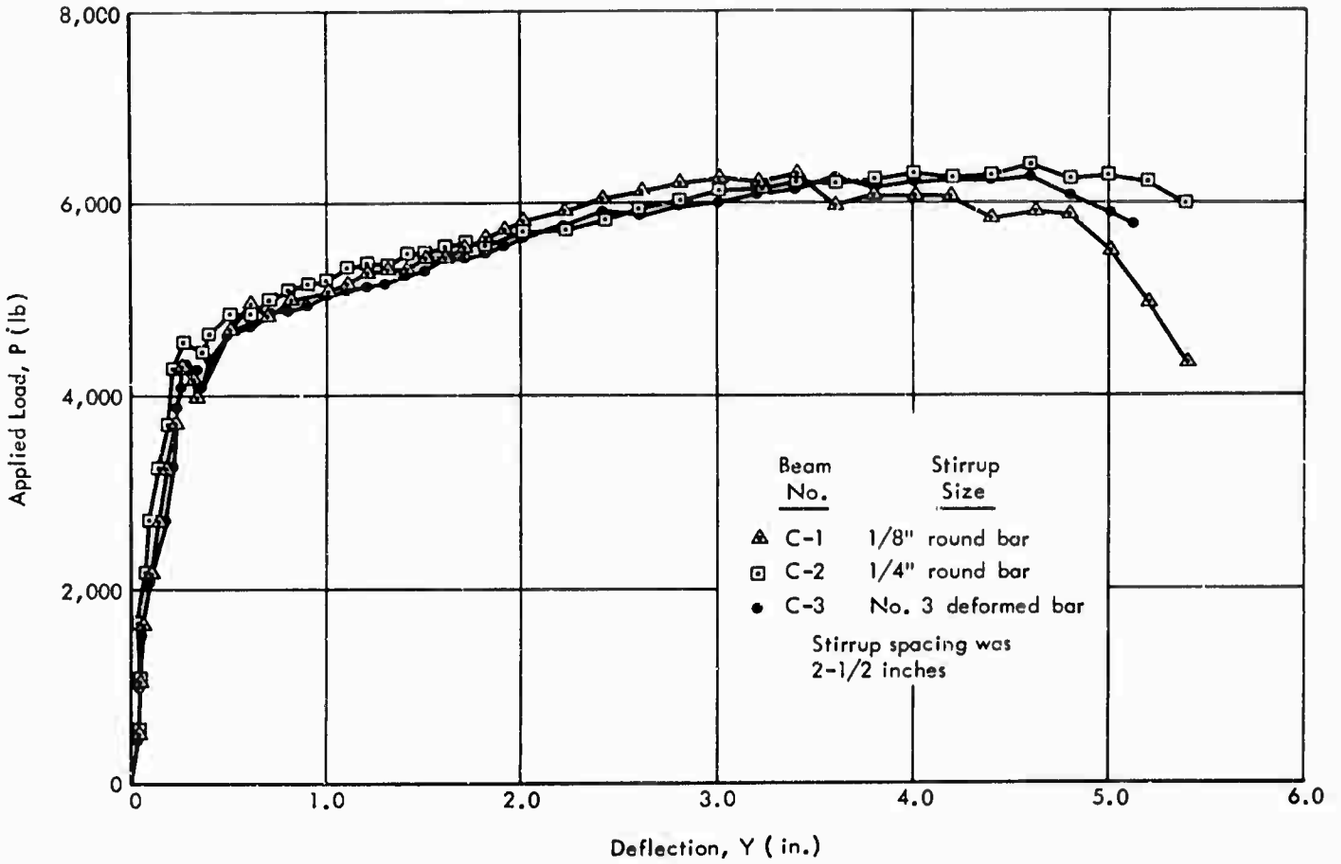

Figure 18. Effect of transverse reinforcement size.

ANALYSIS

This section is divided into two parts: (1) an analysis of the yield stage and (2) an analysis of post-yield behavior. For under-reinforced beams, such as those tested in this investigation, the relationship between moment and curvature or moment and deflection is approximately linear prior to the yield stage; thus, prediction of the moment, curvature, and deflection at yield provides a description of the pre-yield behavior, as well as the stage at which hinging begins.

The post-yield deformations are dependent primarily on the hinging mechanism and are discussed separately. To provide a comparison between the actual and computed hinge characteristics, both the end rotation and deflection of the beams were calculated. The end rotation provides a measure of the magnitude of hinge rotation, because the increase in the end rotation beyond yield results primarily from hinge rotation. In computing deflections, the location of the center of rotation must be considered; thus, deflection calculations reflect the magnitude of hinge rotation and the hinge geometry.

The behavior of beams under dynamic loads will be considered in each part of the analysis.

Yield Stage

Static Tests. The values of moment, curvature, and deflection at yield were computed by the conventional straight-line theory, which requires the following assumptions:

1. A linear distribution of strain over the depth of the beam.

2. A linear stress-strain relationship for the concrete. The modulus of elasticity of the concrete, E_c, was defined[5] as

$$E_c = \frac{30,000}{0.006 + \frac{10}{f_c'}} \tag{2}$$

3. No tensile stresses in the concrete.

The stress-strain relationship for the tension and compression reinforcement was obtained from static tensile tests. A modulus of elasticity equal to 29,000,000 psi was used in the analysis.

Figure 19 shows the stress and strain distributions at the yield stage. By satisfying equilibrium conditions and utilizing the assumptions listed previously, the depth of the compression zone, kd, can be computed. The equation for k is

$$k = \sqrt{2\left[pn + p'(n-1)\frac{d'}{d}\right] + \left[pn + p'(n-1)\right]^2} - \left[pn + p'(n-1)\right] \tag{3}$$

Referring to Figure 19, the yield moment can be computed by taking moments of the internal forces about the level of the tension reinforcement:

$$M_y = C_c\left(d - \frac{kd}{3}\right) + C_s(d - d') \tag{4}$$

To satisfy equilibrium,

$$C_c = T_s - C_s = A_s f_y - A_s' f_s' \tag{5}$$

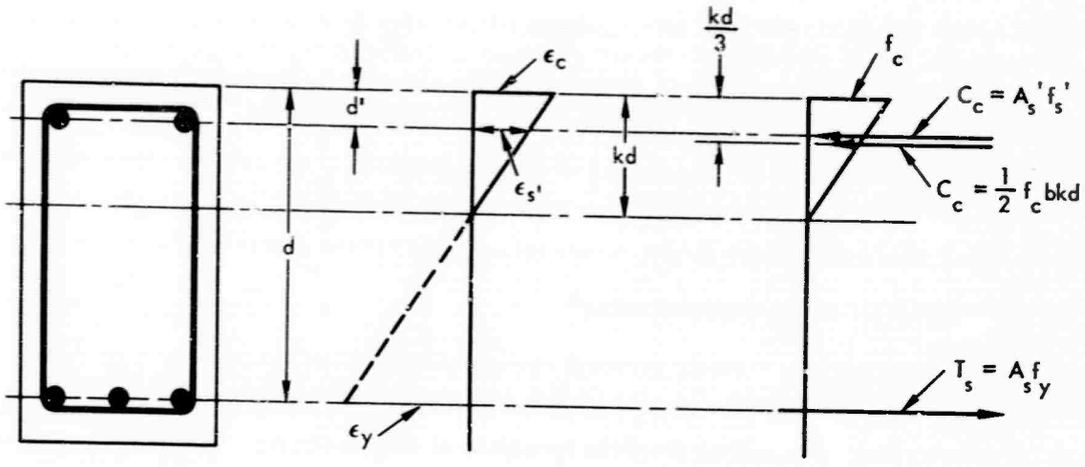

Figure 19. Stress and strain distributions at the yield stage.

and, therefore, Equation 4 becomes

$$M_y = (A_s f_y - A_s' f_s')\left(d - \frac{kd}{3}\right) + A_s' f_s'(d - d') \tag{6}$$

The average stress in the compression reinforcement is

$$f_s' = \frac{kd - d'}{d - kd} f_y \leq f_y' \tag{7}$$

Based on the strain distribution at yield (Figure 19), the curvature at yield is

$$\phi_y = \frac{\epsilon_y}{d(1 - k)} \tag{8}$$

The deflections at yield were computed assuming a linear relationship between moment and curvature. Thus, the distribution of curvature was the same as that for moment, ϕ_y being the maximum value of curvature. The midspan deflection at yield, then, is

$$Y_y = \frac{\phi_y L^2}{12}\left[1 + \frac{a}{L} - \frac{1}{2}\left(\frac{a}{L}\right)^2\right] \tag{9}$$

For the centrally loaded beams, a was assumed to be equal to the width of the load-bearing plate, 2 inches.

Based on the results of previous investigations (References 3, 4, 5, 8, and 11), the value of deflection computed by the straight-line theory generally can be expected to be less than the measured value as shown by the results in Figure 20. The differences between the computed and measured yield deflections have been attributed, in part or entirely, to the following:

1. The modulus of elasticity, E_s, based on the nominal area of the reinforcement being less than 30,000,000 psi [4]

2. A departure from a linear stress-strain relationship for the concrete [4,8]

3. E_c being less than the assumed value [8]

4. The effect of a strain gradient across a section of the tension reinforcement on the magnitude of ϵ_s at yield [6]

5. Additional rotation resulting from the formation of diagonal tension cracks in the region of maximum moment [5]

To provide more accurate estimates of the yield deflections, some investigators have developed empirical procedures to correct the values computed by the straight-line theory.[4,5] Burns and Siess [4] increased the value of the yield strain in Equation 8 by 0.0003; thus,

$$\phi_y = \frac{\epsilon_y + 0.0003}{d - kd} \tag{10}$$

where

$$\epsilon_y = \frac{f_y}{30,000} \tag{11}$$

The computed deflections were in good agreement with the measured values. Burns and Siess noted that Equation 10 would not be valid for beams with high q-values. In their tests, q varied between 0.10 and 0.27.

Subsequently, Yamashiro and Siess [5] found that this procedure provided computed deflections greater than the measured values for beams with small p-values (p = 0.67 percent) and computed deflections less than the measured values for beams with large p-values (p = 3.33 percent). They attributed the difference between the measured and computed values to an additional beam rotation resulting from the formation of diagonal tension cracks adjacent to the maximum moment region. Using their test results and those in References 4 and 11. they developed a procedure for computing this additional rotation, which was found to be dependent on ϵ_y, $f_s A_s/\Sigma 0$, and $1/\ell$. They were then able to obtain good correlation between the experimental and computed values of yield deflections for their results as well as those in References 4 and 11.

To determine the correlation between certain parameters and the difference between the measured and computed values of yield deflection, a stepwise regression analysis procedure was used.[10] The dependent variable was

$$\frac{(Y_y)_{exp}}{(Y_y)_{comp}} - 1 \tag{12}$$

The independent variables were f_y, f_c', A_s, $\Sigma 0$, and ℓ; b and d were used to develop dimensionless parameters. Values of the dependent and independent variables were obtained from References 3, 4, 5, 6, 8, and 11, and the present tests.

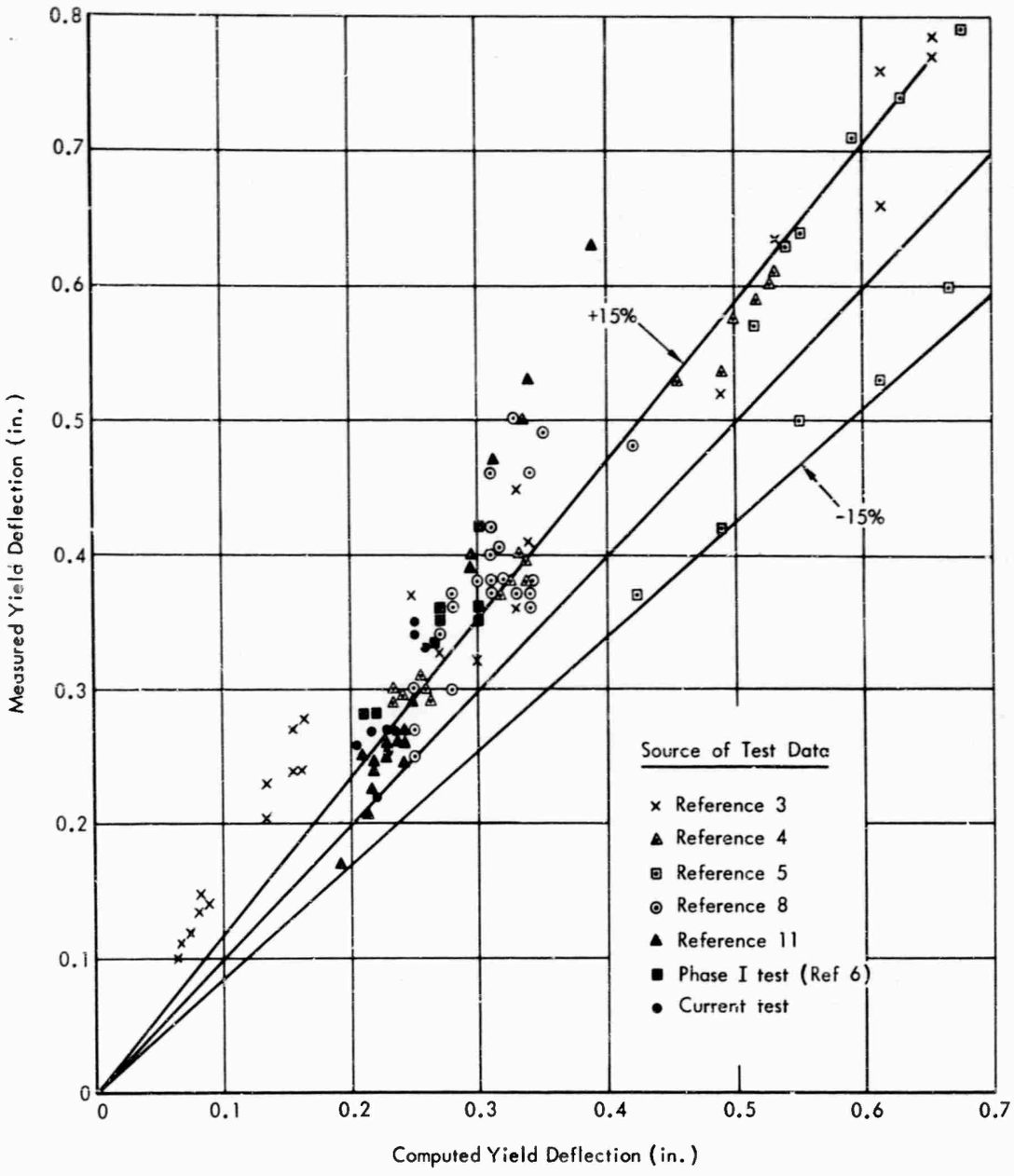

Figure 20. Comparison of measured yield deflections and those computed using the straight-line theory.

The tests described in References 4, 5, and 11 were conducted on simply supported beams loaded through a column stub at midspan. In the deflection calculations, the distribution of curvature across the stub was assumed to be uniform and equal to ϕ_y (Equation 8); this is the same distribution as that assumed in References 4 and 11.

The results of the analysis indicated that

$$q = \frac{pf_y}{f'_c}$$

had the best correlation, using data from all the references. As q increases, nonlinearity of stress in the compression zone is more likely, and therefore deviation between experiment and theory would be expected. Thus, q is a reasonable parameter. The analysis revealed, further, that there were other factors causing the difference noted. However, these other factors could not be established from the parameters investigated. Further study is required involving new parameters and different forms of the parameters used previously.

Using the results of the regression analysis, Equation 8 was modified for beams in which $q \geq 0.1$ as follows:

$$\phi_y = \frac{\epsilon_y}{d(1 - k)}(1 + q) < 1.6\frac{\epsilon_y}{d(1 - k)} \tag{13}$$

For $q < 0.1$, Equation 8 can be used unchanged. Althrough q varied from 0.06 to 0.95 in the test results examined in the regression analysis, there was only one case in which q exceeded 0.6. Equation 13 is not valid for $p > 0.04$.

Dynamic Tests. The yield stage for the dynamically loaded beams was computed using the same procedure as that for the statically loaded beams, except that the dynamic yield strength of the reinforcement was used in the computations. The increase in the yield strength was determined using the experimental strain rate data and results of dynamic tensile tests reported in Reference 6.

By differentiating Equation 8 with respect to time, a relationship between strain rate and curvature rate is obtained:

$$\frac{d\epsilon_s}{dt} = d(1 - k)\frac{d\phi}{dt} \tag{14}$$

Prior to yielding, the maximum curvature rate can be related to maximum deflection rate by differentiating Equation 9:

$$\frac{dY}{dt} = \frac{d\phi}{dt}\frac{L^2}{12}\left[1 + \frac{a}{L} - \frac{1}{2}\left(\frac{a}{L}\right)^2\right] \tag{15}$$

Combining Equations 14 and 15 yields a relationship between strain rate and deflection rate:

$$\frac{d\epsilon_s}{dt} = \frac{12}{L^2} \frac{d(1-k)}{\left[1 + \frac{a}{L} - \frac{1}{2}\left(\frac{a}{L}\right)^2\right]} \frac{dY}{dt} \tag{16}$$

The strain rate at yield was computed by using the measured deflection rate at yield in Equation 16. The value of k was determined by Equation 3.

The relationship between strain rate and percent increase in yield strength was assumed to be that shown in Figure 21. The measured deflection rates, computed strain rates. and percent increase in yield strength are listed in Table 1.

Table 1. Percent Increase in Yield Resistance - Dynamically Loaded Beams

Beam No.	Measured Deflection Rate at Yield (in./sec)	Strain Rate (in./in./sec)	Increase in Yield Resistance (%)
C-4	80	0.66	34
C-5	88	0.70	34
C-6	91	0.72	35
C-9	89	0.82	36
C-10	100	0.84	36
C-12	119	1.01	38
C-13	111	1.09	38
C-14	97	0.76	35
C-15	138	1.08	38
4-7	71	0.46	31
4-8	76	0.49	31
4-9	76	0.50	31
4-10	78	0.51	32
4-11	92	0.60	33
4-14	123	0.81	36
4-15	121	0.78	36
4-16	81	0.54	32

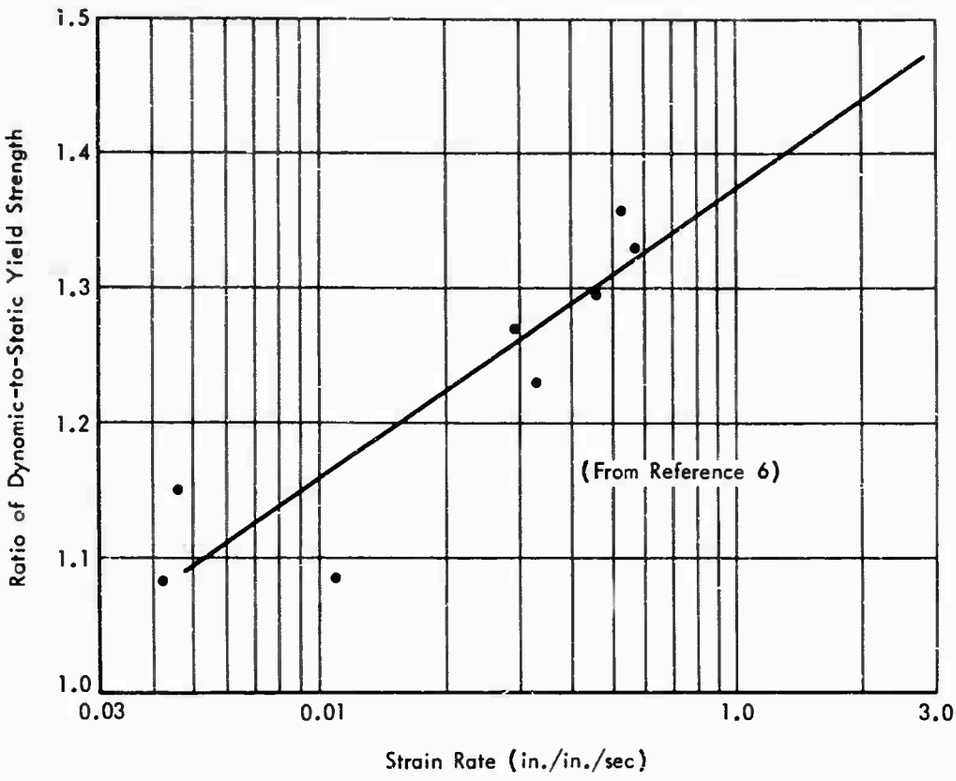

Figure 21. Effect of strain rate on yield resistance.

Post-Yield Behavior

Static Tests. The moment-curvature relationship beyond the yield stage was computed on the basis of the following assumptions:

1. The stress-strain relationship for the tension and compression reinforcement is as shown in Figure 22.

2. The concrete carries no tension.

3. The stress-strain relationship for the compressed concrete may be represented by the diagrams shown in Figure 23.

4. The confined concrete is that concrete within the shaded region shown in the cross section sketch of Figure 23.

5. The distribution of strain is linear across the depth of the beam.

The reinforcement stress-strain relationship in the strain hardening range is a modified form of the relationship presented in Reference 4. An ultimate strain equal to 0.15 inch/inch and a ratio of ultimate tensile strength to yield strength equal to 1.63 is assumed in the equation in Figure 22. These two values are averages of the tensile test data of the present study and those of References 4 and 8. In Figure 22, test data from two reinforcement bars on which strain gages were used are compared with the assumed relationship, and the correlation justifies the use of the equation.

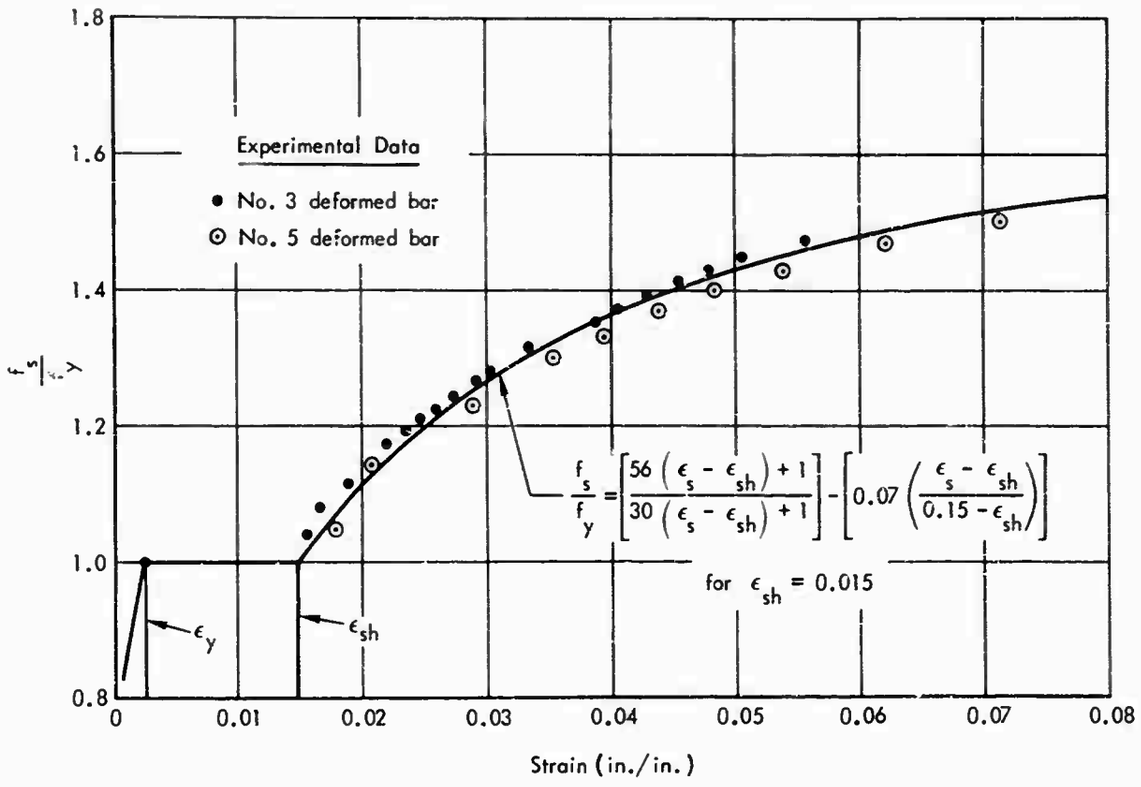

Figure 22. Tensile test data.

The stress-strain relationship for the unconfined concrete up to maximum stress is based on the data obtained previously from standard cylinder tests.[6] The limiting strain of the unconfined concrete has usually been found to be between 0.003 and 0.005 inch/inch,[4,5,6,8] and this was true in the present study. In this analysis, a value of 0.004 was assumed. Therefore, the stage at which ϵ_c reaches 0.004 inch/inch corresponds to the crushing stage which was defined earlier.

The increase in concrete ductility resulting from confinement is well known.[12,13] However, little is known about the stress-strain characteristics of concrete under various degrees of confinement, and therefore, in the present study, it was assumed on the basis of the best knowledge available. The maximum stress was assumed to be equal to that for the unconfined concrete, and the limiting strain was determined using the experimental moment-end rotation data for Beam C-7. A good fit between the experimental computed values was obtained by trial and error.

With the assumed stress-strain relationships for the concrete and the linear strain distribution assumption, the neutral axis must move downward after crushing occurs ($\epsilon_c > 0.004$ inch/inch) in order to attain equilibrium. However, test observations reveal that flexural cracks continue to expand throughout the loading sequence. Therefore, these assumptions are subject to reconsideration. They were made to provide a simple but adequate model of beam behavior. Further study should be conducted using higher maximum stresses for the confined concrete; higher stresses would relieve the necessity of the neutral axis moving down after crushing.

The values of moment and curvature were computed on an IBM 1620 computer. The quantity ϵ_c was incremented by 0.001 starting with $\epsilon_c = 0.001$. For a given value of ϵ_c, a trial compression zone depth was selected. Then, the strains in the tension and compression reinforcement were computed. Next, the forces in the reinforcement and concrete were calculated. If the internal forces were not in equilibrium, the compression zone depth was incremented up or down as required, and the forces for the new conditions were recomputed; this process was continued until the difference between the compressive and tensile forces was within the prescribed limits.

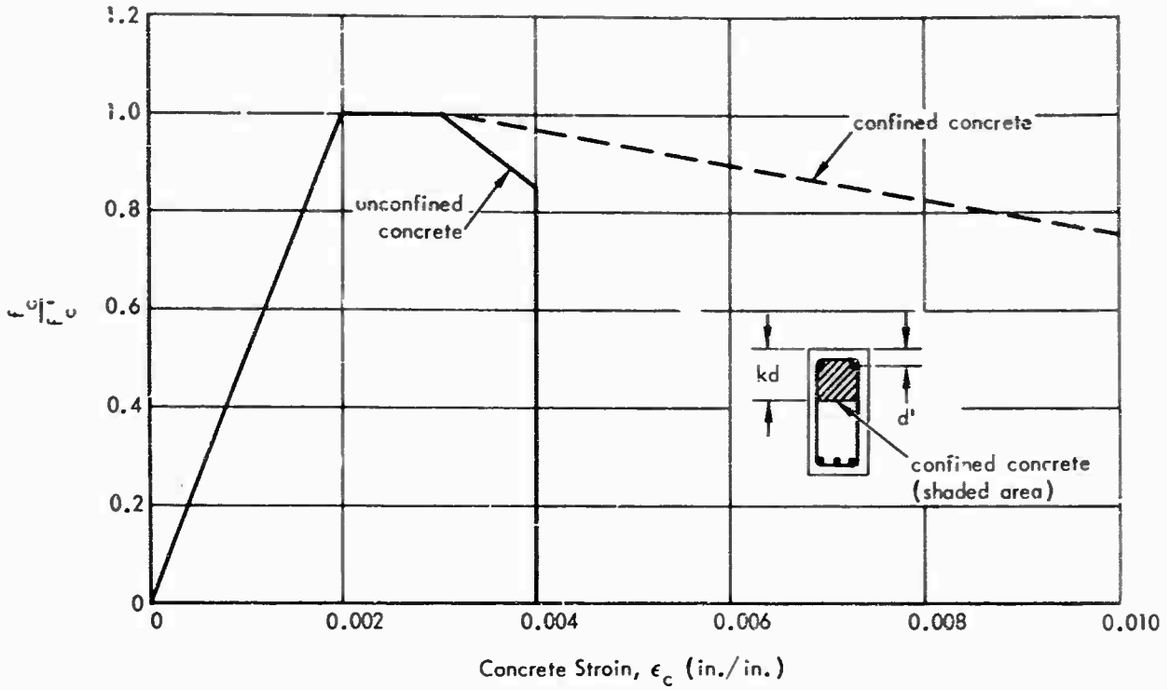

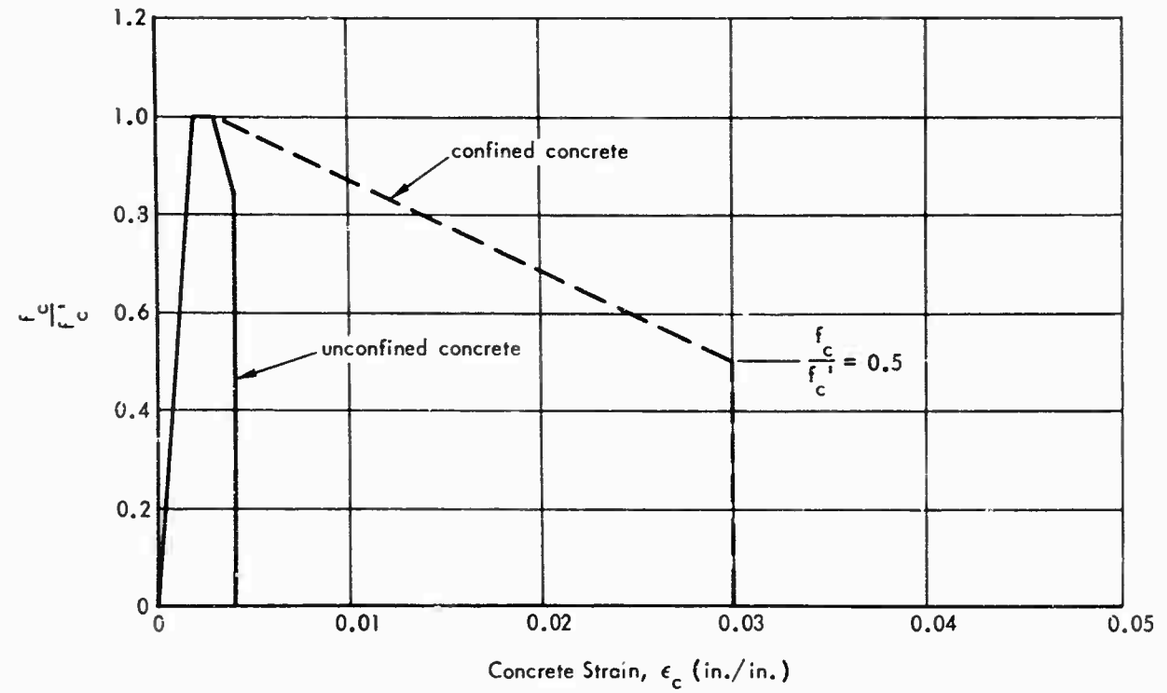

Figure 23. Stress-strain relationship for confined and unconfined concrete.

After equilibrium was obtained, the resisting moment was computed by taking moments of the compressive forces about the line of action of the tensile force. The curvature was determined by

$$\phi = \frac{\epsilon_c}{k_i d} \tag{17}$$

Then, ϵ_c was incremented and the procedure of establishing equilibrium and computing M and ϕ was repeated. The value of ϵ_c was incremented until (1) the computed moment was 10 inch-kips less than the previous maximum value, (2) the tension reinforcement strain reached 15 percent, which meant that the ultimate strength of the reinforcement had been attained, or (3) the strain at the extreme fiber of the confined concrete core reached 0.030 inch/inch (value of ultimate strain).

In some cases, just beyond the crushing stage, the moment decreased approximately 5 percent or less and then increased again, as shown in Figure 24. This decrease resulted from a reduction in the magnitude of the moment arm. As noted earlier, after crushing occurs and the compression reinforcement yields, equilibrium requires that the depth to the neutral axis be increased. This increase results in a corresponding increase in the depth to the center of gravity of the compressive force, and the magnitude of the moment arm is thereby reduced. The amount of decrease in moment was dependent on the amount of tension reinforcement and the value of d'.

In computing the end rotation and deflection of the beams, this temporary decrease in moment after crushing was neglected. A linear relationship between moment and curvature was assumed through this region, as illustrated in Figure 24. Furthermore, a linear distribution was assumed between all other points on the M-ϕ diagram. Symmetry about midspan was also assumed.

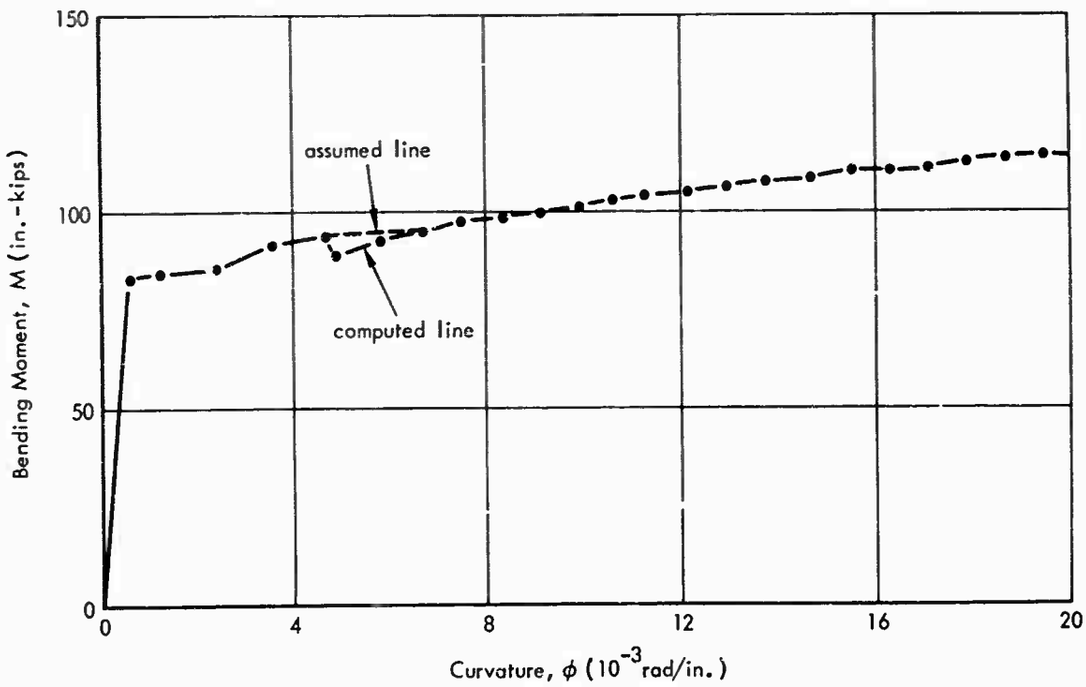

Figure 24. Moment-curvature relationship.

Referring to Figure 25, a hypothetical M-ϕ diagram is shown in (a). For a given moment diagram (c), the curvature diagram is shown in (d). A general expression for beam rotation between any two points in the region between the support and the applied load is

$$\theta_i = \left(\frac{\phi_i + \phi_{i-1}}{2}\right)\left(X_i - X_{i-1}\right) \tag{18}$$

where

$$X_i = \frac{M_i}{M_n}\left(\frac{L-a}{2}\right) \leq \frac{L-a}{2} \tag{19}$$

For example, the beam rotation between points X_2 and X_3 (denoted as θ_3) is the area under the curvature diagram between these two points,

$$\theta_3 = \left(\frac{\phi_3 + \phi_2}{2}\right)\left(X_3 - X_2\right) \tag{20}$$

where

$$X_3 = \frac{M_3}{M_n}\left(\frac{L-a}{2}\right)$$

The rotation across the uniform moment region is $\phi_n a$.

The magnitude of the end rotation is equal to one-half the area under the curvature diagram. Therefore

$$\theta_E = \phi_n \frac{a}{2} + \sum_1^n \left(\frac{\phi_i + \phi_{i-1}}{2}\right)\left(X_i - X_{i-1}\right) \tag{21}$$

and, for example, if n = 3,

$$\theta_E = \frac{1}{2}\left[\phi_3 a + \left(\phi_3 + \phi_2\right)\left(X_3 - X_2\right) + \left(\phi_2 + \phi_1\right)\left(X_2 - X_1\right) + \phi_1 X_1\right]$$

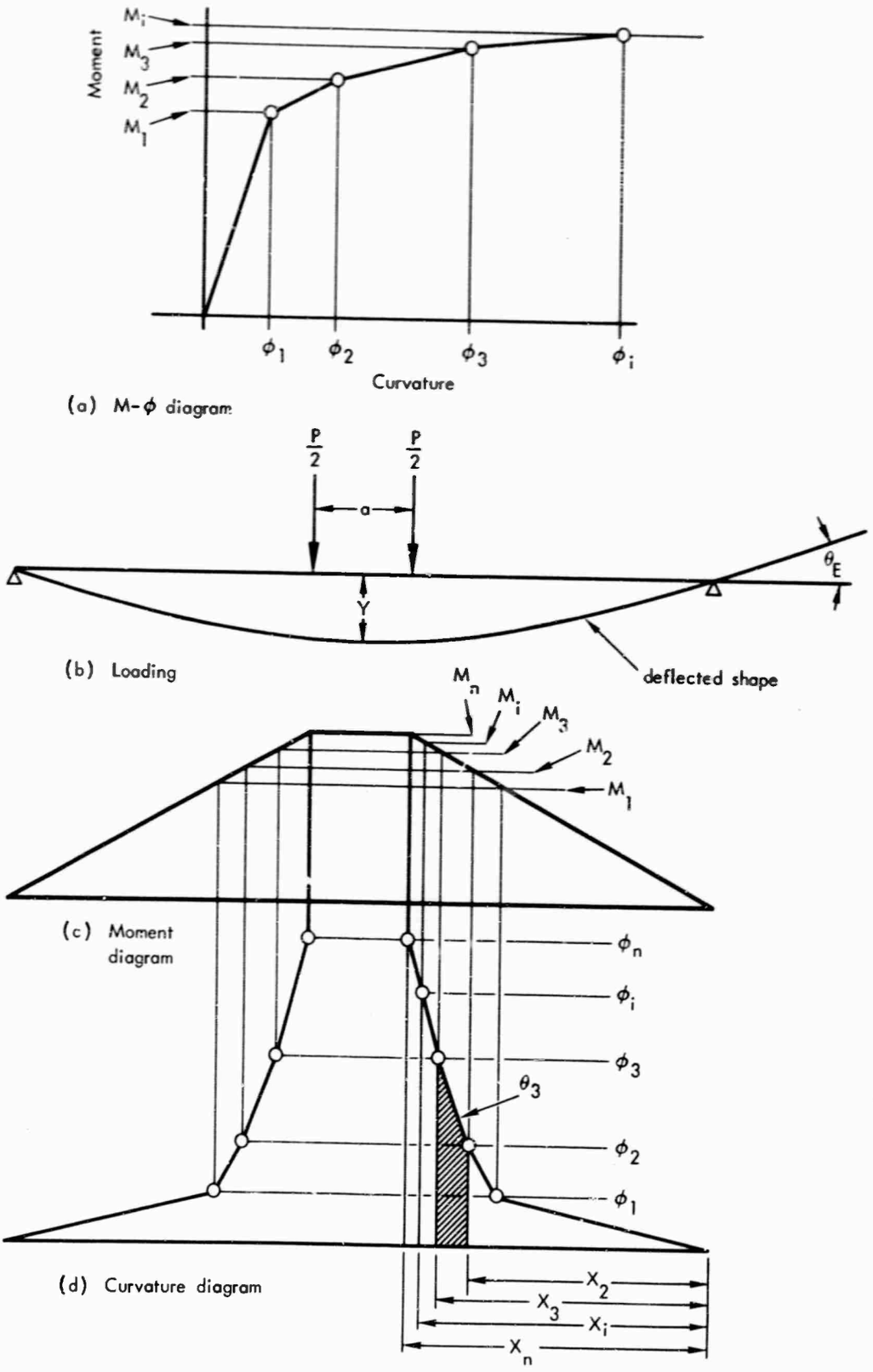

Figure 25. Curvature distribution for deflection calculations.

The midspan deflection is equal to the product of the area of the curvature diagram between midspan and either support multiplied by the distance from the support to the centroid of the area. By considering the moments of the area between each set of points, the equation for midspan deflection may be written

$$Y = \phi_n \frac{a}{2}\left(\frac{L}{2} - \frac{a}{4}\right) + \sum_{i}^{n}\left[\phi_i\left(2X_i^2 - X_iX_{i-1} - X_{i-1}^2\right)\right.$$

$$\left. + \phi_{i-1}\left(X_i^2 + X_iX_{i-1} - 2X_{i-1}^2\right)\right] \tag{22}$$

Dynamic Tests. For the centrally loaded beams, the post-yield behavior was represented by a bilinear relationship which is based on the computed static load-deflection diagram, as shown in Figure 26. Point y on the dynamic resistance diagram corresponds to the yield stage which has already been discussed. Point O is established by first computing Q_{dm} by assuming that

$$Q_{dm} = 1.1\, Q_{sm} \tag{23}$$

in those beams in which the computed stress in the tension reinforcement at maximum beam resistance approaches the ultimate strength of the reinforcement. Equation 23 is based on the results of dynamic tensile tests on intermediate grade reinforcing steels which have shown that the increase in ultimate strength is small, usually in the range of 10 percent.[14] Point O, then, is the point at which the difference between Q_{dm} and Q_s is equal to the difference between the dynamic and static yield resistance.

In one centrally loaded beam (C-14) the computed maximum static resistance was developed at a tension steel stress about 10 percent greater than f_y. In this case, the maximum dynamic resistance was assumed to be equal to

$$Q_{dm} = \frac{Q_{dy}}{Q_{sy}}\, Q_{sm} \tag{24}$$

The deflection at which Q_{dm} was reached was assumed to be the same as that at which Q_{sm} was reached.

For the beams subjected to two concentrated loads, the measured static load-deflection diagram indicated an elastoplastic resistance diagram to be a reasonable assumption. The value of Q_{dm} was assumed to be equal to Q_{dy}.

The dynamic response curves were computed by numerical integration procedures, assuming an undamped single-degree-of-freedom system and using the idealized resistance diagrams and the load data given in Appendix B. These numerical integration procedures are described elsewhere.[15]

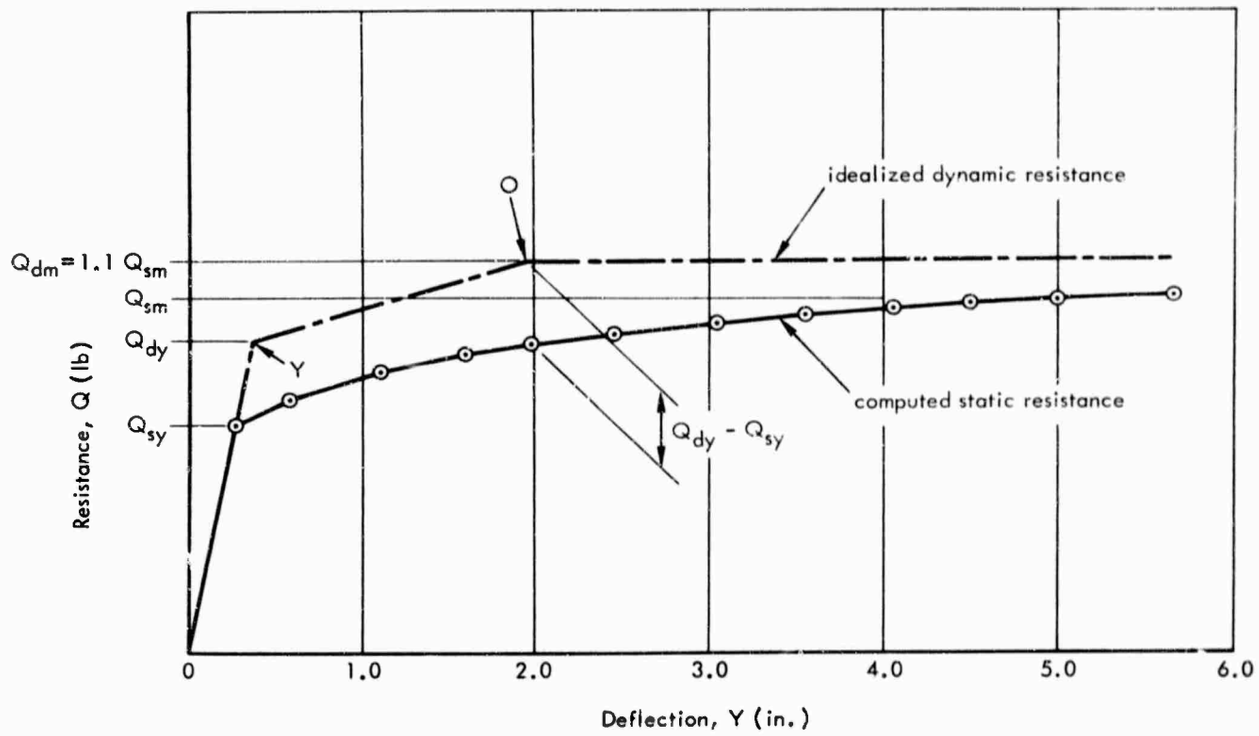

Figure 26. Dynamic resistance-deflection relationship.

COMPARISON OF EXPERIMENTAL AND COMPUTED RESULTS

Yield Stage

Static Tests. In Table 2, yield moments computed using Equation 6 are compared with the experimental yield moments (beam weight is included). Good agreement was obtained between the experimental and computed values; the ratio of experimental to computed yield moment ranged from 0.94 to 1.06 with a mean value of 1.01. Thus, the straight-line theory provides an accurate procedure for predicting the yield moment of under-reinforced beams.

The measured and theoretical yield curvatures are also compared in Table 2 and Figure 27. The yield curvatures were computed by modifying the value of yield curvature calculated using the straight-line theory. As shown in Equation 13, the correction factor is a function of q. Experimental curvatures were calculated using the tension and compression steel strain data. A good correlation between the measured and computed values was obtained. In Table 2, the ratios of experimental to theoretical curvature are between 0.94 and 1.04 with a mean of 0.98. This correlation is as good as that for the yield moments. In Figure 27, experimental data obtained from Reference 3 are presented; computed values were obtained using Equation 13. For the data from Reference 3, the correlation is not as good as that for the present data, the possible error being approximately ±15 percent.

Table 2. Experimental and Computed Yield Stage Data - Static Tests

Beam No.	Bending Moment at Yield, M_y (in.-kips)			Curvature at Yield, ϕ_y [1] (10^{-3} rad/in.)			Midspan Deflection at Yield, Y_y (in.)		
	Exp.	Comp.	Exp./Comp.	Exp.	Comp.	Exp./Comp.	Exp.	Comp.	Exp./Comp.
C-1	78.9	81.3	0.97	0.62	0.65	0.95	0.27	0.28	0.96
C-2	82.3	80.9	1.02	0.61	0.65	0.94	0.26	0.28	0.93
C-3	78.7	79.5	0.99	0.60	0.64	0.94	0.26	0.28	0.93
C-7	41.0	41.3	0.99	0.57	0.55	1.04	0.22	0.24	0.92
C-8	52.6	56.4	0.94	0.56	0.58	0.97	0.26	0.25	1.04
C-11	53.2	52.5	1.01	--	0.55	--	0.26	0.24	1.08
4-6	75.9	71.5	1.06	0.61	0.60	1.02	0.33	0.31	1.06
4-12	70.9	68.2	1.04	0.56	0.58	0.97	0.35	0.30	1.17
4-13	70.2	68.4	1.03	--	0.58	--	0.34	0.30	1.13
Average			1.01			0.98			1.02
Range			0.94 to 1.06			0.94 to 1.04			0.92 to 1.17

[1] $\phi = \frac{\epsilon_s + \epsilon_s'}{d - d'}$

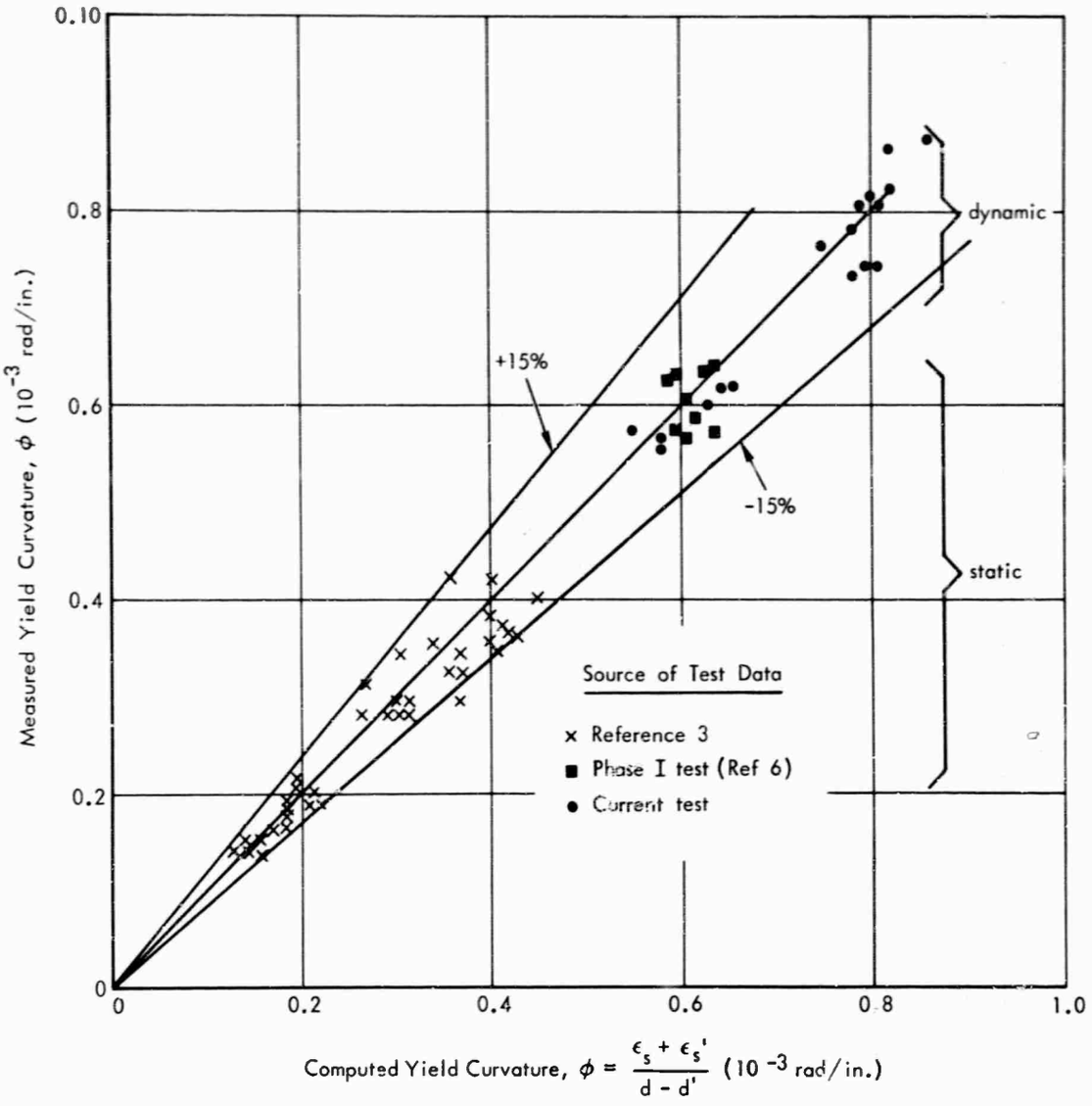

Figure 27. Comparison of measured and computed maximum curvature at yield.

Yield deflections were computed using Equation 9. The ratio of experimental to computed yield deflection varied from 0.92 to 1.17; the mean value was 1.02. In Figure 28, the correlation between measured and computed yield deflections is shown. Data from a large number of tests are presented. Although the correlation shown in Figure 28 is less than desired, it is better than that shown in Figure 20. The yield deflections in Figure 20 were computed using yield curvatures determined by the conventional straight-line theory, Equation 8.

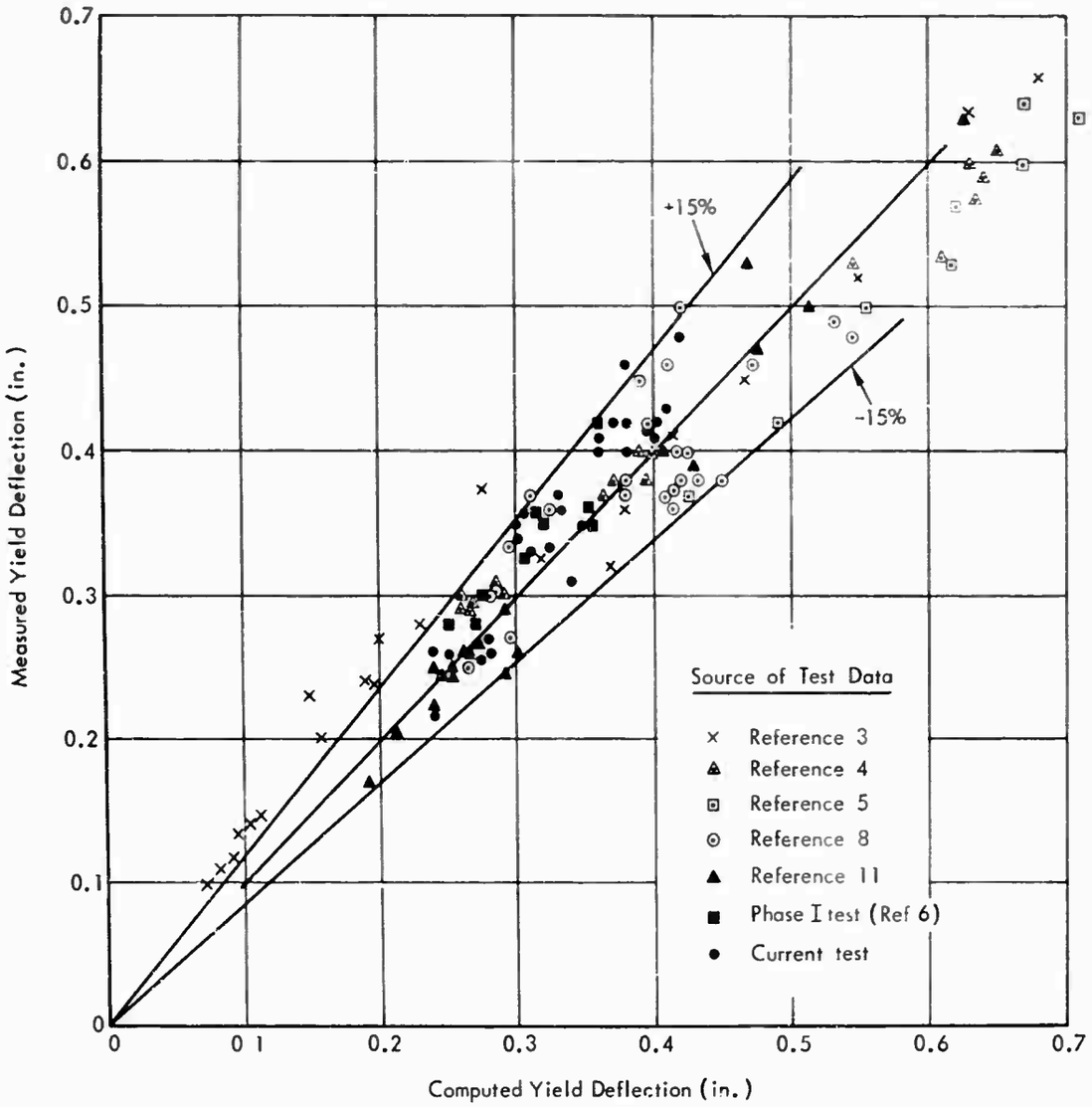

Figure 28. Comparison of measured and computed yield deflections.

Dynamic Tests. The experimental and computed curvatures and deflections are compared in Table 3. For both quantities, the range of the ratio of experimental to computed value is greater than that for the corresponding static data. This difference is to be expected, because the accuracy of the reduced data is not as great as in the static tests. Considering the degree of correlation for the static test results, the agreement between the measured and computed dynamic curvatures and deflections is very good. The data presented in Table 3 are also given in Figures 27 and 28.

The experimental and computed dynamic resistance at yield are not compared here but considered in the next section where the response of the dynamically loaded beams is presented.

Table 3. Experimental and Computed Yield Stage Data - Dynamic Tests

Beam No.	Curvature at Yield, ϕ_y [1] (10^{-3} rad/in.)			Midspan Deflection at Yield, Y_y (in.)		
	Exp.	Comp.	$\frac{\text{Exp.}}{\text{Comp.}}$	Exp.	Comp.	$\frac{\text{Exp.}}{\text{Comp.}}$
C-4	0.80	0.81	0.99	0.40	0.36	1.11
C-5	0.87	0.86	1.01	0.42	0.37	1.13
C-6	0.82	0.82	1.00	0.35	0.35	1.00
C-9	0.74	0.81	0.91	0.31	0.34	0.91
C-10	0.76	0.75	1.01	0.36	0.33	1.09
C-12	--	0.73	--	0.33	0.32	1.03
C-13	--	0.76	--	0.37	0.33	1.12
C-14	--	0.71	--	0.36	0.31	1.16
C-15	0.86	0.82	1.05	0.41	0.36	1.14
4-7	0.80	0.79	1.01	0.43	0.41	1.05
4-8	0.74	0.80	0.92	0.41	0.40	1.02
4-9	0.73	0.78	0.94	0.42	0.40	1.05
4-10	0.78	0.78	1.00	0.42	0.40	1.05
4-11	0.81	0.80	1.01	0.48	0.42	1.14
4-14	--	0.72	--	0.46	0.38	1.21
4-15	--	0.73	--	0.40	0.38	1.05
4-16	--	0.74	--	0.42	0.38	1.10
Average			0.98			1.08
Range			0.91 to 1.05			0.91 to 1.21

[1] $\phi = \frac{\epsilon_s + \epsilon_s'}{d - d'}$

Post-Yield Behavior

Static Tests. Results for the centrally loaded beams are considered first, and then the results for the beams subjected to two concentrated loads.

For the centrally loaded beams, comparisons between the experimental and computed load-deflection relationship and comparisons between the experimental and computed moment-rotation relationship are given in Figures 29 through 34. The value of moment in these figures includes the dead load moment. The experimental and computed curves coincide within reasonable limits. The deviation between the experimental and computed values of moment is greatest for Beam C-7, Figure 32.

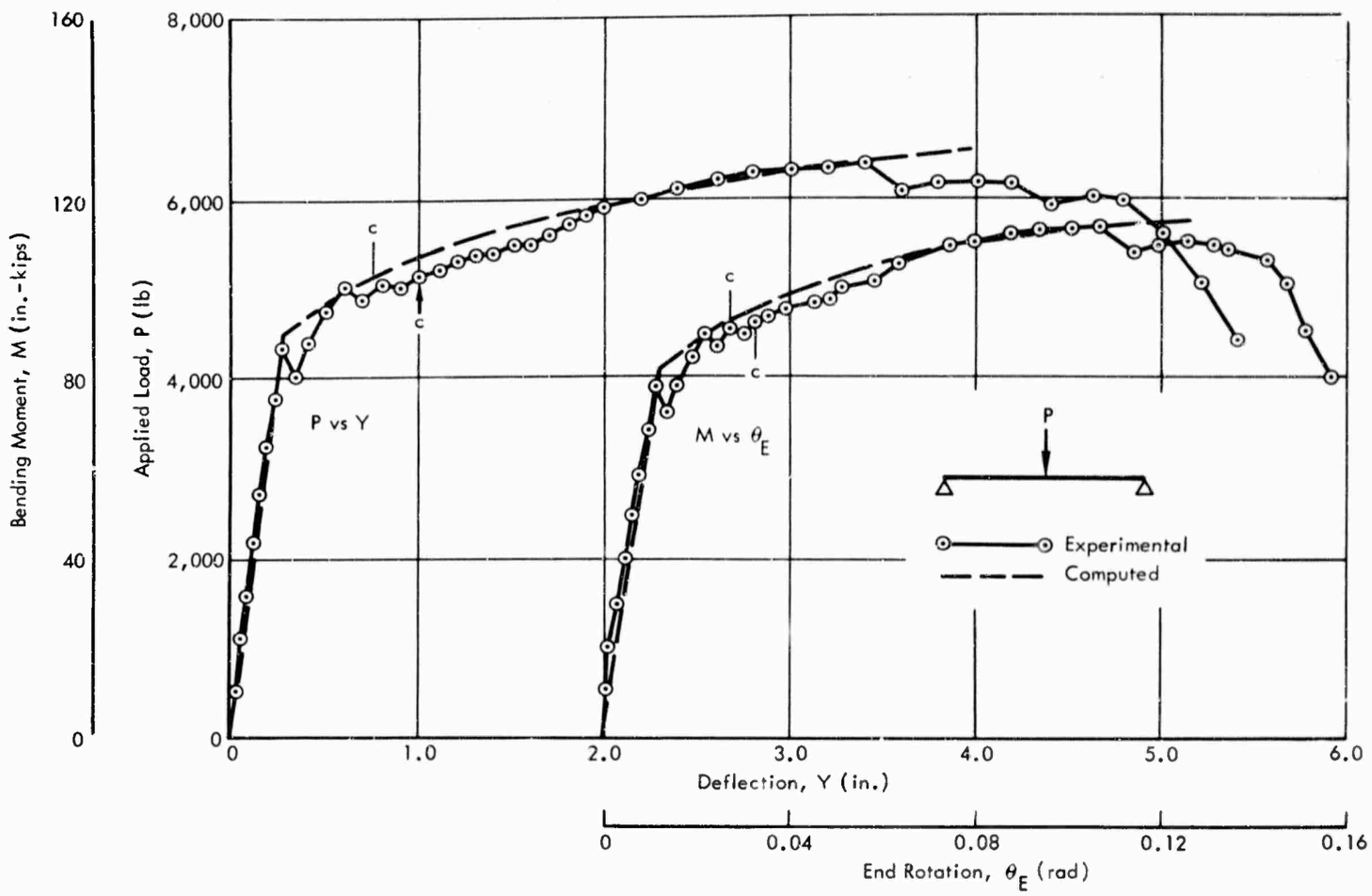

Figure 29. Experimental and computed behavior - Beam C-1.

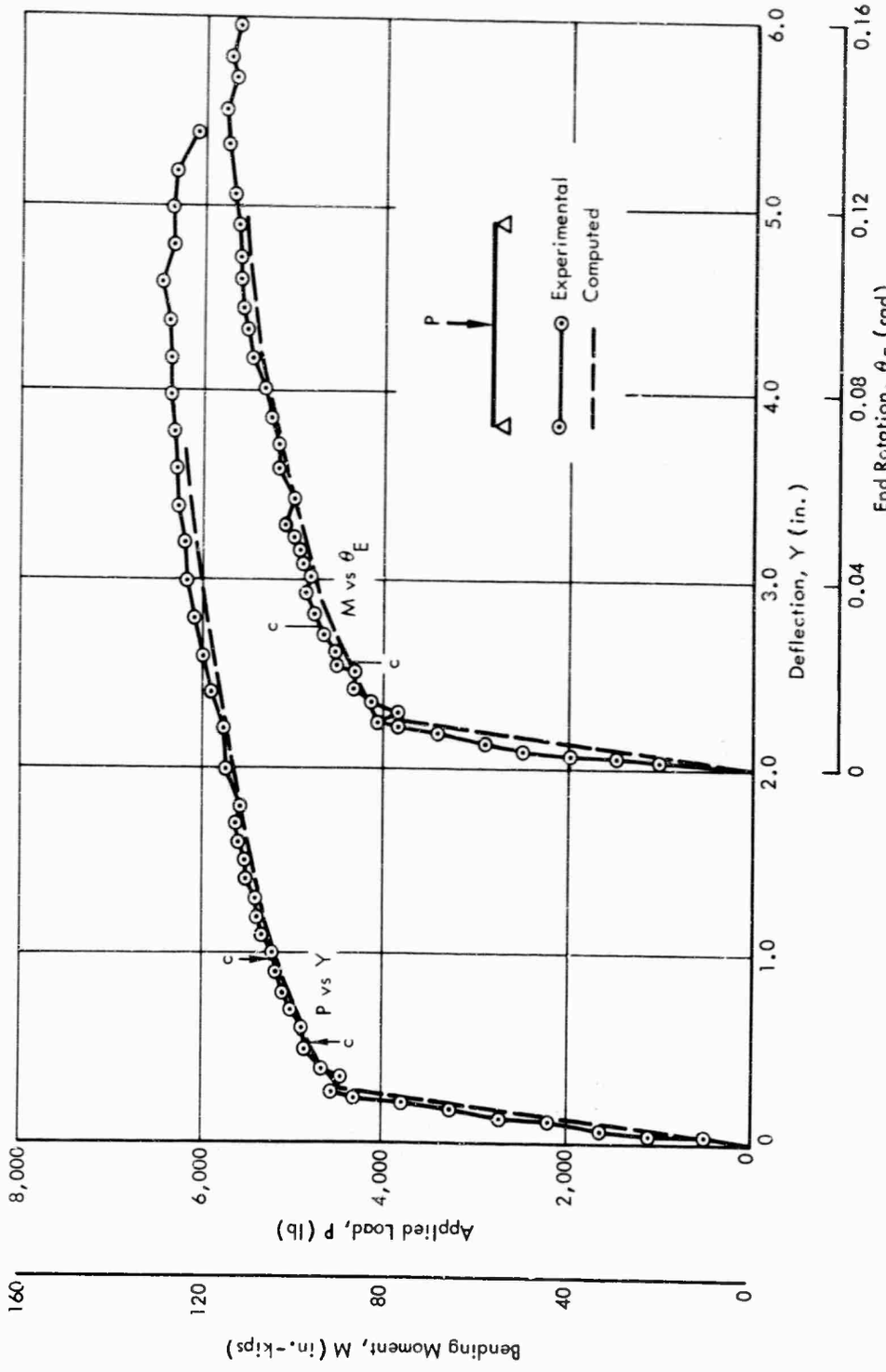

Figure 30. Experimental and computed behavior - Beam C-2.

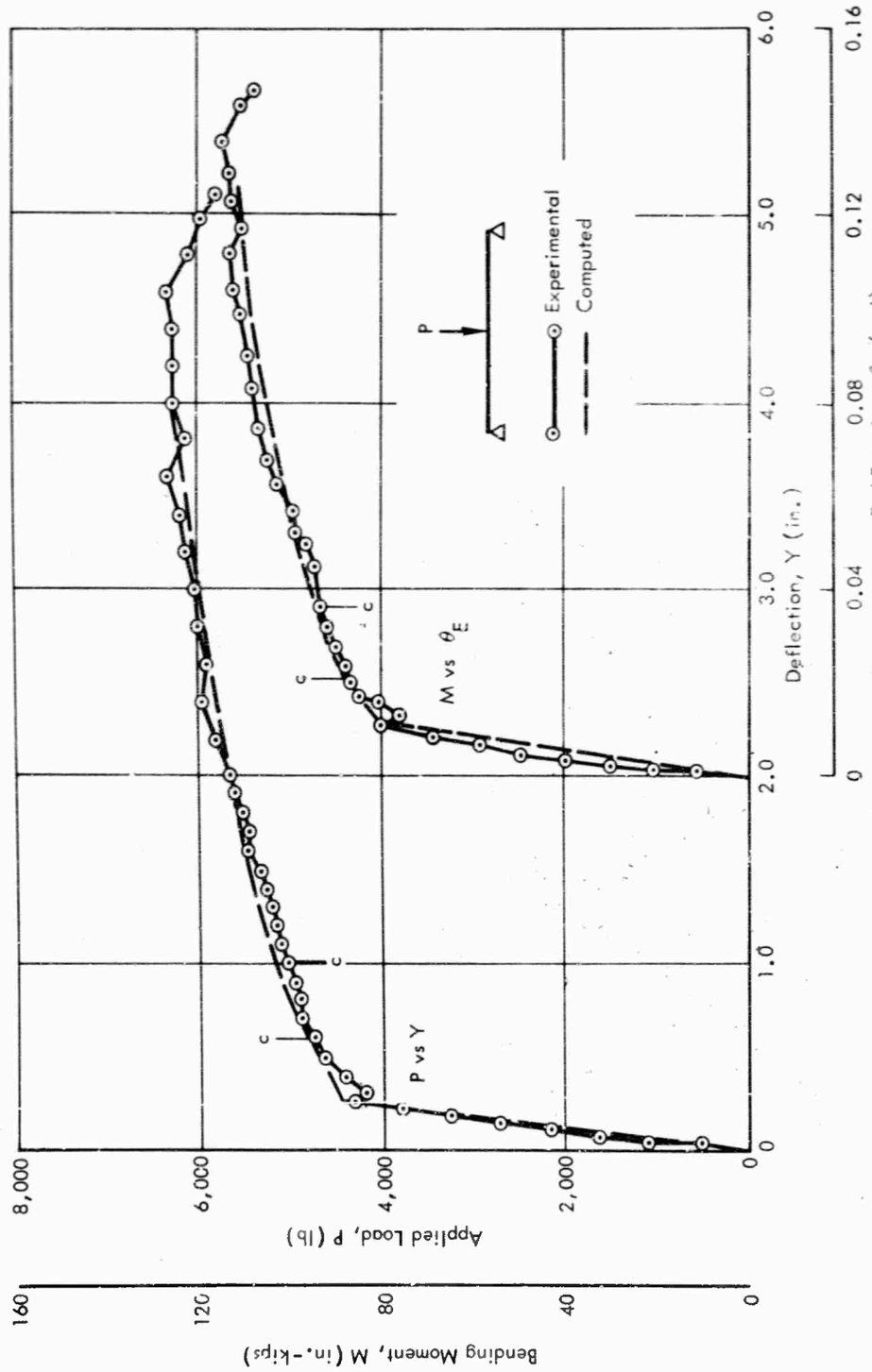

Figure 31. Experimental and computed behavior - Beam C-3.

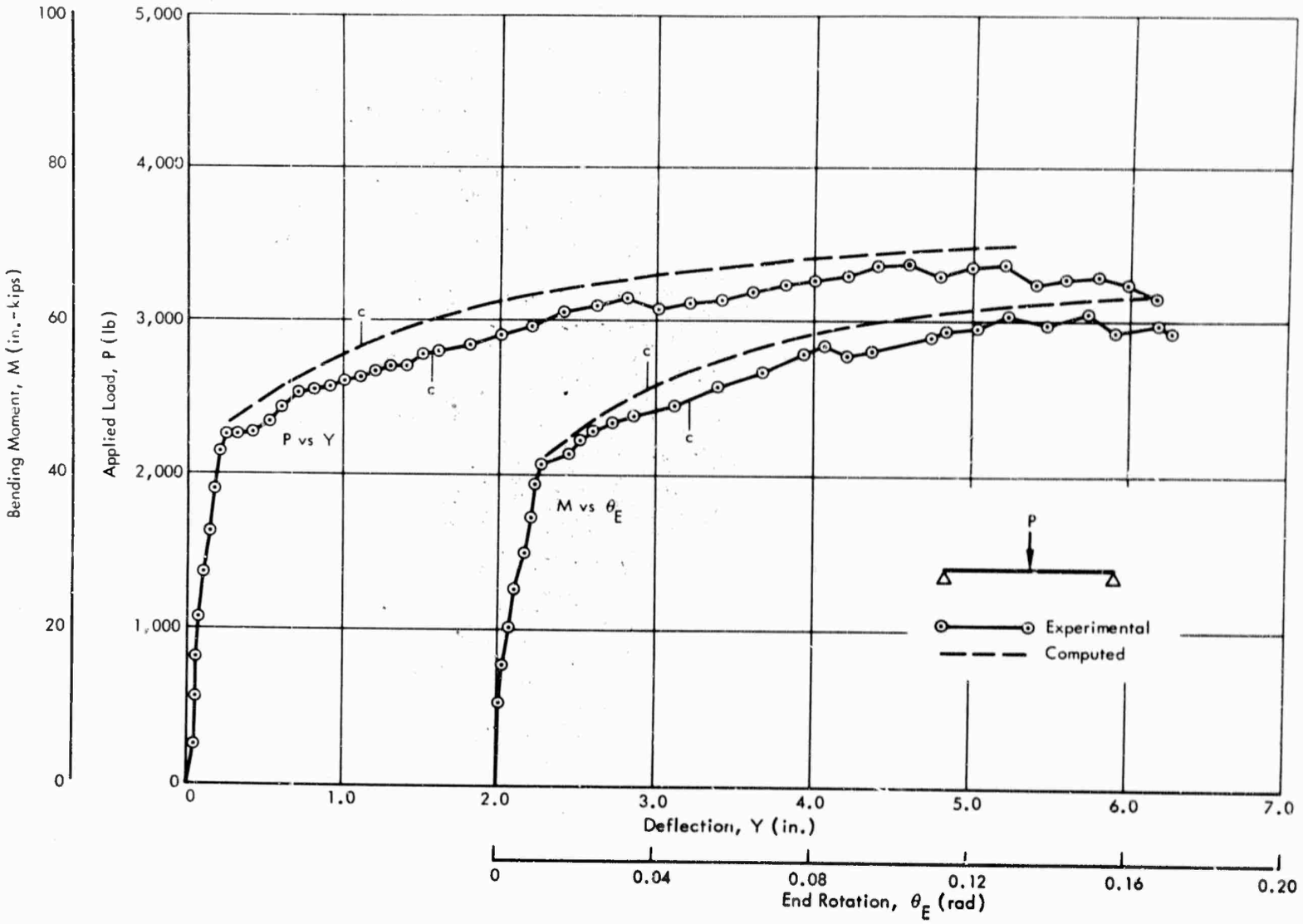

Figure 32. Experimental and computed behavior - Beam C-7.

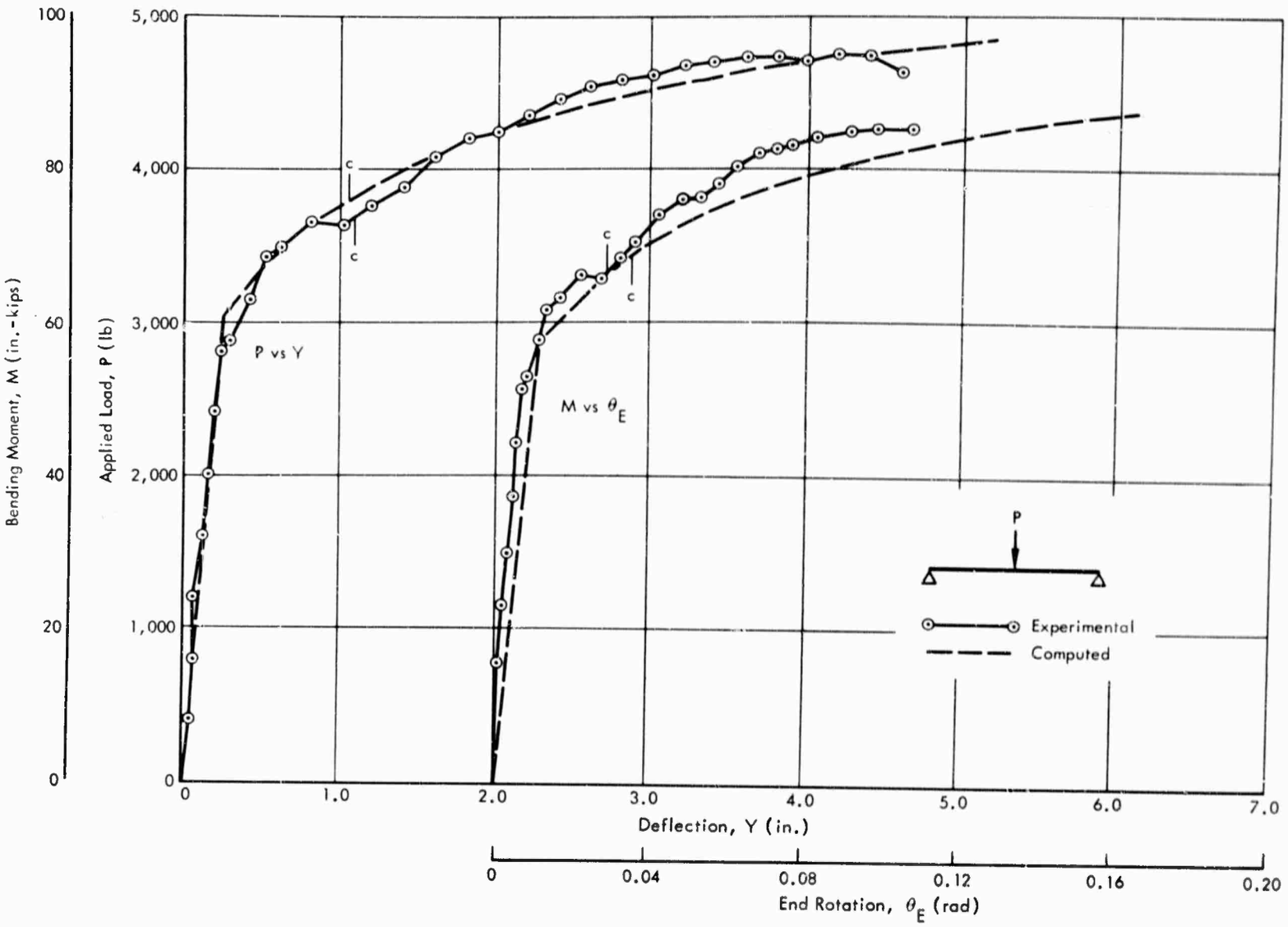

Figure 33. Experimental and computed behavior - Beam C-8.

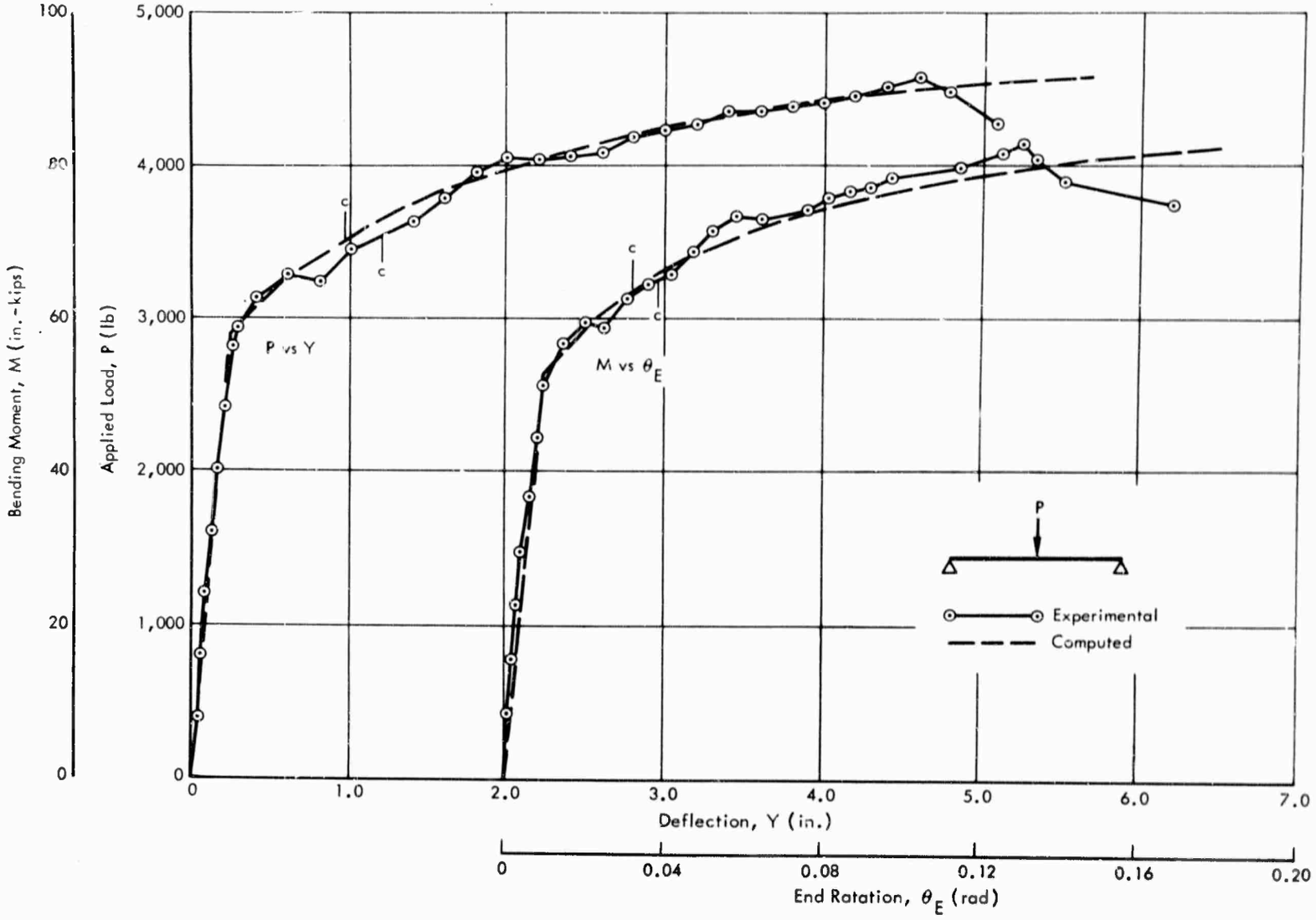

Figure 34. Experimental and computed behavior - Beam C-11.

The experimental and computed values of moment, deflection, and end rotation at the crushing stage for these beams are compared in Table 4. The ratio of experimental to computed crushing moment ranged from 0.97 to 1.07 with a mean of 1.01; this is a good correlation. For the crushing deflections, the ratio of the experimental to computed value varied from 1.03 to 1.69 with a mean of 1.37. For the end rotation at crushing, the ratio was between 0.86 and 1.56 with a mean of 1.26. Thus, the correlation for deflections and rotations is not too satisfactory. However, as noted in a previous section, the crushing stage was an arbitrary one in these tests. No indication of this stage was observed on the load-deflection diagram. Furthermore, the reserve rotation capacity beyond crushing up to maximum load, expressed as the ratio of Y_m to Y_c, ranged from 3.3 to 4.8. For these beams, an accurate prediction of the deformation at this stage is not required.

Table 4. Experimental and Computed Data at Crushing Stage - Static Tests

Beam No.	Bending Moment at Crushing, M_c (in.-kips)			Midspan Deflection at Crushing, Y_c (in.)			End Rotation at Crushing, $\frac{\theta_{E1} + \theta_{E2}}{2}$ (10^{-3} rad)		
	Exp.	Comp.	$\frac{\text{Exp.}}{\text{Comp.}}$	Exp.	Comp.	$\frac{\text{Exp.}}{\text{Comp.}}$	Exp.	Comp.	$\frac{\text{Exp.}}{\text{Comp.}}$
C-1	89.8	92.6	0.97	0.97	0.77	1.26	34.4	26.8	1.28
C-2	93.6	87.6	1.07	0.95	0.58	1.64	30.4	20.8	1.46
C-3	90.8	86.6	1.05	1.00	0.59	1.69	32.9	21.1	1.56
C-7	50.6	51.2	0.99	1.55	1.10	1.41	48.2	37.1	1.30
C-8	66.2	68.4	0.97	1.05	1.02	1.03	29.6	34.5	0.86
C-11	64.4	63.4	1.01	1.20	0.99	1.21	37.7	33.3	1.13
Average			1.01			1.37			1.26
4-6	83.7	81.2	1.03	1.90	1.51	1.26	--	53.2	--
4-12	74.4	72.3	1.03	1.63	1.50	1.09	44.6	51.7	0.86
4-13	76.5	71.9	1.06	1.80	1.23	1.46	60.1	42.9	1.40
Average			1.04			1.27			--

However, closer correlation could have been obtained by assuming that the maximum computed curvature at crushing was uniformly distributed over that region of the beam resisting a moment greater than M_y; this assumption was used previously.[6] This assumption was not used in the present study because it was not in agreement with the measured curvature distribution and, at later stages of deformation, resulted in excessively large values of deflection.

In Figure 35, the measured and computed curvature distributions are plotted for the crushing stage. As shown, the measured curvature (6-inch gage length) at midspan is greater than the computed value, but the distributions of curvature appear to be similar.

In Table 5, the experimental and computed values of moment, deflection, and end rotation at maximum load are compared. The experimental and computed moments are in good agreement; the ratio of the experimental to computed value ranged from 0.96 to 1.04 with a mean of 1.00.

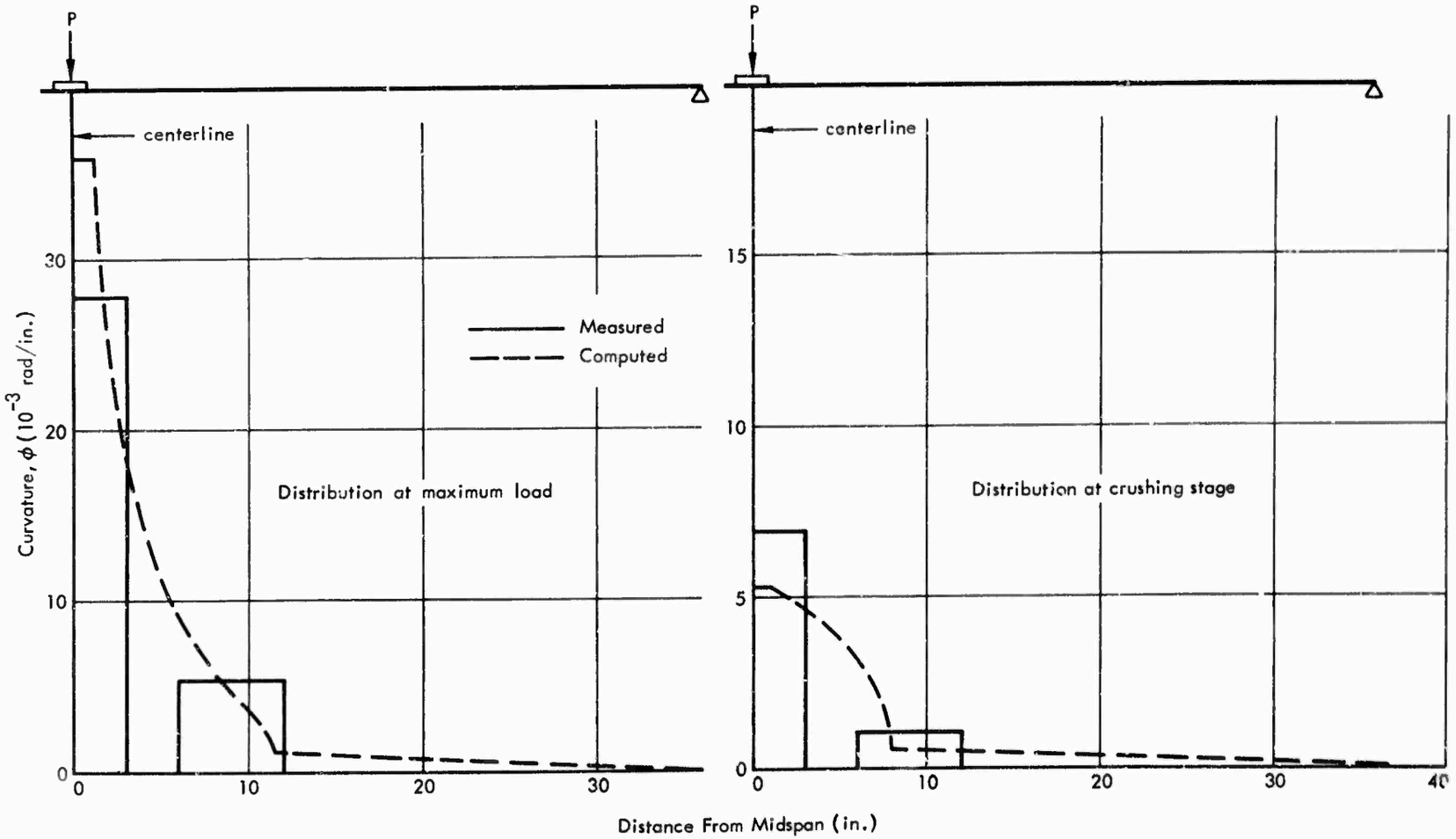

Figure 35. Measured and computed curvature distribution - Beam C-7.

Table 5. Experimental and Computed Data at Maximum - Load-Static Tests

Beam No.	Bending Moment at Max Load, M_m (in.-kips)			Midspan Deflection at Max Load, Y_m (in.)			End Rotation at Max Load, $\frac{\theta_{E1} + \theta_{E2}}{2}$ (10^{-3} rad)		
	Exp.	Comp.	$\frac{\text{Exp.}}{\text{Comp.}}$	Exp.	Comp.	$\frac{\text{Exp.}}{\text{Comp.}}$	Exp.	Comp.	$\frac{\text{Exp.}}{\text{Comp.}}$
C-1	113.4	117.0	0.97	3.40	3.95	0.86	112	126	0.89
C-2	115.3	111.0	1.04	4.60	3.70	1.24	140	118	1.19
C-3	113.2	111.3	1.02	4.60	3.95	1.16	142	126	1.13
C-7 1/	61.1	63.6	0.96	5.20	5.26	0.99	150	166	0.90
C-8	85.7	87.5	0.98	4.20	5.19	0.81	112	165	0.68
C-11 1/	82.6	82.3	1.00	4.60	5.66	0.81	136	179	0.76
Average			1.00			0.98			0.93
4-6	--	82.0	--	--	1.68	--	--	59	--
4-12	77.7	76.0	1.02	2.43	1.89	1.29	70	65	1.08
4-13	77.8	71.9	1.08	2.24	1.23	1.82	74	43	1.72

1/ The computed values correspond to the stage at which $\epsilon_s = 0.15$, the assumed ultimate strain for the reinforcement.

In the discussion of the test results, the increase in moment beyond M_y was found to be primarily the result of strain hardening of the tension reinforcement. The good agreement between the computed and experimental maximum moment, therefore, was possible because strain hardening of the tension reinforcement was taken into account using the relationship given in Figure 22.

The ratio of experimental to computed maximum deflection ranged from 0.81 to 1.24; similar results were obtained in the comparison of the experimental and computed end rotations at maximum load. This correlation is thought to be good for this advanced stage of deformation; the deflections at maximum load ranged from 12 to 25 times the yield deflection.

Because the analysis is empirical and all the beams had the same transverse reinforcement spacing, the results cannot be generalized to include other transverse reinforcement arrangements.

As shown in Figure 35, the computed curvature distribution at maximum load is in good agreement with the experimental curvature measurements obtained with the mechanical rotation gage. In addition, the computed curvature distribution is also compatible with the distribution of permanent tension reinforcement strain (Figure 12).

A further comparison between the experimental and computed results is shown by the typical data in Figures 36 and 37. The development of the computed tension reinforcement strain (Figure 36) is similar to that for the experimental case. The strain gage became defective at a high strain, but the strain continued to increase. For this example, the computed strain was approximately 7.5 percent at maximum load.

The difference between the experimental and computed compression steel strains (Figure 37) can be attributed to the strain measurements being taken at midspan directly below the load-bearing plate. The crushed section was adjacent to this plate and, therefore, the actual strains in the crushed zone probably increased more rapidly than those shown.

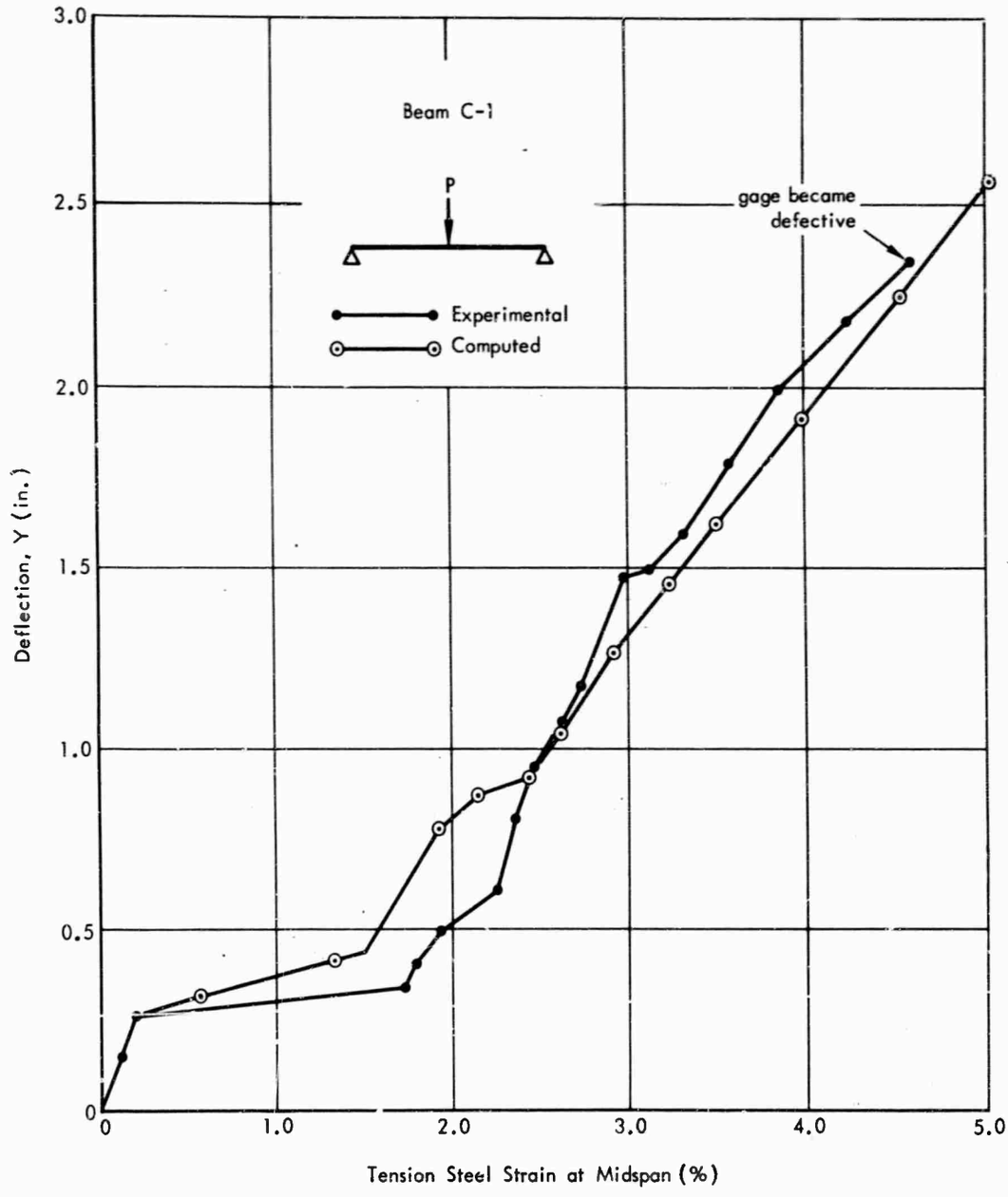

Figure 36. Measured and computed tension steel strain - Beam C-1.

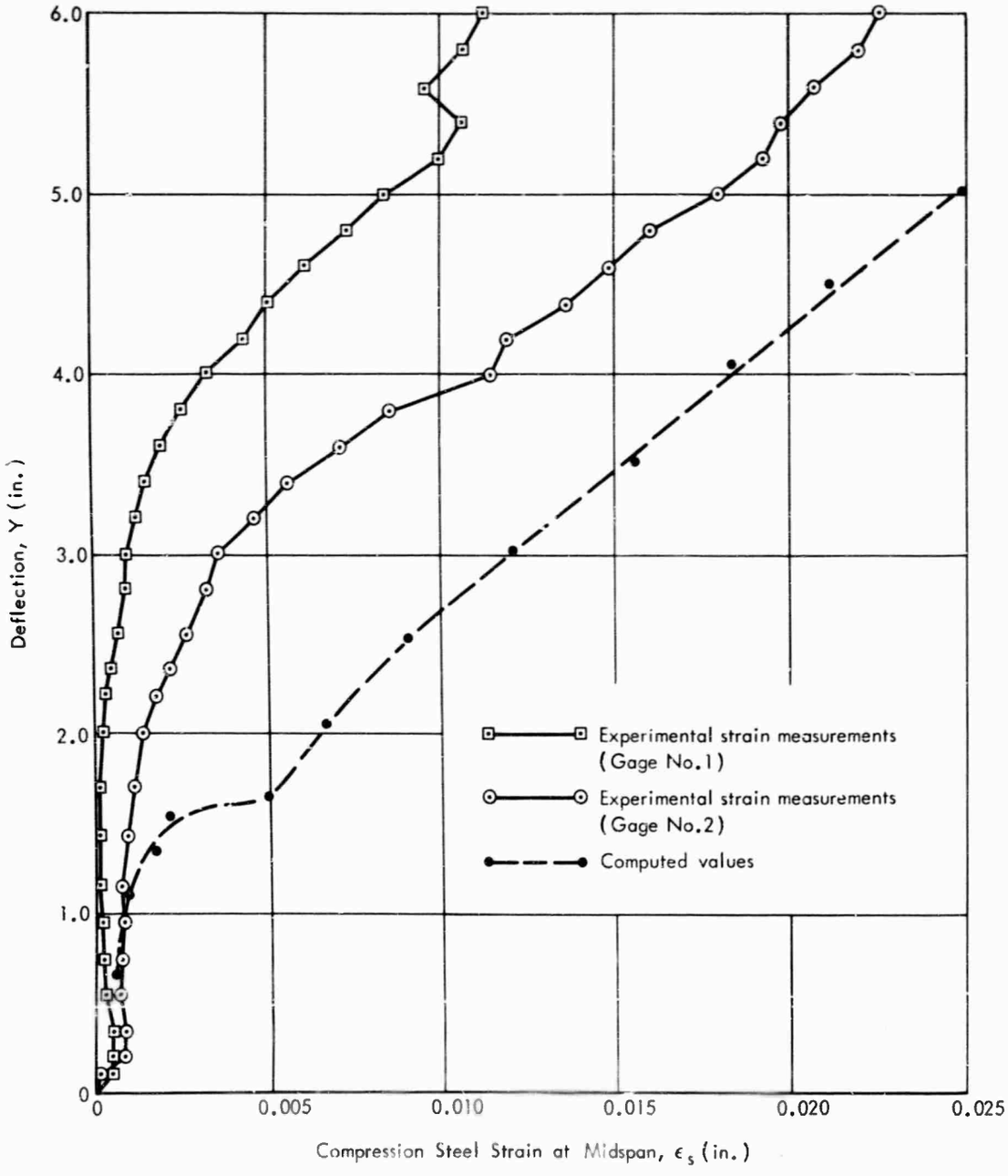

Figure 37. Comparison of measured and computed compression steel strains - Beam C-7.

For the beams subjected to two concentrated loads 18 inches apart, the experimental and computed load-deflection diagrams are presented in Figure 38 and the moment-end rotation diagrams in Figure 39. In addition, Tables 4 and 5 provide comparisons between the experimental and computed moment, deflection, and end rotation at crushing. The experimental and computed moments at the crushing stage and at maximum load are in good agreement. The correlation is as good as that between the experimental and computed yield moments.

As shown in Table 4, all the experimental and computed values of deflection and end rotation at crushing are not in satisfactory agreement. The experimental and computed moment-curvature diagrams for each of these beams are presented in Figures 40 through 42. As shown, in two cases (Figures 40 and 41), the computed curvatures at crushing are equal to or greater than the measured curvatures. Accordingly, for these two beams, the agreement between the computed and experimental crushing deflection is reasonable. For the other beam (4-13, Figure 42), the computed curvature, deflection, and rotation are less than the corresponding measured values. The computed curvature is lower than the values in the other two cases because the measured value of d', which was used in the analysis, is significantly greater than that in the other cases.

In this analysis, the significant reserve rotation capacity beyond the crushing stage was not predictable, because the amount of confined concrete was negligible. After crushing occurred in the analysis (ϵ_c = 0.004 in./in.), the computed resistance decreased. In these beams crushing localized the subsequent hinge rotation. By this localization, the reserve rotation can possibly result from an increase in strength of the compression steel due to strain hardening or the increased resistance of the concrete in the critical region. Nonetheless, the present analysis does provide reasonable estimates of maximum moment and conservative estimates of the maximum deflection and hinge rotation.

Dynamic Tests. The test results revealed that hinge geometry is not significantly affected by the type of load, i.e., static or dynamic. Furthermore, previous studies have shown that the maximum deformation capacity of under-reinforced beams is not detrimentally affected by dynamic loadings.[6,7] Therefore, once the static behavior is established, the problem is to determine the dynamic resistance. The dynamic resistance was determined using the computed static load-deflection diagram and taking into account the effect of strain rate on the yield strength of the reinforcement. This procedure is discussed in the section titled Analysis. For the beams subjected to two concentrated loads, an elastoplastic resistance was assumed.

The resistance-deflection diagrams are shown in Figures 43 through 55; the computed static and dynamic curves, and the experimental dynamic resistance curves are presented. Equation 1 was used to calculate the experimental dynamic resistance values. In some cases, the beams were loaded statically following the dynamic test or tests; these experimental data also are shown in Figures 43 through 45 and 52 through 54.

In general, the correlation between the experimental and computed dynamic resistance is good. For the centrally loaded beams, the experimental dynamic resistance equals or exceeds the computed value. In addition, the experimental static data in Figures 43 through 45 are in close agreement with the computed data. For the beams subjected to two concentrated loads, the agreement between the maximum experimental and computed dynamic resistance is within 5 percent.

To further investigate the accuracy of the computed dynamic resistance, the response of the beams to the experimental load data was calculated using the computed dynamic resistance diagram as discussed in the section titled Analysis. The experimental and computed beam responses are compared in Table 6 and Figures 56 through 60. With few significant exceptions, the computed maximum response was greater than the experimental value. Thus, the estimates of dynamic resistance were conservative estimates.

For the centrally loaded beams, the ratio of experimental to computed maximum response ranged from 0.64 to 1.14 with a mean of 0.85, and for the beams subjected to two concentrated loads, the ratio varied between 0.58 and 1.59 with a mean of 1.02. The agreement is very good considering that small changes in resistance can have an appreciable effect on the maximum response; for example, a 10 percent change in the maximum resistance could result in a 40 to 50 percent change in the maximum deflection.

The close correlation between the experimental and computed response for the centrally loaded beams was achieved because the effect of strain hardening in the tension reinforcement was considered, as well as the effect of strain rate.

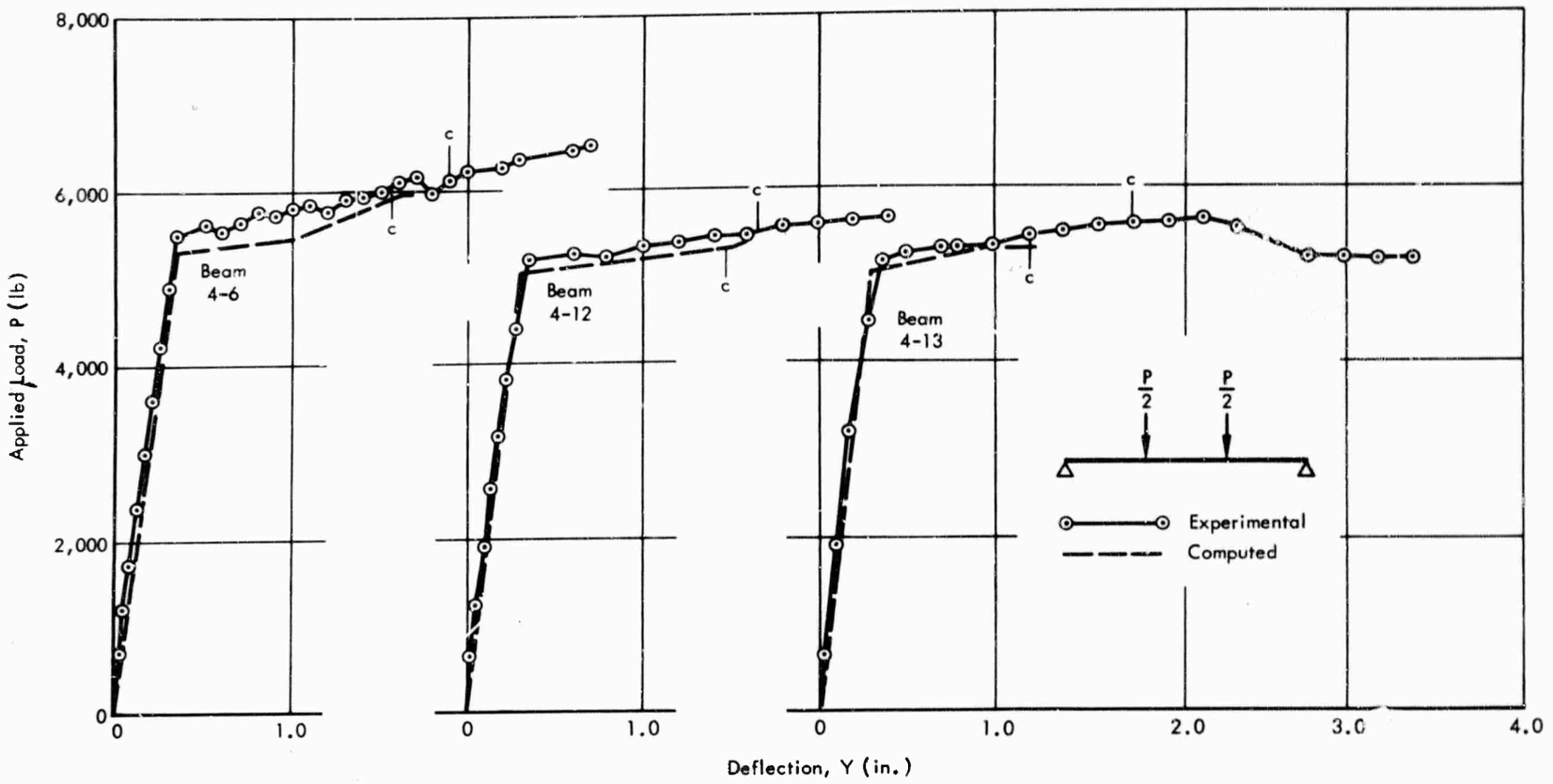

Figure 38. Experimental and computed P-Y relationship.

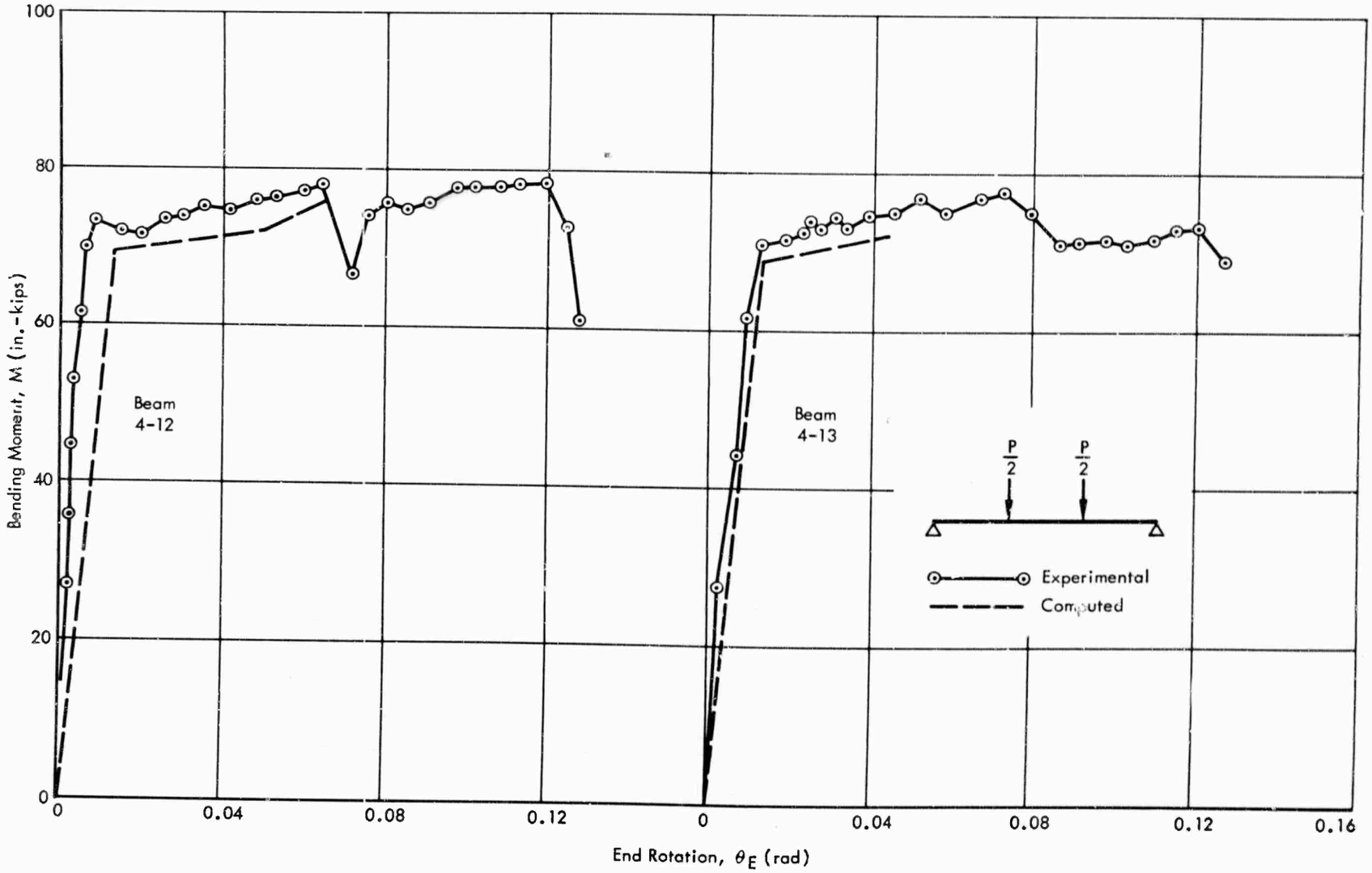

Figure 39. Experimental and computed M versus θ_E relationship.

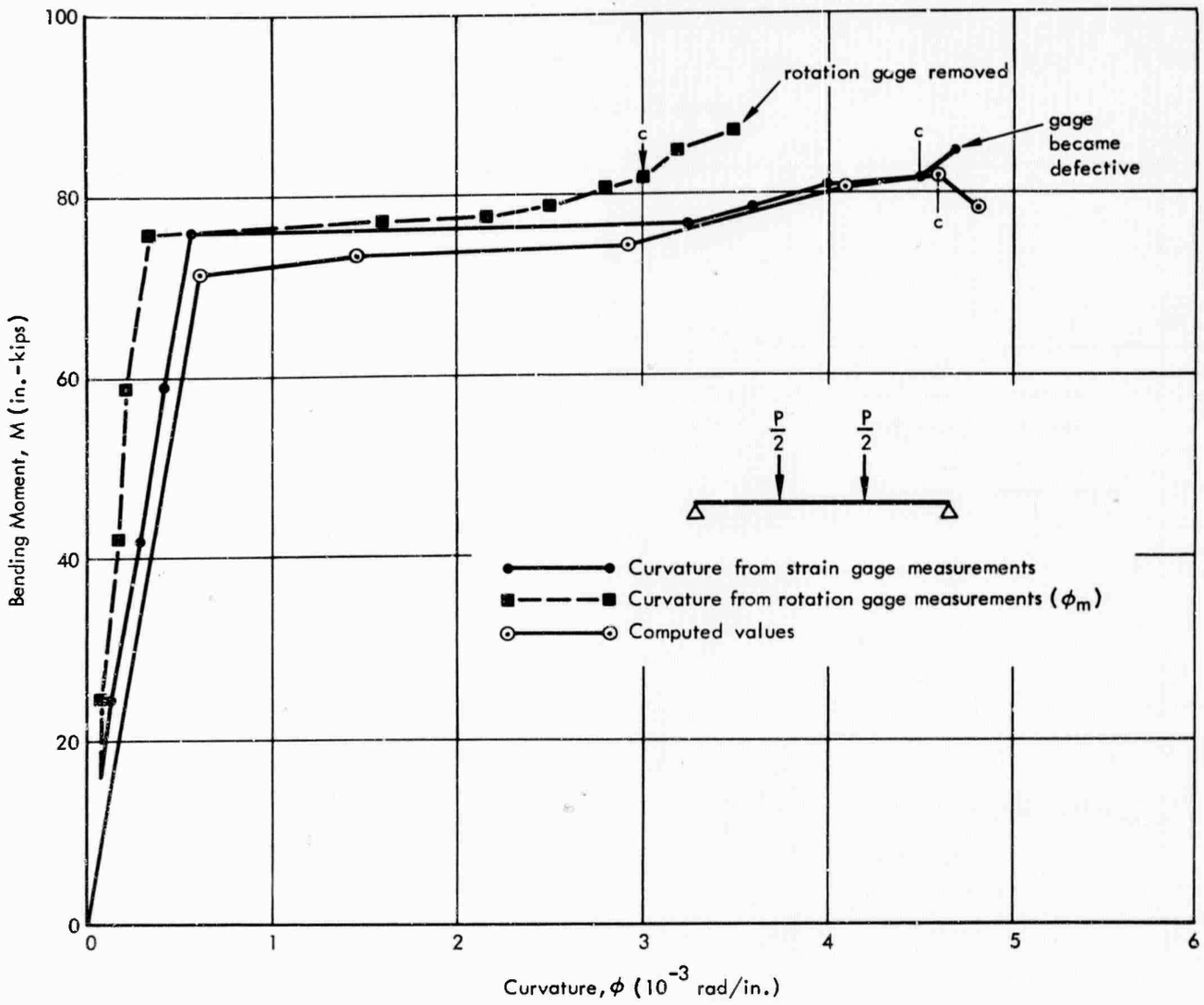

Figure 40. Experimental and computed M-ϕ relationship - Beam 4-6.

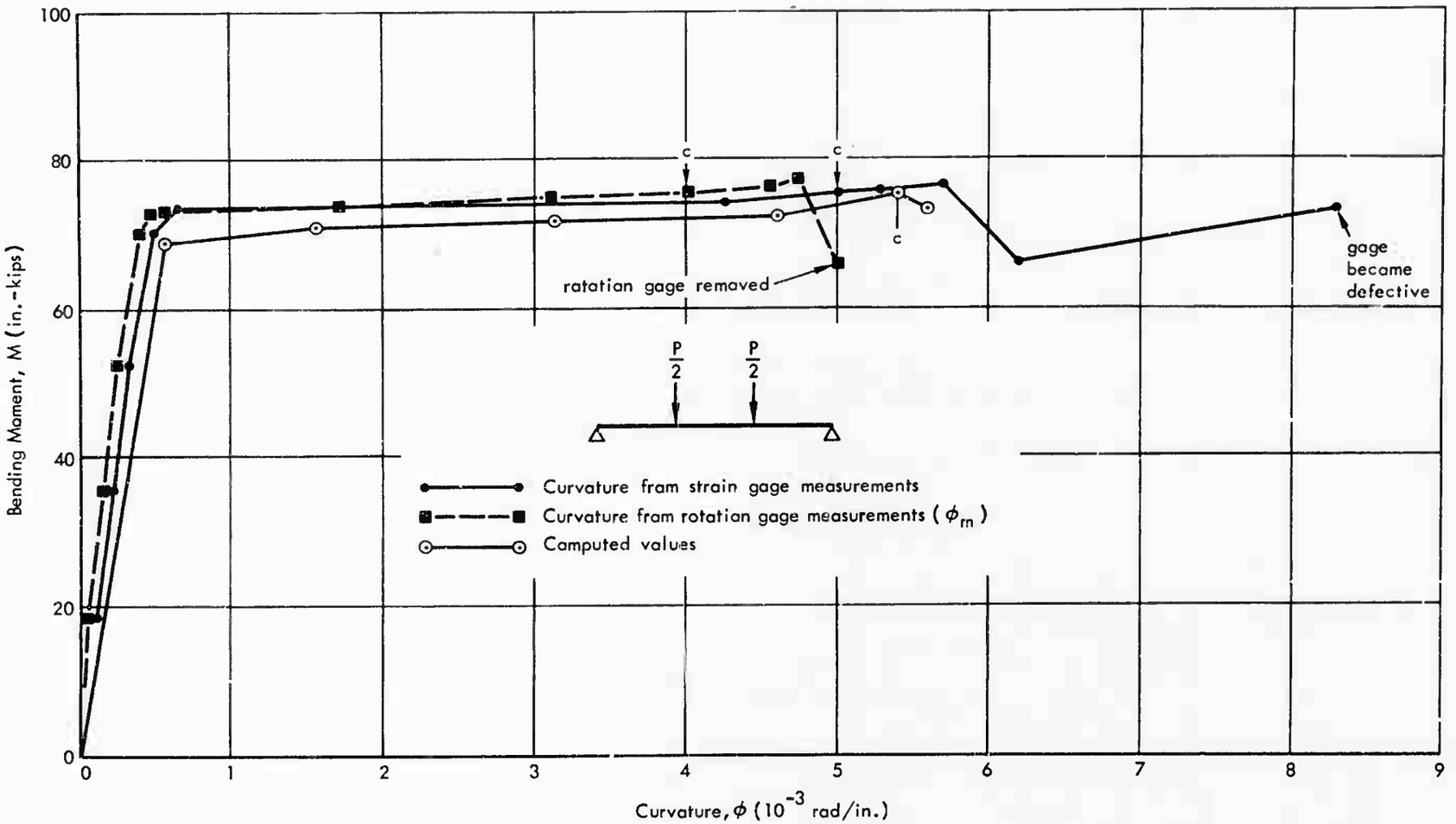

Figure 41. Experimental and computed M-ϕ relationship - Beam 4-12.

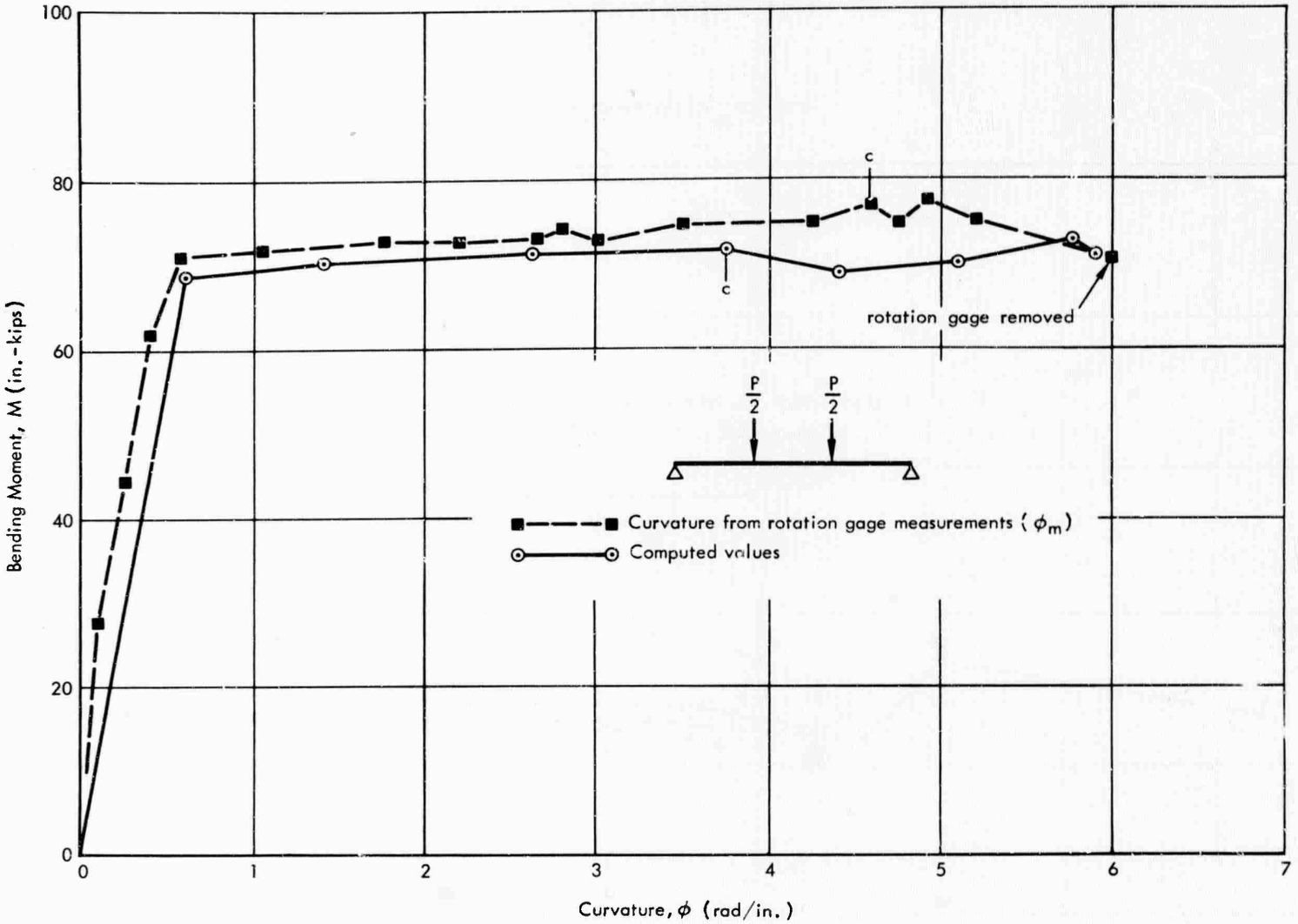

Figure 42. Experimental and computed M-ϕ relationship - Beam 4-13.

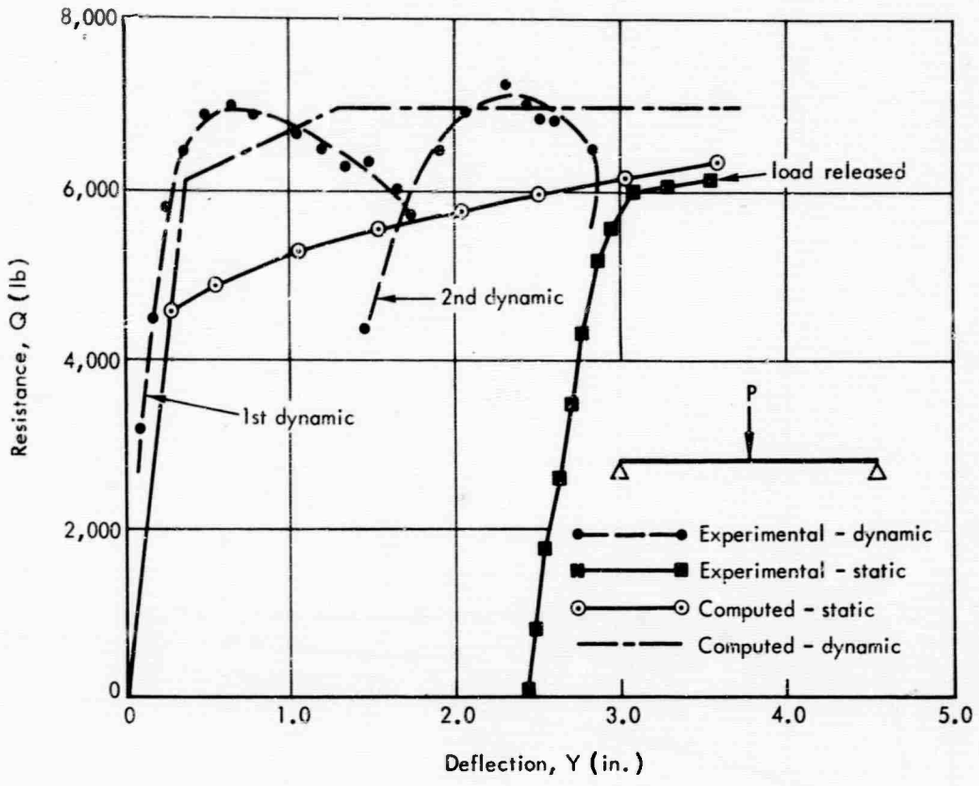

Figure 43. Resistance versus deflection - Beam C-4.

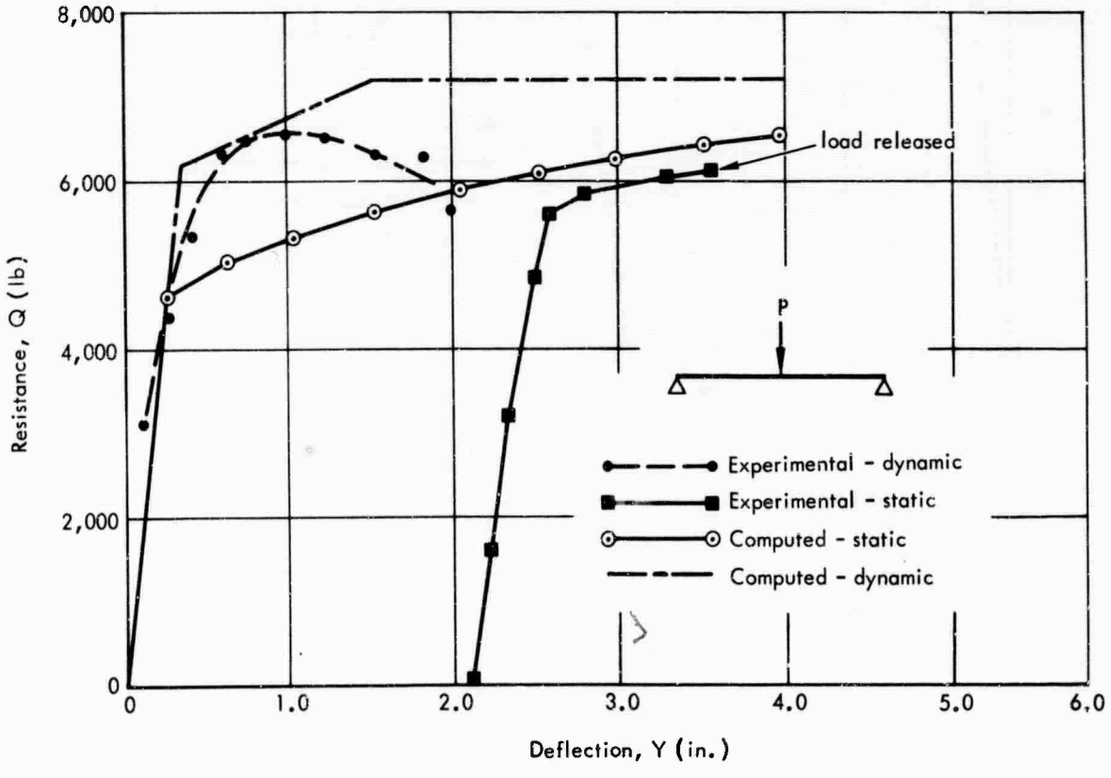

Figure 44. Resistance versus deflection - Beam C-5.

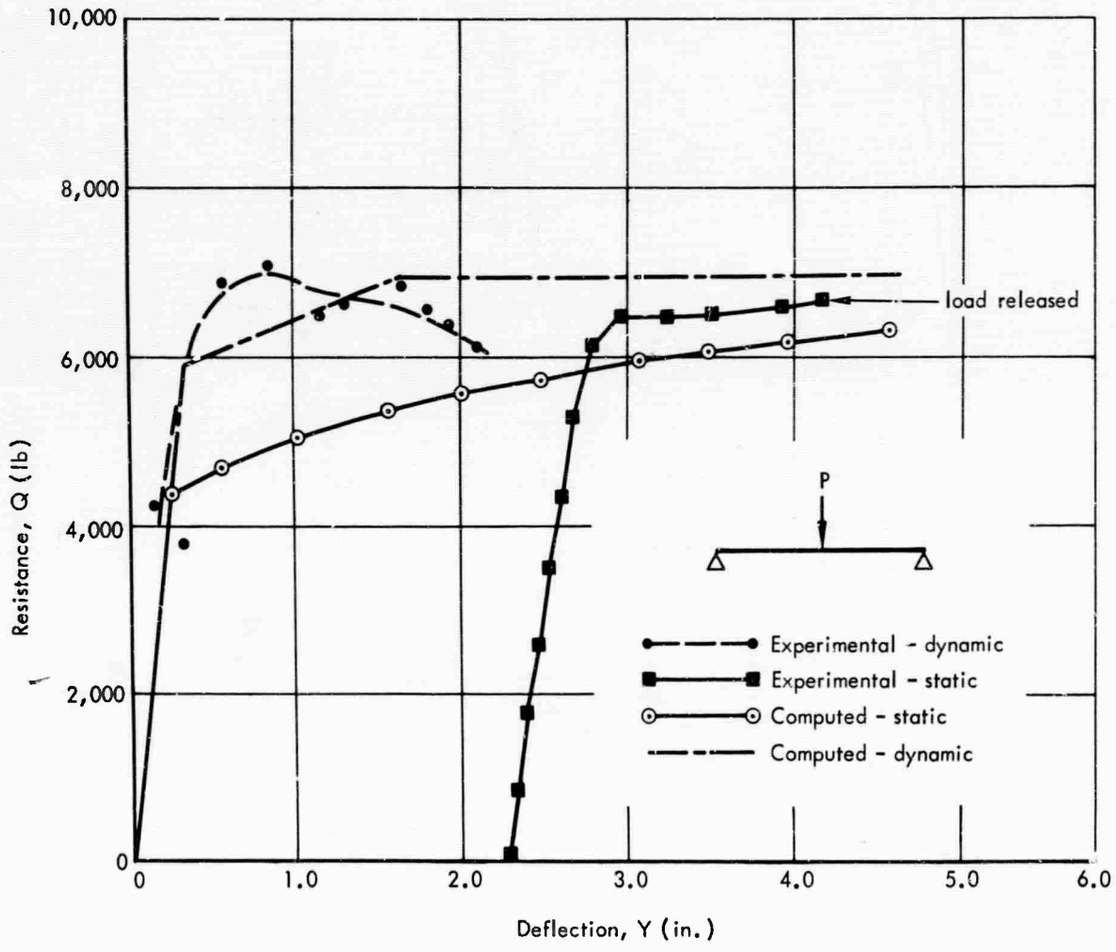

Figure 45. Resistance versus deflection - Beam C-6.

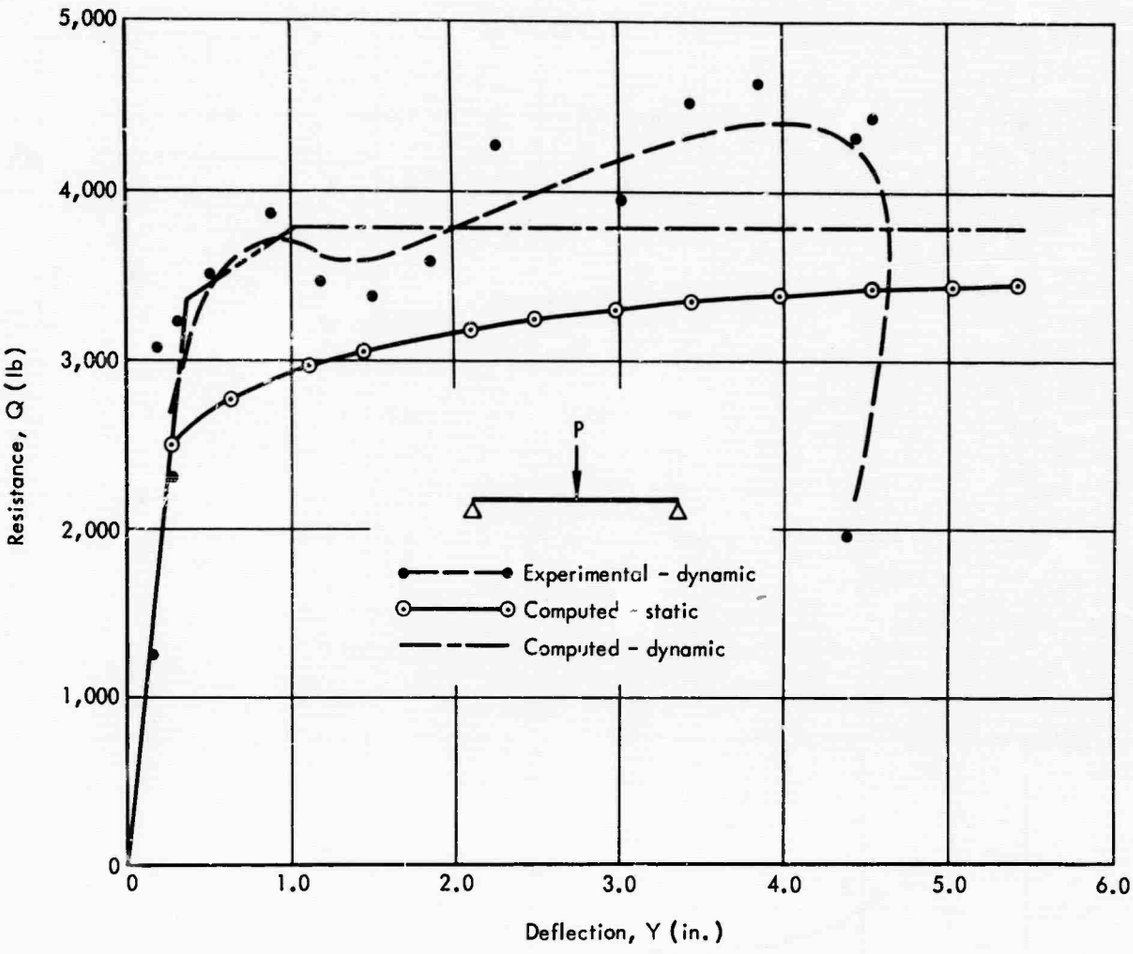

Figure 46. Resistance versus deflection - Beam C-9.

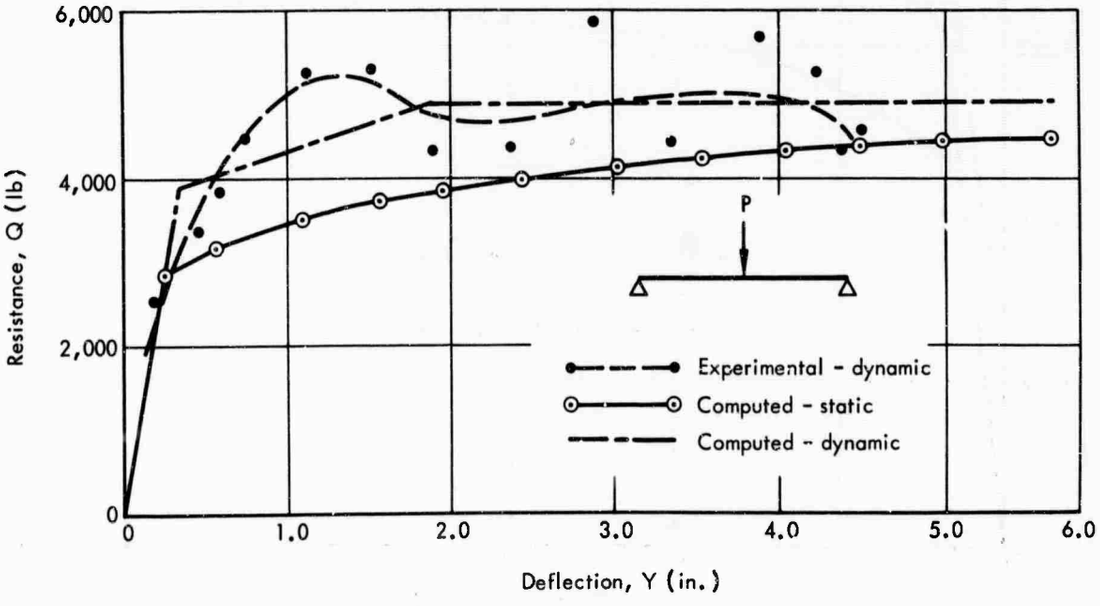

Figure 47. Resistance versus deflection - Beam C-10.

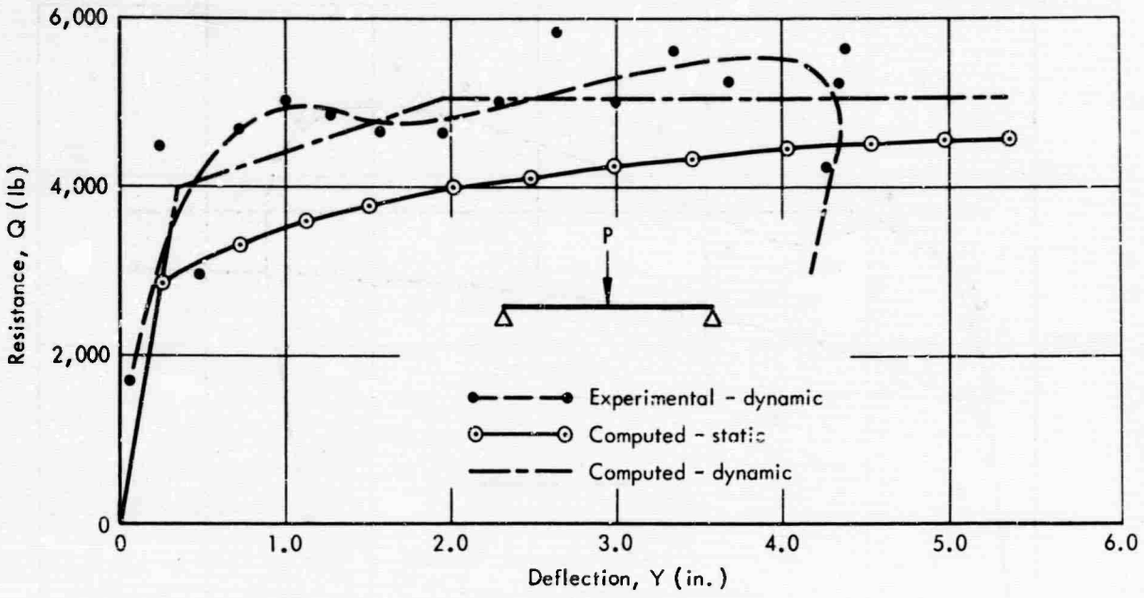

Figure 48. Resistance versus deflection - Beam C-12.

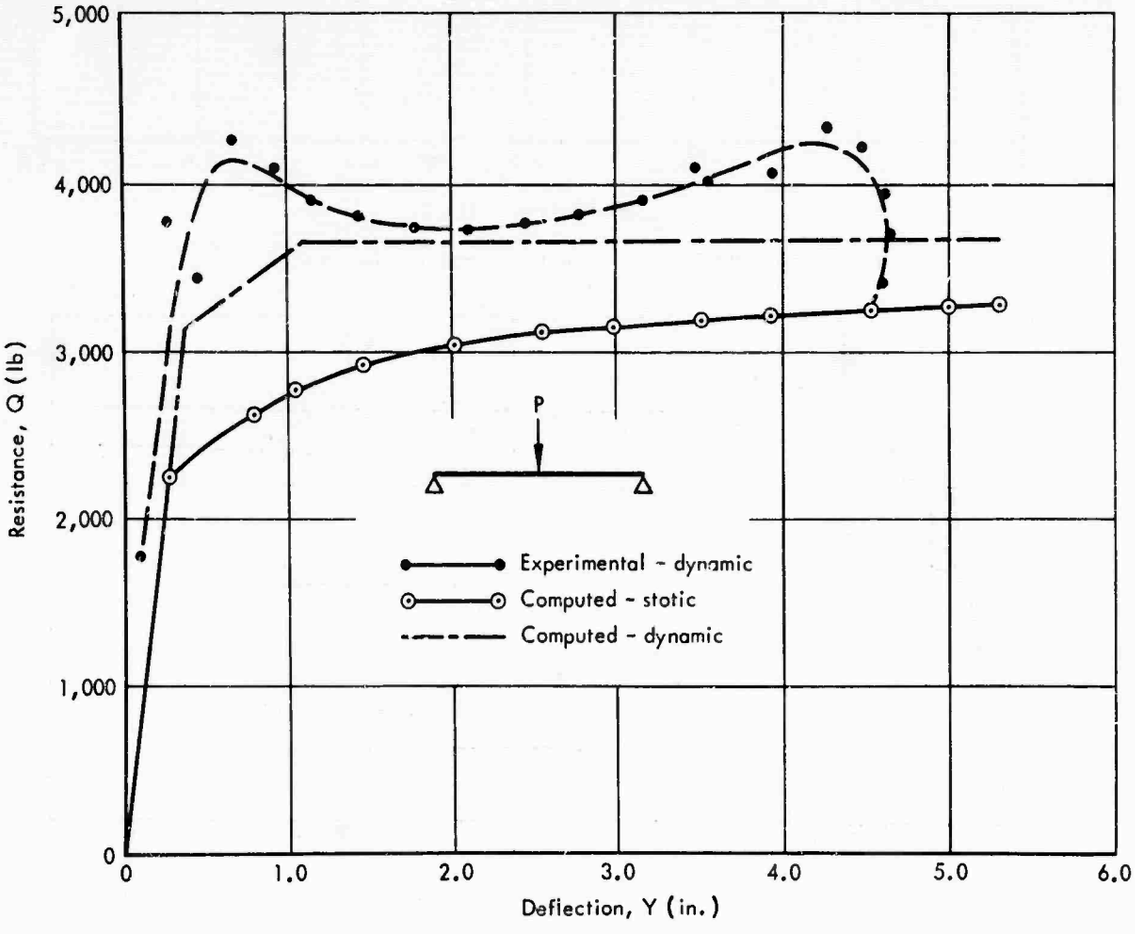

Figure 49. Resistance versus deflection - Beam C-13.

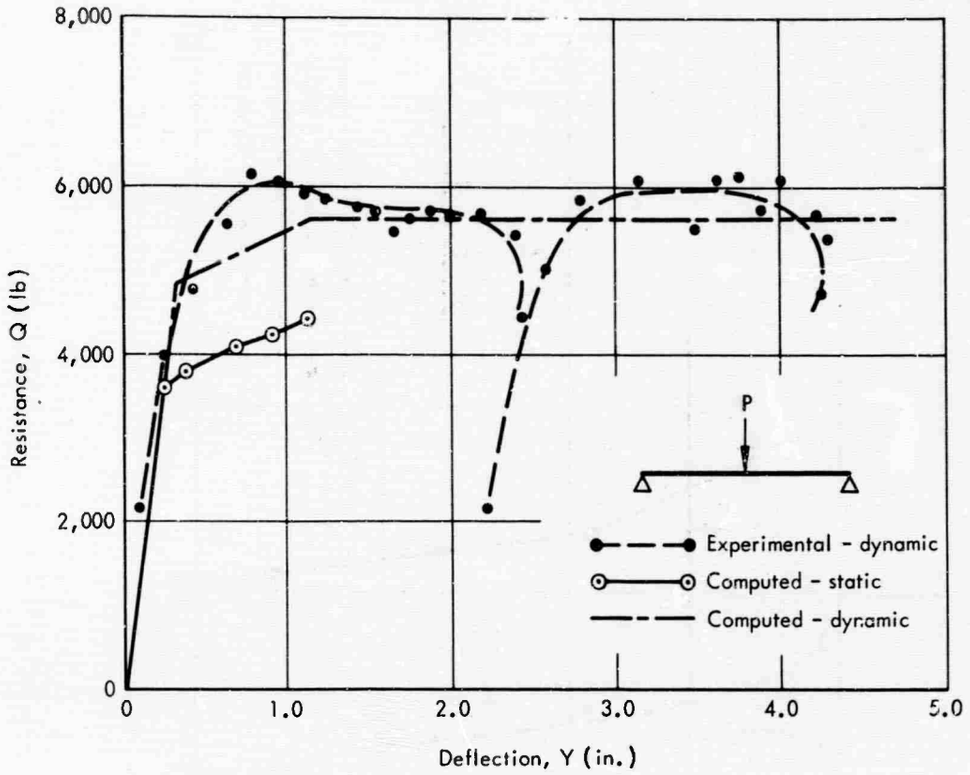

Figure 50. Resistance versus deflection - Beam C-14.

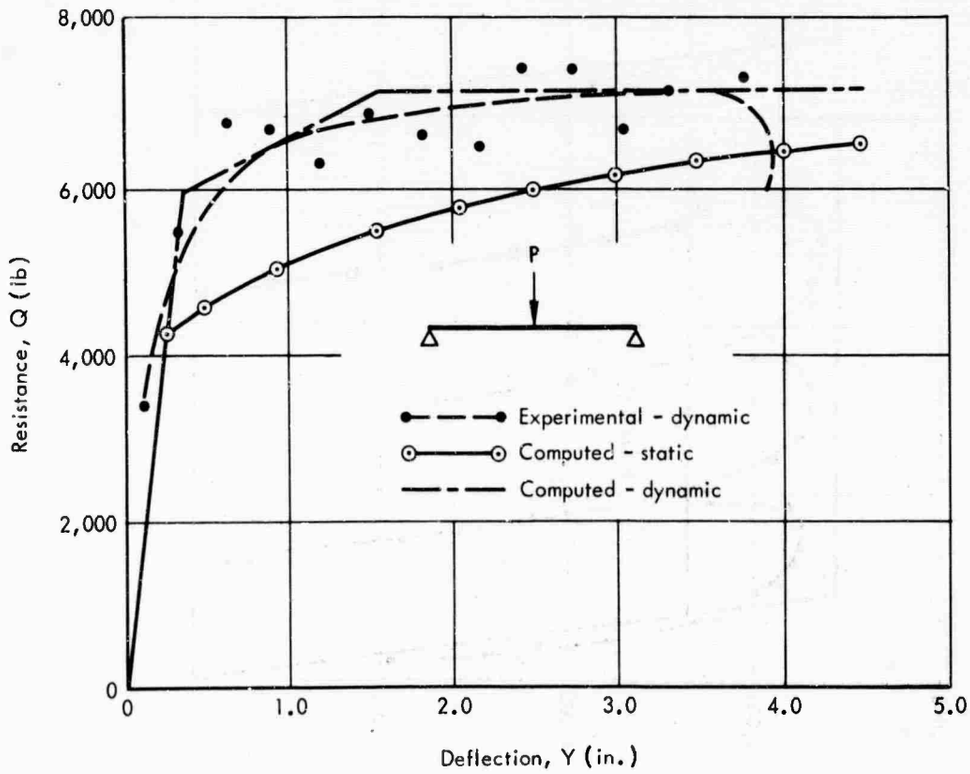

Figure 51. Resistance versus deflection - Beam C-15.

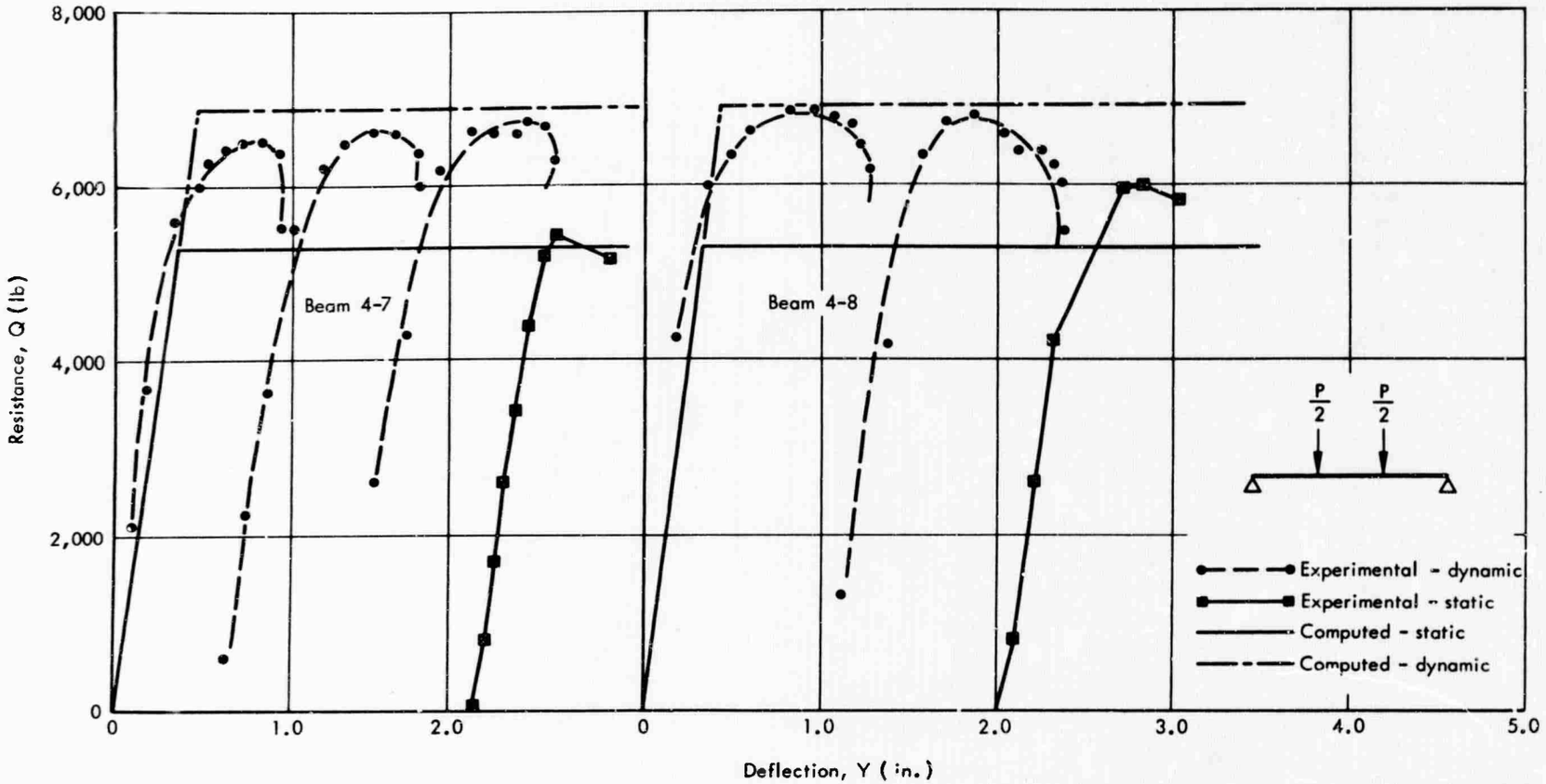

Figure 52. Resistance versus deflection - Beams 4-7 and 4-8.

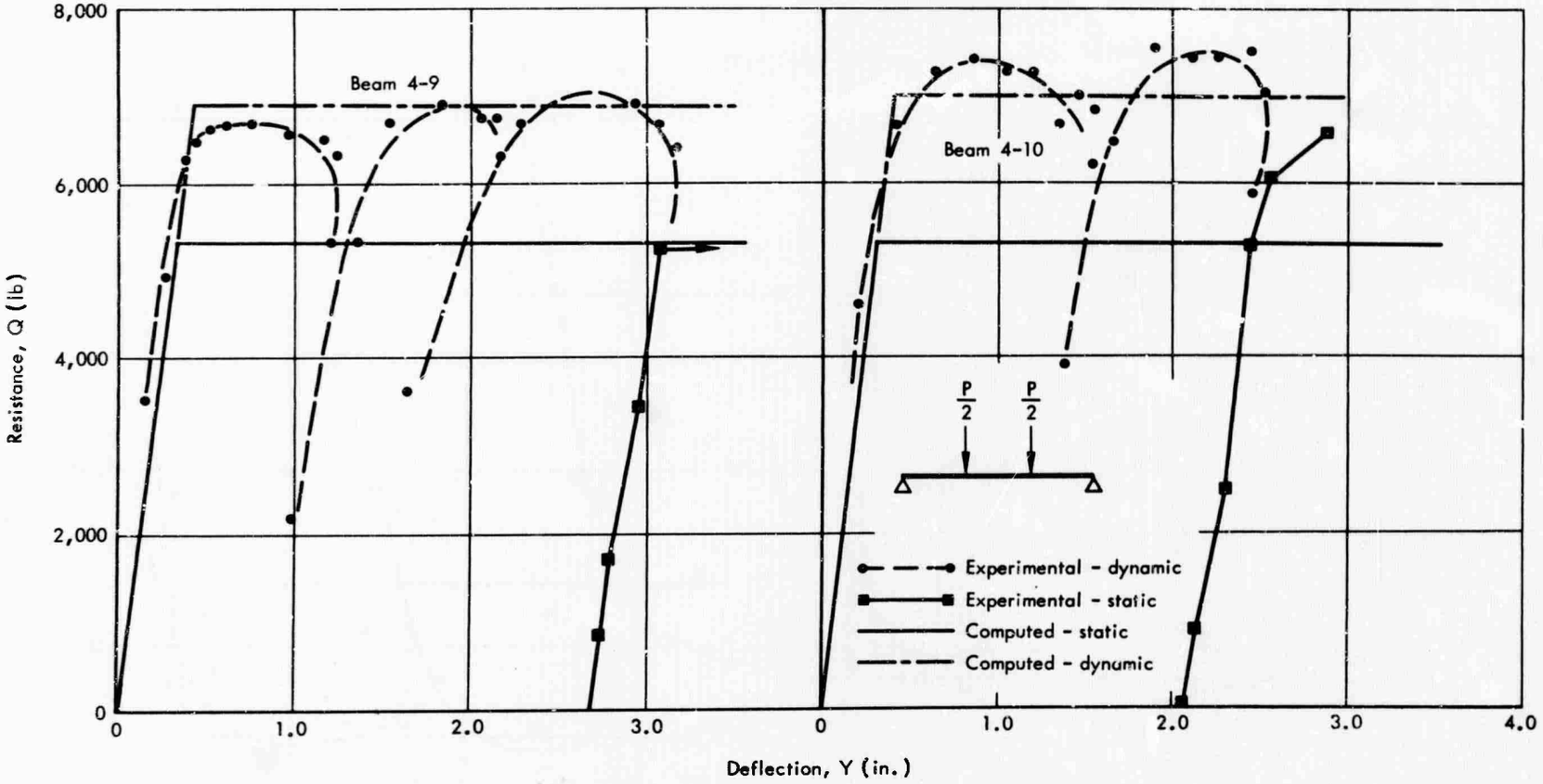

Figure 53. Resistance versus deflection - Beams 4-9 and 4-10.

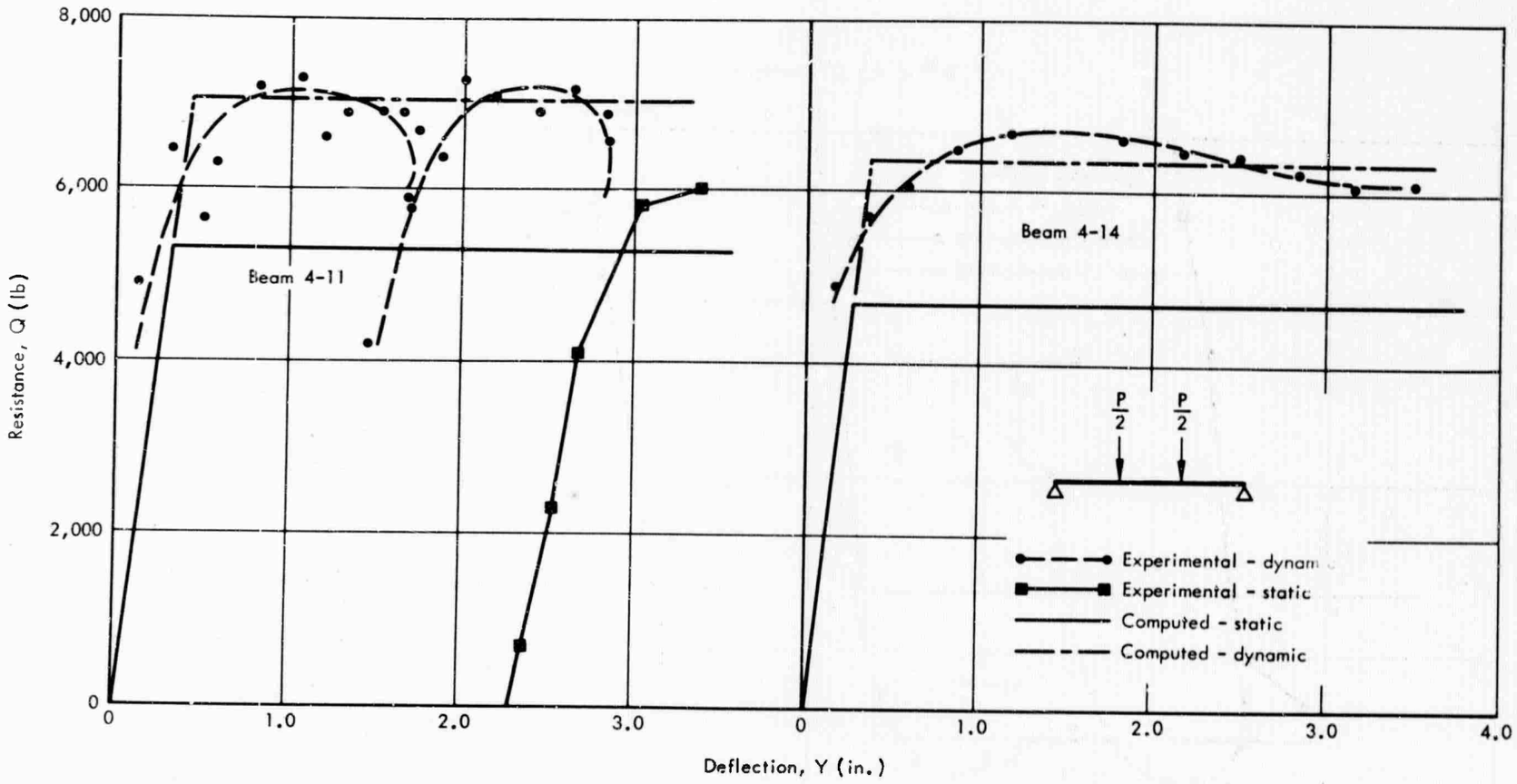

Figure 54. Resistance versus deflection - Beams 4-11 and 4-14.

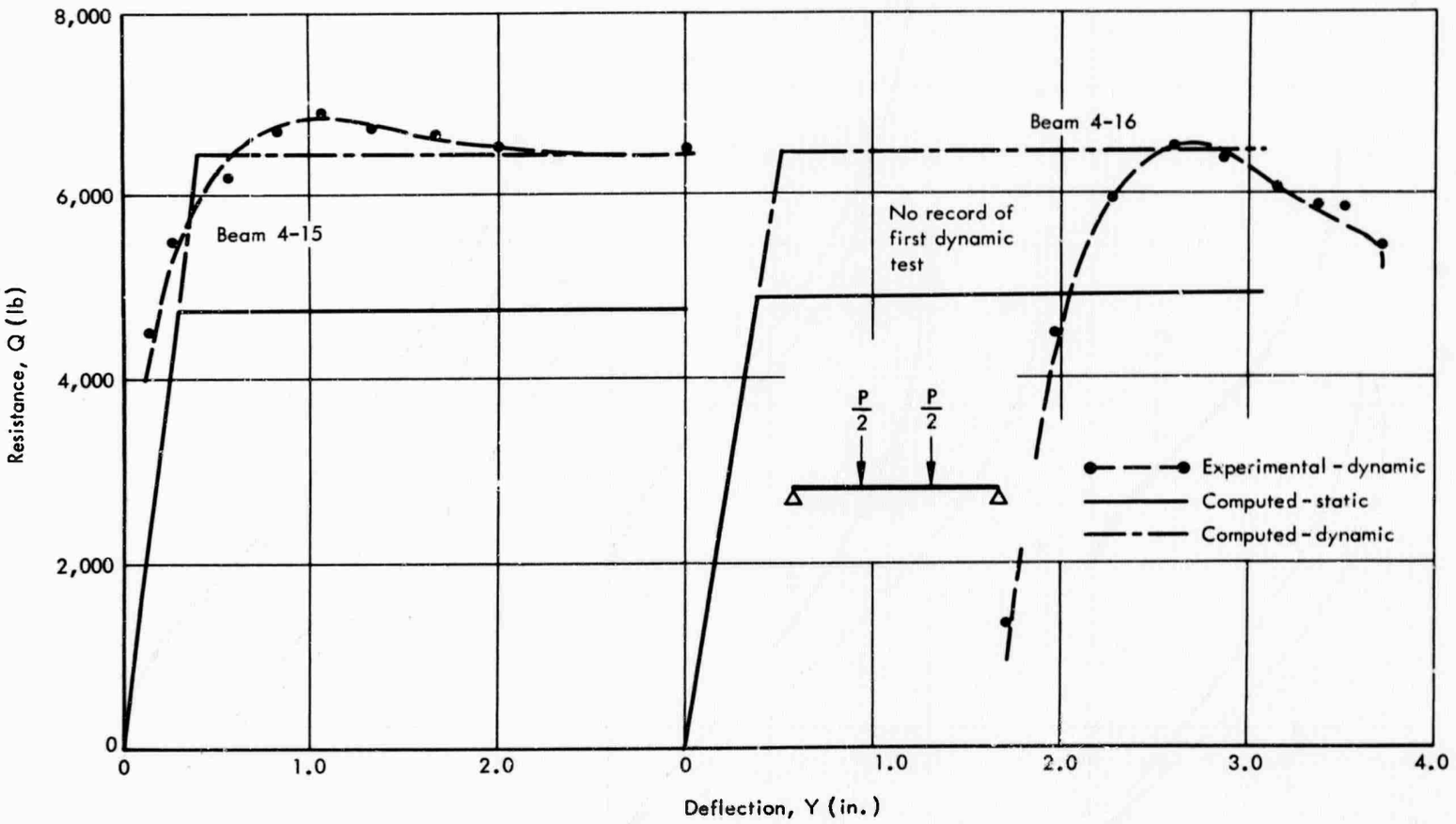

Figure 55. Resistance versus deflection - Beams 4-15 and 4-16.

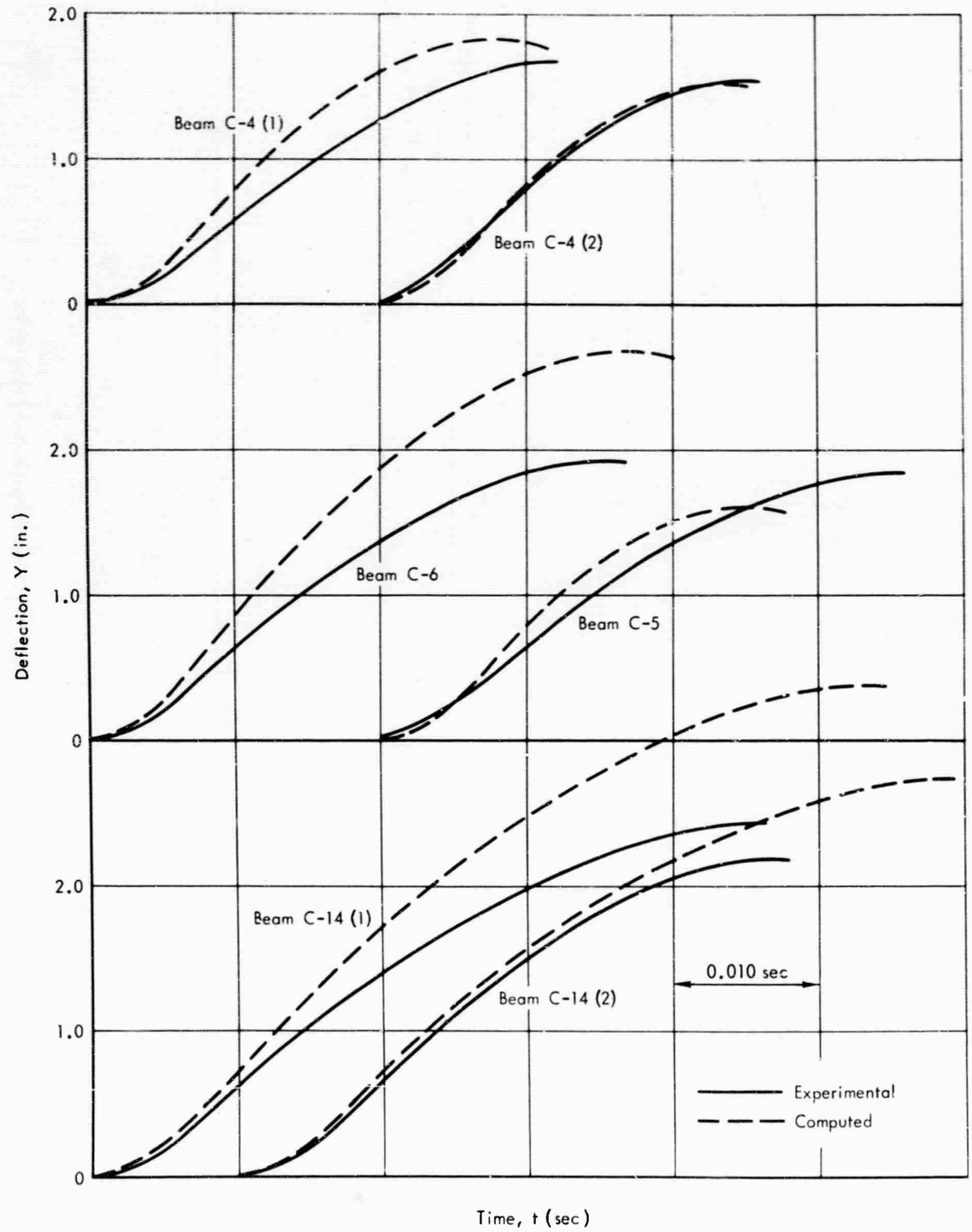

Figure 56. Experimental and computed response curves.

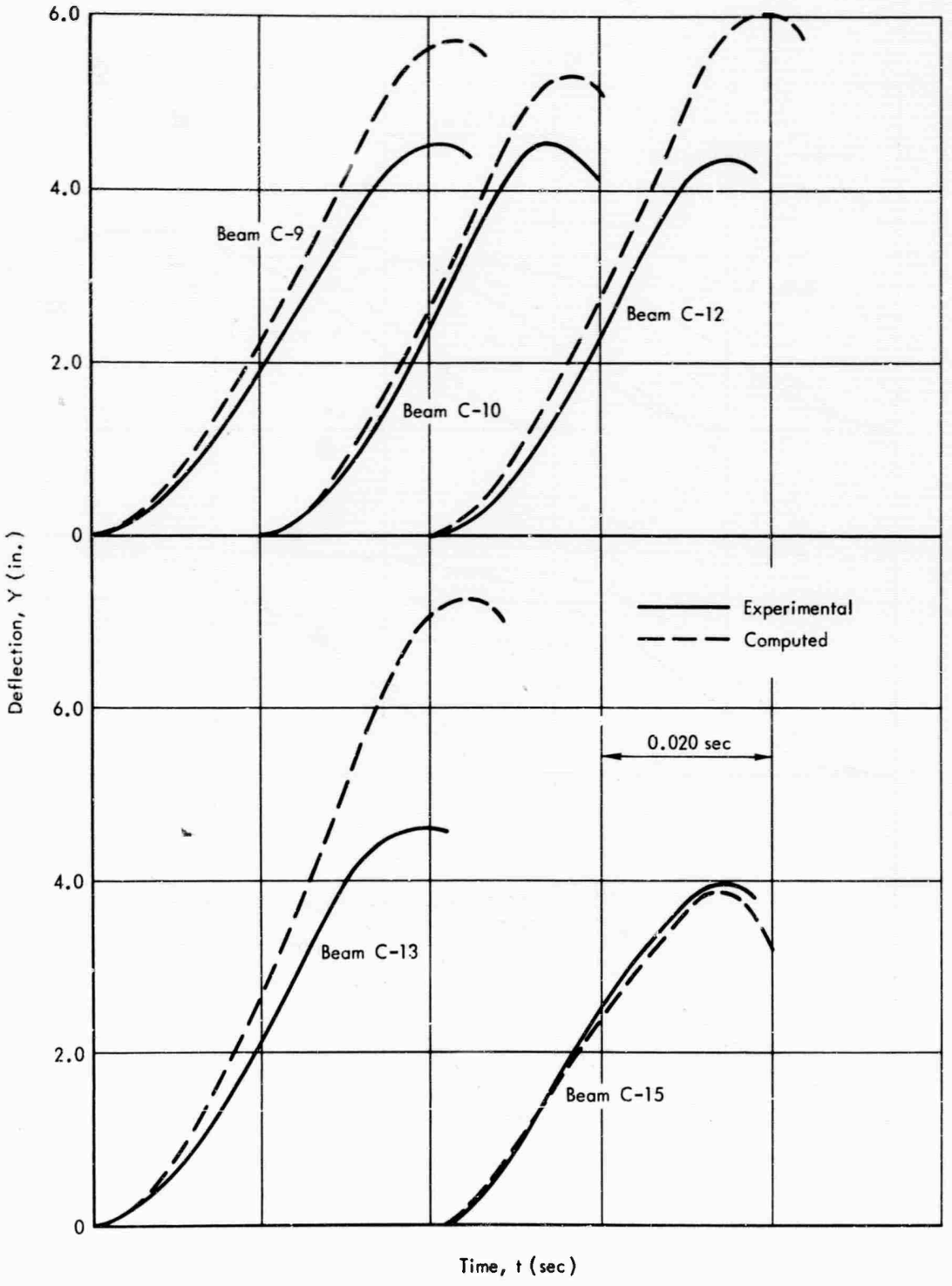

Figure 57. Experimental and computed response curves.

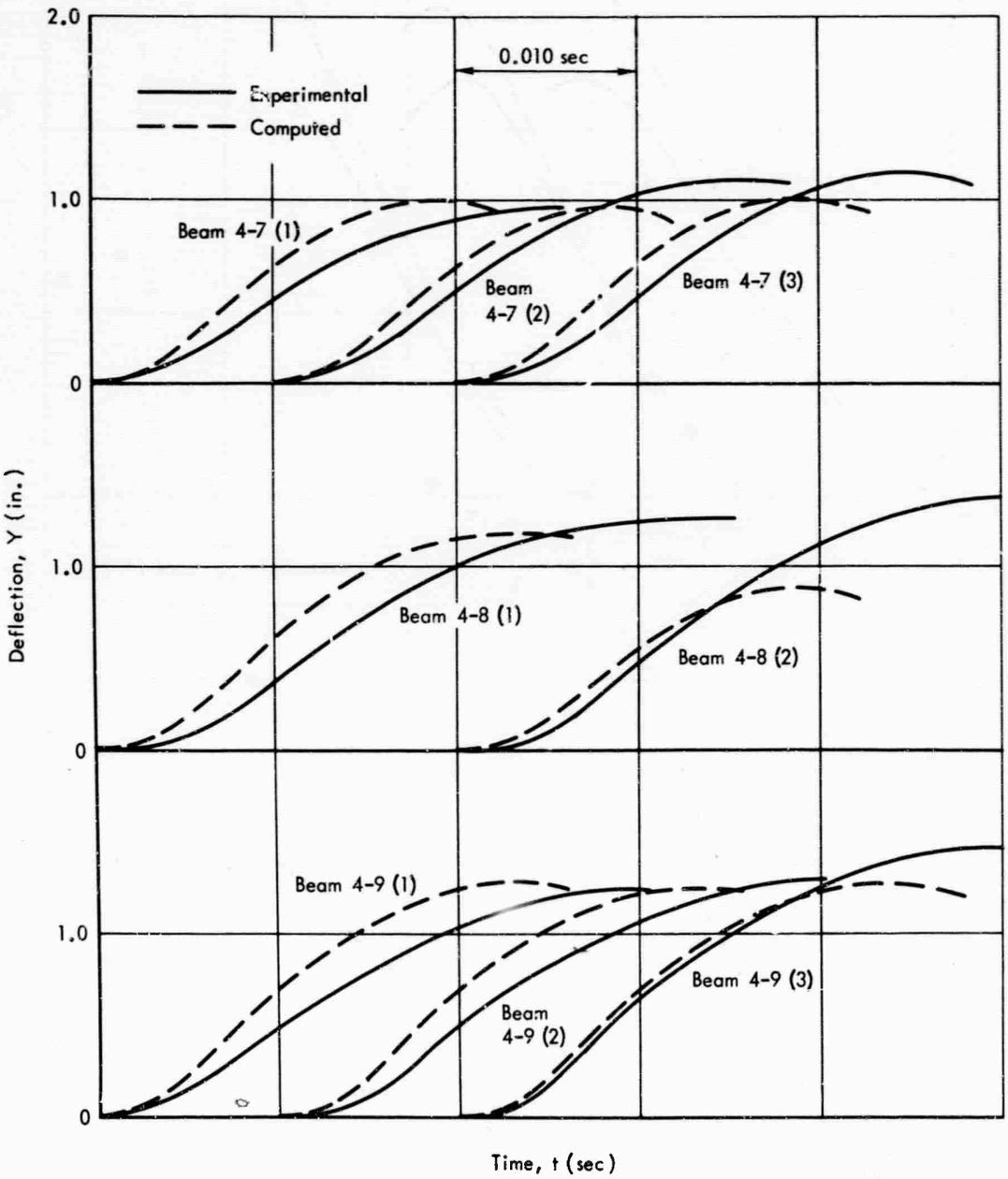

Figure 58. Experimental and computed response curves.

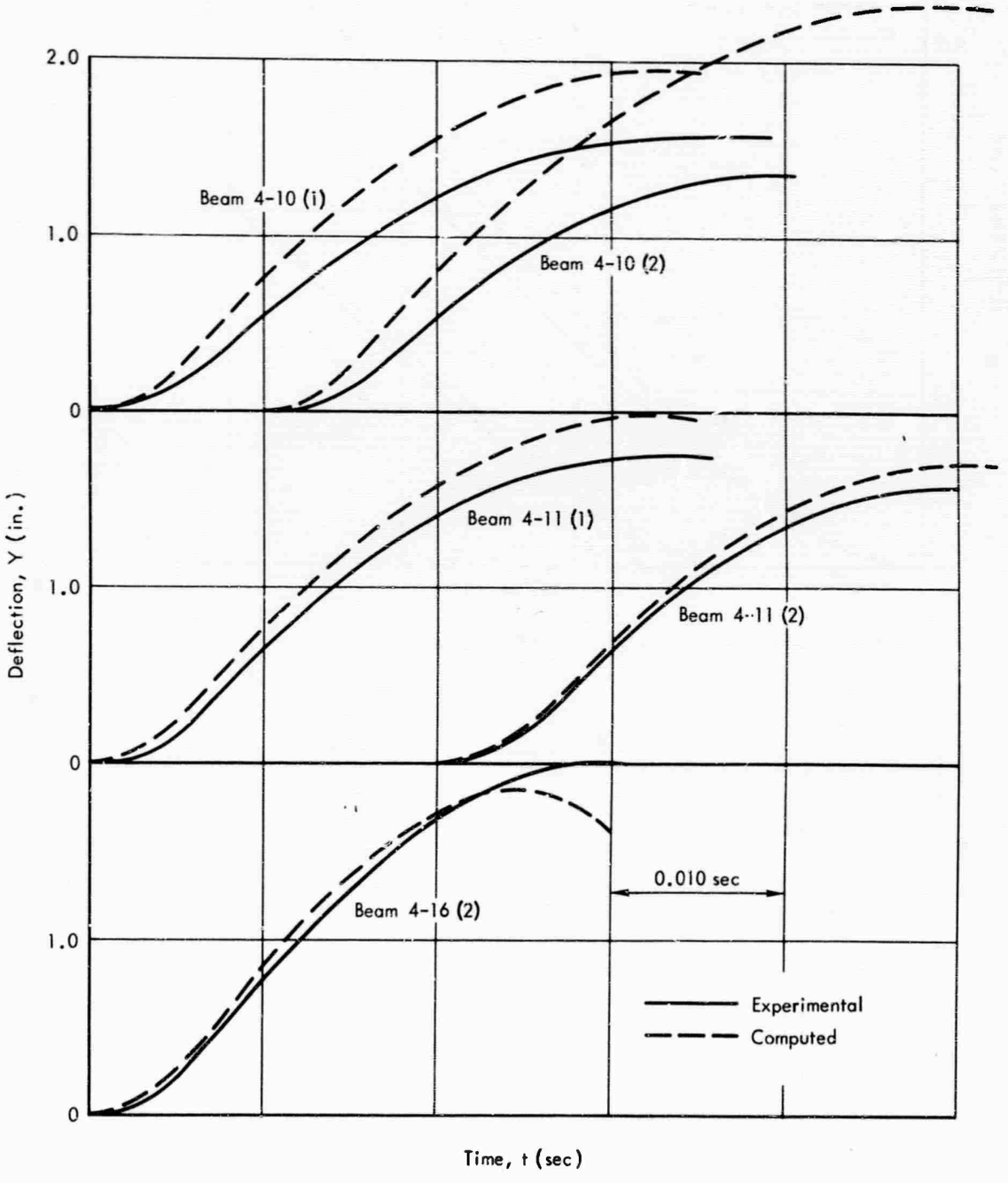

Figure 59. Experimental and computed response curves.

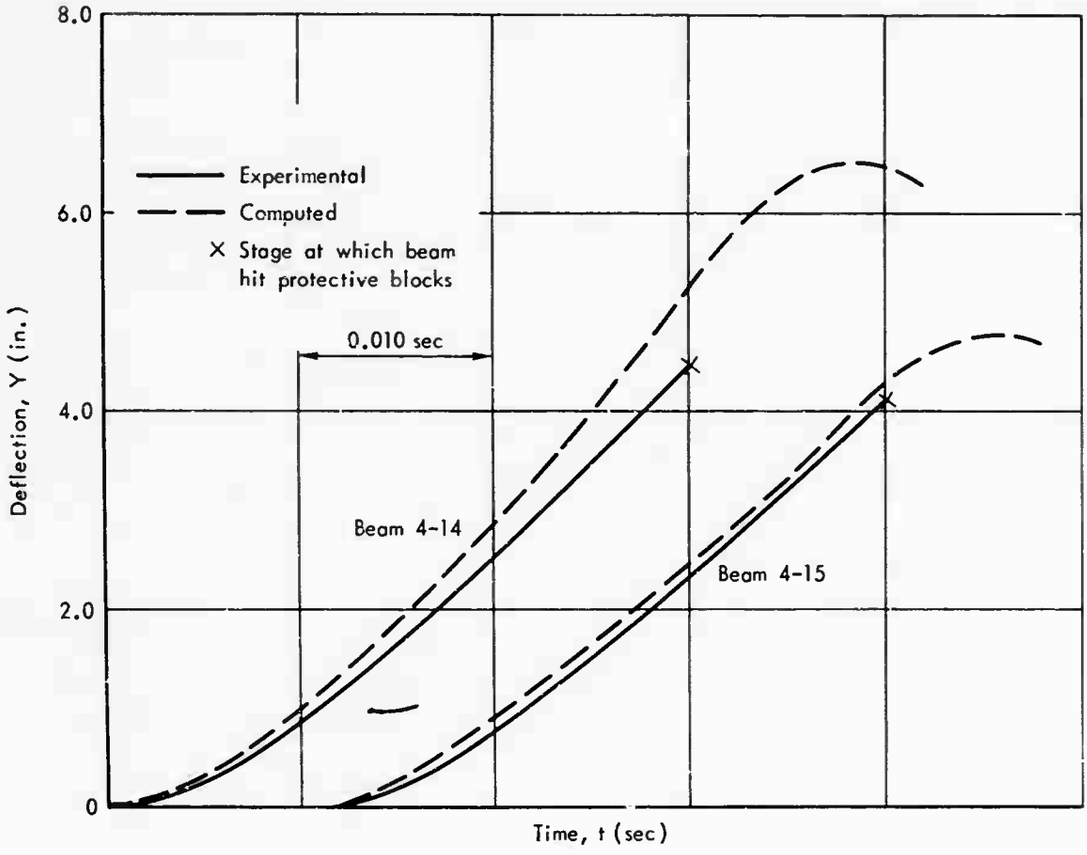

Figure 60. Experimental and computed response curves.

Table 6. Experimental and Computed Data at Maximum Deflection - Dynamic Tests

Beam No.	Initial Max Deflection, Dynamic Test, Y_{md} (in.)			Beam No.	Initial Max Deflection, Dynamic Test, Y_{md} (in.)		
	Exp.	Comp.	Exp./Comp.		Exp.	Comp.	Exp./Comp.
C-4(1)	1.66	1.80	0.93	4-7(1)	0.92	1.00	0.92
(2)	1.52	1.47	1.03	(2)	1.09	0.94	1.16
C-5	1.82	1.59	1.14	(3)	1.14	1.00	1.14
C-6	1.92	2.66	0.72	4-8(1)	1.23	1.20	1.02
C-9	4.56	5.73	0.80	(2)	1.38	0.87	1.59
C-10	4.50	5.29	0.85	4-9(1)	1.26	1.29	0.98
C-12	4.39	6.01	0.73	(2)	1.23	1.26	0.98
C-13	4.66	7.25	0.64	(3)	1.46	1.29	1.16
C-14(1)	2.41	3.35	0.72	4-10(1)	1.55	1.91	0.81
(2)	2.19	2.72	0.81	(2)	1.32	2.27	0.58
C-15	3.96	3.93	1.01	4-11(1)	1.72	1.96	0.88
				(2)	1.55	1.67	0.93
				4-14	>4.40	6.45	--
				4-15	>4.06	4.73	--
				4-16(1)	2.09	--	--
				(2)	2.04	1.83	1.11
Average			0.85	Average			1.02

FINDINGS AND CONCLUSIONS

Static Tests

1. The yield stage analysis predicted moments and curvatures which were within 6 percent of the measured values. Except for two cases, the yield deflections were predicted within 10 percent of the measured values. Test results from other sources were examined using Equations 9 and 13. The correlation was not as close as that noted above. However, the correlation was better than that obtained using the conventional straight-line theory.

2. The post-yield analysis (yield to maximum load) predicted moments within 8 percent of the measured values. Furthermore, there was good correlation between the computed and experimental load-deflection curves and between the computed and experimental moment-rotation curves for the centrally loaded beams. The analysis did not satisfactorily predict the maximum load stage for the beams subjected to two concentrated loads.

3. Hinging results from the propagation of yielded zones in the tension reinforcement. In consequence, the stiffness of the beam beyond the yield stage is dependent on strain hardening in the tension reinforcement and the length of the maximum moment region.

4. The extent of the hinge zone was essentially limited to the region of the beam resisting a moment greater than the yield moment. Beam curvature and plastic deformation of the tension reinforcement were a maximum at midspan for the centrally loaded beams and at the crushed section for the beams subjected to two loads (Figures 12 and 35).

5. For beams with well-tied compression reinforcement, the onset of crushing is not a limiting stage. The ratio of deflection at maximum load to deflection at onset of crushing ranged from 1.2 to 4.8; the larger values were for the centrally loaded beams. Furthermore, additional rotation capacity at high load was usually available beyond maximum load.

6. In the centrally loaded beams in which the percentage of tension reinforcement was varied (p = 0.9, 1.3, and 2.0 percent), the deflection and the magnitude of high rotation at the crushing, maximum load, and ultimate stages increased as p decreased. At ultimate, the two beams with the small values of $q - q'$ (1.7 percent) failed when the tension reinforcement fractured and the other two beams ($q - q'$ = 3.6 and 7.5 percent) failed when the compression reinforcement buckled.

7. In the centrally loaded beams, the ductility of the tension steel was being utilized completely, so that the addition of more compression reinforcement would have a negligible effect on the rotation capacity of the beams.

8. The effect of the size of the transverse reinforcement (closed stirrups) had a negligible effect on the rotation capacity of the centrally loaded beams because two of the beams failed by fracture of the tension reinforcement. Transverse reinforcement should have a greater effect in beams with larger reinforcement percentages ($p > 2.0$ percent) and small amounts of compression steel ($p'/p < 0.6$ percent).

9. Increasing the amount of confined concrete resulted in a greater ultimate rotation capacity and a greater maximum resistance (Figure 2).

10. The ductility factor, expressed as the ratio of ultimate to yield deflection, ranged from 18 to 28 for the centrally loaded beams. Thus, large rotation capacities can be obtained in reinforced concrete beams. This ratio was approximately equal to 7 for the beams subjected to two concentrated loads.

Dynamic Tests

1. Hinge formation and propagation is not detrimentally affected by dynamic loads. The deflections at crushing were generally less than those measured in the static tests; for three beams subjected to two concentrated loads, the crushing deflections were approximately 40 percent less than the average static value. However, this decrease was not found to be detrimental, because the beam resistance or response was not affected by this premature crushing.

2. Ductility factors, expressed as a ratio of maximum dynamic deflection to dynamic yield deflection, equal to 15 for the centrally loaded beams were obtained without failure. For the beams subject to two loads, ratios equal to 10 were obtained without a failure.

3. The analysis of the dynamic behavior provided conservative but realistic estimates of the dynamic resistance. For the centrally loaded beams, strain hardening and the strain rate effect were considered. For the beams subjected to two concentrated loads, only the strain rate effect was considered and an elastoplastic resistance diagram was used.

4. For the centrally loaded beams, the ratio of experimental to computed maximum deflection ranged from 0.64 to 1.14 with a mean of 0.95; for the beams subjected to two concentrated loads, this ratio varied between 0.58 and 1.59 with a mean of 1.02. In the latter case, except for the two extreme values, the ratio ranged from 0.81 to 1.16. In general, the degree of accuracy is reasonable and acceptable.

DESIGN RECOMMENDATIONS

1. Within the limits noted, Equation 13 can be used to compute the yield curvature pending further study. The percent increase in yield curvature for strain rates between 0.3 and 1.10 in./in./sec for intermediate grade reinforcement can be obtained from Figure 21.

2. For maximum strength and ductility, compression reinforcement should be tied securely to transverse reinforcement which, in turn, should be detailed to enclose as much of the compression zone as possible.

3. For beams with low reinforcement percentages ($p < 2.0$ percent), failure can occur after strain hardening has developed in the tension reinforcement. In such cases, the steel reinforcement stress-strain diagram in Figure 22 can be used to obtain a more accurate prediction of maximum steel stress; it is appropriate for steels with yield strengths of approximately 50,000 psi.

4. For beams with well-tied compression reinforcement and adequate shear reinforcement, failure does not occur when the maximum concrete strain reaches 0.003 to 0.004 in./in. as normally assumed. Although there is no generally accepted method for computing the maximum resistance and ductility for such beams, the procedures outlined in this report and in References 2, 3, 4, and 5 can be used to provide reasonable estimates for these quantities.

LIST OF SYMBOLS

A_s	Area of tension steel reinforcement $(in.^2)$
A_s'	Area of compression steel reinforcement $(in.^2)$
a	Distance between concentrated loads (in.)
b	Width of beam (in.)
C_c	Total compressive force in concrete (lb)
C_s	Force in compression reinforcement (lb)
c	Crushing stage
cr	Cracking stage
comp	Subscript denoting a computed value
d	Distance from outer fiber in compression to centroid of tension reinforcement (in.)
d'	Distance from outer fiber in compression to centroid of compression reinforcement (in.)
E_c	Modulus of elasticity of concrete (psi)
E_s	Modulus of elasticity of steel (psi)
exp	Subscript denoting an experimental value
f_c	Stress in concrete (psi)
f_c'	Compressive strength of 6- by 12-inch cylinder (psi)
f_s	Steel stress (ksi)
f_s'	Average stress in compression steel reinforcement (ksi)
f_y	Yield stress of tension steel reinforcement (ksi)
f_y'	Yield stress of compression steel reinforcement (ksi)
h	Height of beam (in.)
k	Coefficient defining position of neutral axis at yield stage
kd	Depth of compression zone (in.)
k_i	Coefficient defining position of neutral axis at a stage beyond yield
L	Span length (in.)
ℓ	Shear span length (in.)
M	Bending moment (in.-kips)
M_c	Bending moment at crushing stage (in.-kips)

M_i	Bending moment at which $\phi = \phi_i$ (see Figure 25) (in.-kips)
M_m	Bending moment at maximum load (in.-kips)
M_u	Bending moment at ultimate stage (in.-kips)
M_y	Bending moment at yield stage (in.-kips)
m	Maximum load stage
m_e	Equivalent mass of beam (lb-sec^2/in.)
n	E_s/E_c
P	Applied load (lb)
P_c	Applied load at crushing stage (lb)
P_m	Maximum applied load (lb)
P_u	Applied load at ultimate stage (lb)
P_y	Applied load at yield stage (lb)
p	A_s/bd = tension steel ratio
p'	A_s'/bd = compression steel ratio
Q	Resistance (lb)
Q_d	Dynamic resistance (lb)
Q_{dm}	Maximum dynamic resistance (lb)
Q_{dy}	Dynamic yield resistance (lb)
Q_s	Static resistance (lb)
Q_{sm}	Maximum static resistance (lb)
Q_{sy}	Static yield resistance (lb)
q	pf_y/f_c'
q'	$p'f_y'/f_c'$
T	Natural period of vibration (sec/cycle)
T_s	Force in tension reinforcement (lb)
t	Time (sec)
t_d	Time to load release (msec)
t_m	Time to reach Y_{md} (msec)
t_r	Rise time of load (msec)
t_y	Time to Y_y, dynamic tests (msec)

t_z	Time to zero load (msec)
u	Ultimate stage
X_i	Distance from reaction to point where $M = M_i$ and $\phi = \phi_i$ (in.)
Y	Deflection (in.)
Y_c	Deflection at midspan, crushing stage (in.)
Y_m	Deflection at midspan, maximum load (in.)
Y_{md}	Initial maximum deflection, dynamic test (in.)
Y_p	Permanent deflection (in.)
Y_u	Deflection at midspan, ultimate stage (in.)
Y_y	Deflection at midspan, yield stage (in.)
y	Yield stage
Δ_B	Deflection between bottom ends of mechanical rotation gage angles (in.)
Δ_T	Deflection between top ends of mechanical rotation gage angles (in.)
ϵ_c	Concrete strain at outer fiber in compression
ϵ_s	Strain in tension steel reinforcement
ϵ_s'	Strain in compression steel reinforcement
ϵ_{sh}	Steel strain at strain hardening
ϵ_y	Yield strain of tension steel reinforcement
θ	Beam rotation as measured by mechanical gages (rad)
$\theta_E, \theta_{E1}, \theta_{E2}$	End rotation (rad)
θ_i	Beam rotation between point X_i and X_{i-1} (rad)
θ_m	Beam rotation at midspan as measured by mechanical gages (rad)
θ_r, θ_ℓ	Beam rotation at load point for beam with a = 18 inches and at location adjacent to θ_m for beam with a = 0; see Figure A-2 for exact location (rad)
$\Sigma 0$	Sum of perimeters of tension reinforcement bars
ϕ	Curvature (rad/in.)
ϕ_{avg}	$(\phi_\ell + \phi_m + \phi_r)/3$ (rad/in.)
ϕ_i	Curvature at which $M = M_i$ (see Figure 25) (rad/in.)
ϕ_ℓ	Curvature, $\theta_\ell/6$ (rad/in.)
ϕ_m	Curvature, $\theta_m/6$ (rad/in.)

ϕ_{max}	ϕ_ℓ, ϕ_m, or ϕ_r, whichever is largest (rad/in.)
ϕ_r	Curvature, $\theta_r/6$ (rad/in.)
ϕ_u	Curvature at ultimate stage (rad/in.)
ϕ_y	Curvature at yield stage (rad/in.)

Appendix A

MATERIALS, INSTRUMENTATION, AND TEST PROCEDURE

MATERIALS

The geometrical and mechanical properties of each beam are presented in Tables A-1 and A-2. The location of the reinforcement was determined by measurements taken after the test, the concrete being chipped away to expose the reinforcement. The reinforcement stress-strain data represent the average of the results from two tensile tests on 2-foot-long bars removed from one or each end of the beam.

The concrete mix design is presented below:

Cement (lb, dry wt)	Sand (lb, dry wt)	Coarse Aggregate* (lb, dry wt)	Water (lb)	Water/ Cement Ratio	Slump (in.)
33.5	125.4	83.6	23.2	0.60	1.5

Three standard concrete control cylinders were moist cured with each beam for 22 to 23 days. Thirty to thirty-two days after casting, a beam and the corresponding control cylinders were tested on the same day. The average concrete cylinder strength was 4,980 psi.

Except for four beams, the stirrups were 1/8-inch round bars having a yield strength (0.2 percent offset) of 85,000 psi. Bars 1/4-inch in diameter with a yield strength of 50,000 psi were used in Beams C-3 and C-5, and No. 3 deformed bars in Beams C-2 and C-6. In all four beams the larger stirrups were used only in the region within 14 inches each side of midspan; the 1/8-inch round stirrups were used in the remainder of the shear span over to the supports.

EQUIPMENT

Dynamic loads were applied with the NCEL 10,000-pound rapid load machine (Figure A-1). The load is developed by a differential pressure acting on a piston connected to a load strut, the pressure being obtained from bottled nitrogen gas. The load strut was locked in position during the pressurizing operation and was released automatically at the desired time.

Static loads were applied with a 20,000-pound hydraulic jack reacting against a steel bracket secured to the test frame of the rapid load machine, the pressure chamber assembly being raised to a higher position in the test frame in order to provide the necessary clearance.

INSTRUMENTATION

The instrumentation layouts are presented in Figure A-2.

Load

Dynamic loads were measured in terms of strain in the load strut. Four foil-type strain gages having a 1-inch gage length were bonded to the strut in a symmetrical pattern, two gages parallel and two perpendicular to the longitudinal axis of the strut. The output of this bridge was calibrated using a 50,000-pound-capacity load cell as a standard. This load cell was also used to measure the total applied load on those beams subjected to two concentrated loads located 9 inches each side of midspan. Furthermore, in tests on these beams the static and dynamic reactions at one end of the distributing beam were measured with a 20,000-pound-capacity load cell. This cell was also used to measure the total static load on the centrally loaded beams.

*Maximum size aggregate - 3/8 inch.

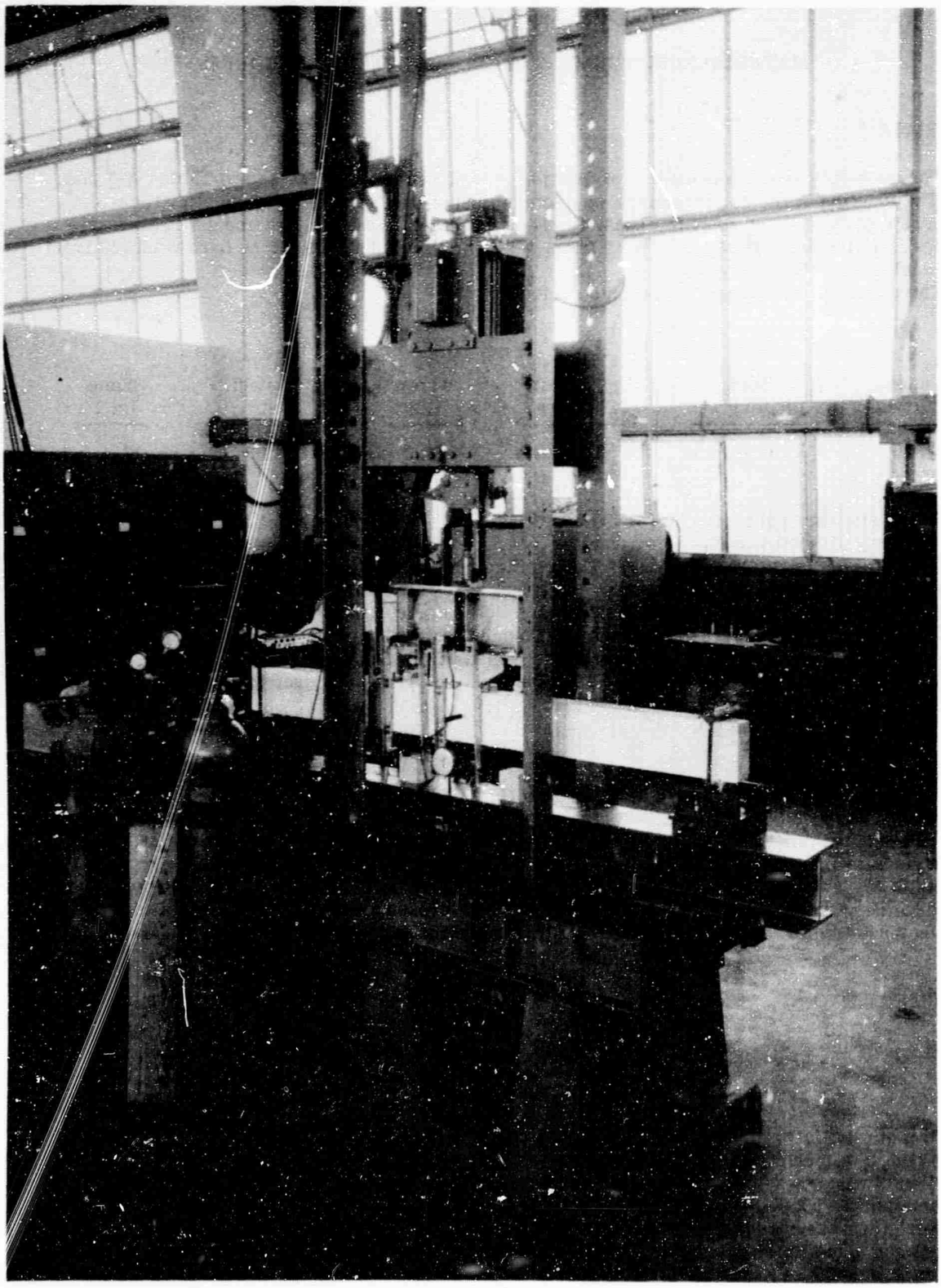

Figure A-1. NCEL 10,000-pound rapid load machine.

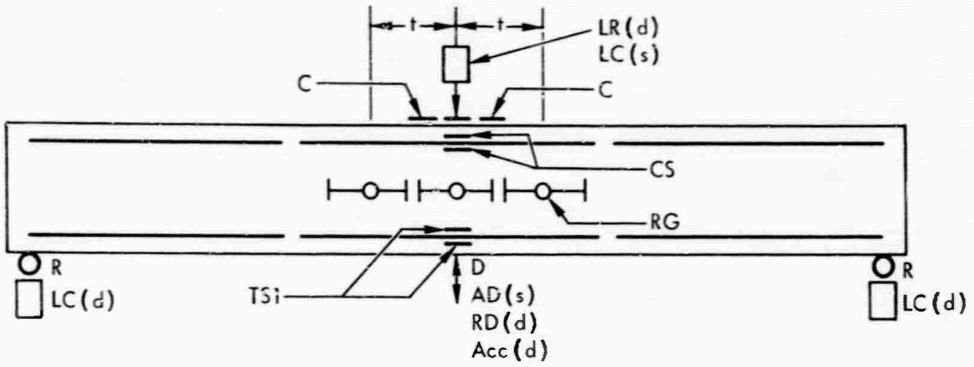

(a) Beams with a = 0

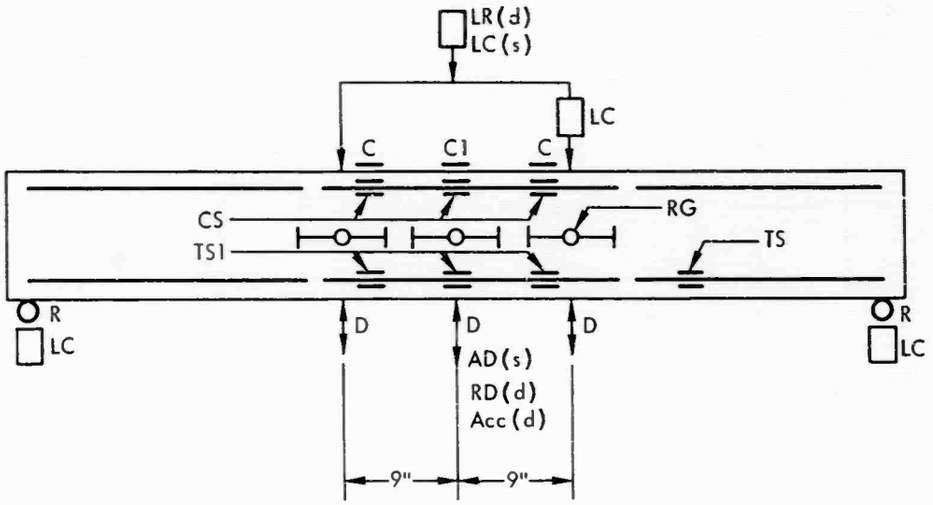

(b) Beams with a = 18"

Load

LC = Load cell
LR = Gaged load strut

Deflection

AD = Ames dial
D = Linear Potentiometer
RD = Rotating drum

Rotation

R = Angular differential transducer
RG = Rotation gage (6" gage length)

Strain Gages

C = Concrete strain (3/4" gage length)
CS = Compression steel strain
C1 = Concrete strain (4" gage length)
TS = Tension steel strain
TS1 = Tension steel strain (high-elongation gage)

Acc = Acceleration
(d) = Dynamic tests only
(s) = Static tests only
t = 9" Beams
C-1 through C-9
t = 6" Beams
C-10 through C-15

Note: Gages an reinforcement omitted for Beams C-11 through C-14 and 4-13 through 4-16.

Figure A-2. Instrumentation layout.

Table A-1. Properties of Beams Loaded at Midspan (L = 72 in., b = 3-1/8 in., h = 6-1/2 in., Stirrup Spacing = 2-1/2 in.)

Beam No.	Type of Test[1]	d (in.)	d' (in.)	f_c' (psi)	Reinforcement[2]					
					f_y (ksi)	f_y' (ksi)	Amount and Size		p (%)	p' (%)
							Tension	Compression		
C-1	S	5.40	0.60	4,860	52.0	52.0	3 No. 3	2 No. 3	2.0	1.3
C-2	S	5.40	0.75	4,850	52.2	50.0	3 No. 3	2 No. 3	2.0	1.3
C-3	S	5.40	0.75	4,910	51.3	51.4	3 No. 3	2 No. 3	2.0	1.3
C-4	D	5.65	0.85	4,720	51.0	50.0	3 No. 3	2 No. 3	1.9	1.2
C-5	D	5.45	0.70	5,040	52.9	53.4	3 No. 3	2 No. 3	1.9	1.3
C-6	D	5.42	0.80	5,770	50.5	51.7	3 No. 3	2 No. 3	2.0	1.3
C-7	S	5.45	0.62	4,740	56.2	61.3	3 No. 2	2 No. 2	0.9	0.7
C-8	S	5.40	0.55	4,820	53.3	58.4	2 No. 3	3 No. 2	1.3	0.9
C-9	D	5.48	0.53	4,960	61.0	61.2	3 No. 2	2 No. 2	0.9	0.7
C-10	D	5.33	0.66	4,930	50.0	56.8	2 No. 3	3 No. 2	1.3	0.9
C-11	S	5.35	0.63	5,090	50.3	62.6	2 No. 3	3 No. 2	1.3	0.9
C-12	D	5.37	0.56	5,140	49.1	61.3	2 No. 3	3 No. 2	1.3	0.9
C-13	D	5.43	0.50	4,870	56.2	58.2	3 No. 2	2 No. 2	0.9	0.7
C-14	D	5.37	0.83	5,630	44.8	50.6	1 No. 5	1 No. 4	1.8	1.2
C-15	D	5.39	0.52	5,440	49.4	52.0	3 No. 3	2 No. 3	2.0	1.3

1/ D = Dynamic, S = Static.

2/ Transverse reinforcement: Beams C-2 and C-6 - No. 3 deformed bars. Beams C-3 and C-5 - 1/4-inch round bars. All other beams - 1/8-inch round bars.

Table A-2. Properties of Beams Subjected to Two Concentrated Loads (L = 72 in., b = 3-1/8 in., h = 6-1/2 in.)

Reinforcement: tension, 1 No. 5 deformed bar (p = 1.8%); compression, 1 No. 4 deformed bar (p' = 1.2%); transverse, 1/8-inch round bars, 1-1/2 inches apart in shear span.

Beam No.	Type of Test 1/	d (in.)	d' (in.)	f_c' (psi)	f_y (ksi)	f_y' (ksi)
4-6	S	5.38	0.69	4640	49.1	44.0
4-7	D	5.38	0.69	4660	49.6	43.5
4-8	D	5.38	0.69	4730	50.0	43.1
4-9	D	5.44	0.69	4680	49.1	42.5
4-10	D	5.44	0.75	4860	49.7	43.5
4-11	D	5.40	0.70	4870	49.6	45.0
4-12	S	5.34	0.65	4690	47.1	44.2
4-13	S	5.40	0.95	5010	47.4	44.4
4-14	D	5.41	1.00	5400	44.7	51.3
4-15	D	5.37	0.94	5540	45.5	51.3
4-16	D	5.42	0.75	4460	46.0	47.9

1/ D = Dynamic, S = Static.

In all dynamic tests the reactions at both ends of the beam were measured with 20,000-pound-capacity load cells, 1-1/2 inches high. A preload was applied to these load cells through a holddown arrangement (Figure A-3) which prohibited the ends of the beam from moving upward as a result of whiplash when the dynamic load was applied. Changes in the preload were recorded by measuring the strain in the holddown bars, each of which had two longitudinally oriented strain gages bonded to the bar on diametrically opposite sides.

Deflection

Linear potentiometers were used to measure the deflection at midspan and the load points in the static and dynamic tests. In addition, the deflection at midspan in the static tests was measured with an Ames dial gage in order to provide an accurate measure of the deflection during the progress of the test. In the dynamic tests a check of the maximum deflection was obtained with a rotating drum recorder. This apparatus consists of a spring-loaded pencil secured to the beam and an electrically operated drum attached to the test frame. Deflection is recorded on paper wrapped around the drum.

Strain

Strain in the tension and compression steel was measured over a 0.50-inch-gage length with foil-type strain gages. High-elongation gages were used on the tension reinforcement within the maximum moment region. Two gages diametrically opposed were bonded to the reinforcing bars at selected locations, except for the No. 2 deformed bars on which only one gage was placed. The gages were secured and waterproofed before the beam was cast. Compressive strains on the top surface of the concrete were measured with bonded wire gages with a gage length equal to 0.75 or 4.00 inches. The locations of all the strain gages are shown in Figure A-2.

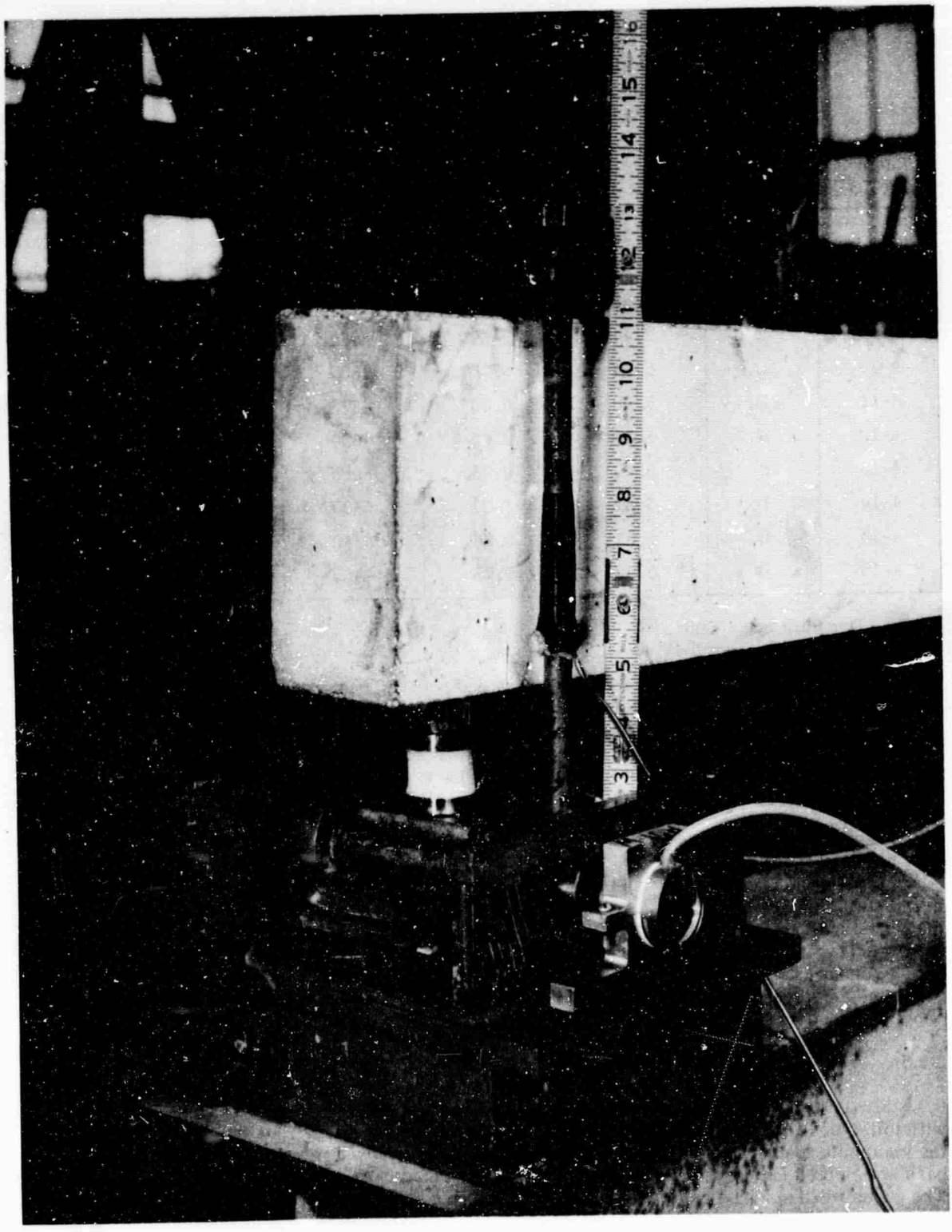

Figure A-3. Instrumentation at beam reaction (load cell and angular transducer).

When strain gages on the tension reinforcement were omitted, the magnitude and distribution of permanent strain were measured with a 2-inch-long Whittemore strain gage. The holes were covered with a small piece of tape to prevent their being filled with concrete. Following the test, the tension reinforcement was removed from the beam and the permanent strain recorded.

Rotation

The magnitude of rotation over a 6-inch length was measured at certain locations (Figure A-2) with the device shown in Figure A-4. The apparatus consisted of two linear potentiometers connected between two aluminum brackets secured to the top and bottom surfaces of the beam. Similar devices have been used previously by others.[16,17]

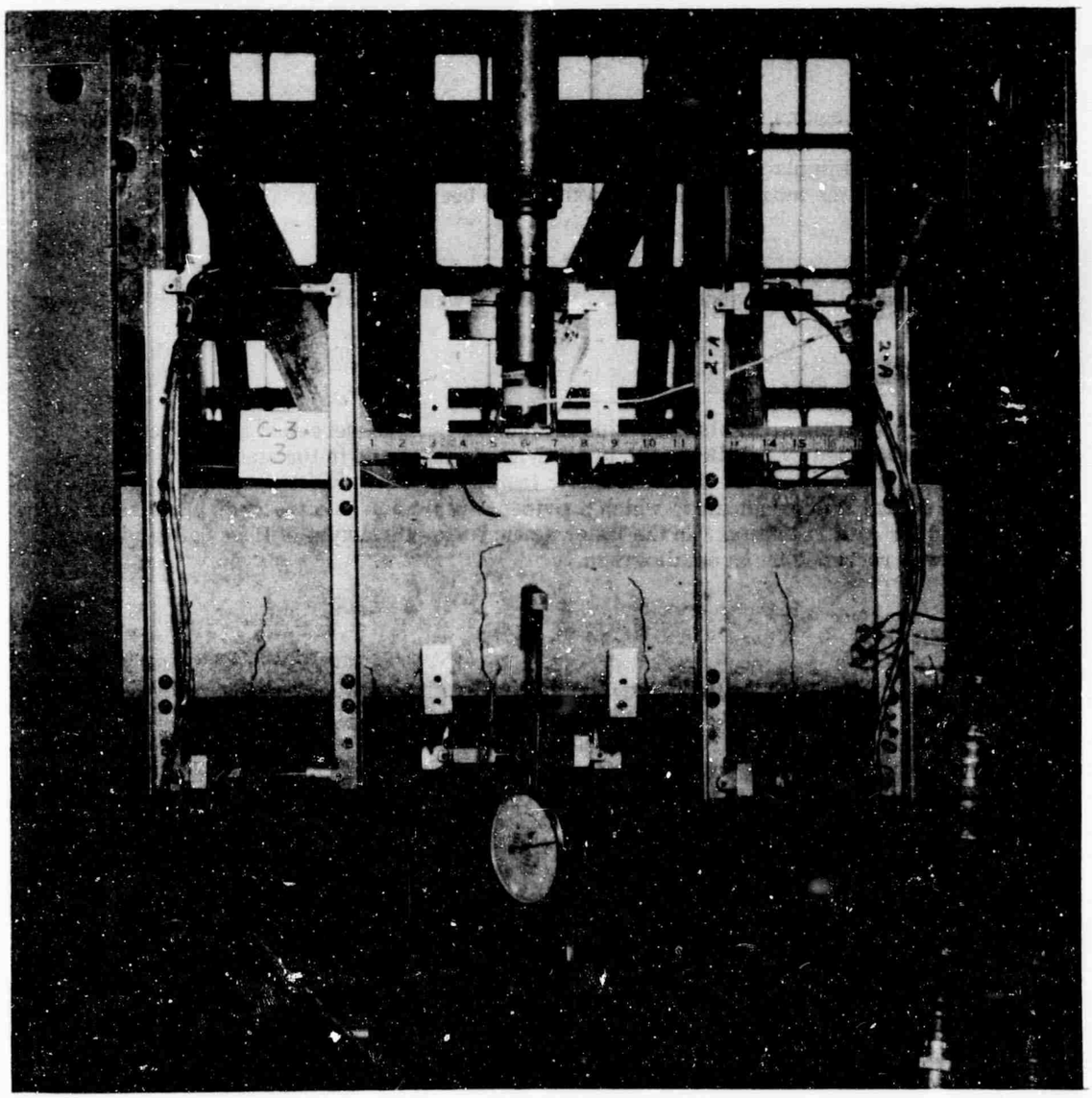

Figure A-4. Mechanical rotation gages.

The gage length (6 inches) was approximately equal to the effective depth of the beams. The distance between the potentiometers was 15 inches, and the values of beam rotation were computed as follows:

$$\theta = \frac{\Delta_T + \Delta_B}{15} \tag{A-1}$$

The average curvature within the gage length is

$$\phi = \frac{\theta}{6} = \frac{\Delta_T + \Delta_B}{90} \tag{A-2}$$

Rotation of the beams at the reactions was measured with angular differential transducers. The rotating stem of this device was secured to the roller reaction which rotated with the beam. The housing was held in place in a bracket (Figure A-3) which moved with the beam only in a direction parallel to the initial longitudinal axis of the beam.

Acceleration

In the dynamic tests the acceleration of the beam was measured at midspan with a 100-g accelerometer.

Recording Equipment

Signal outputs from all resistance-type measuring devices were sent through carrier amplifiers and recorded by oscillographs in all dynamic tests and in the static tests of Beams A-6, C-1, C-2, and C-3. In all the other static tests, the outputs were recorded on an automatic multichannel digital strain indicator, which provided a rapid means of recording and reduced the time required for data reduction. In the latter static tests, the output of the angular differential transducers was recorded by an oscillograph.

TEST PROCEDURE

In the static tests load, deflections, strains, and rotations were recorded by the oscillographs on the digital strain indicator at regular load intervals up to and just beyond the deflection at yield of the tension reinforcement. Subsequently, records were taken at selected intervals of deflection until the ultimate load was reached or collapse occurred. Photographs were taken during the tests to provide a record of the crack pattern and general appearance of the beam at various stages.

The beams to be loaded dynamically were first loaded statically up to the cracking load in order to develop tension cracks in the concrete. Then the natural period was obtained by striking the beam and recording the tension steel strain or accelerometer output. After the desired pressure was obtained in the control cylinder, the procedure for the dynamic tests was governed by means of an automatic interval controller. Time intervals were preset between start of oscillographs, release of load ram, release of load, and stop of oscillographs. Thus, one switch triggered the sequence of events from start to finish. Depending on the timer settings, step load or triangular load pulses were obtained. However, problems were encountered in trying to obtain the triangular load pulse. The repeatability of the mechanical releases was such that the loads were not always released at the desired time even though the pretest trials were satisfactory. Also, some beams deflected beyond the stroke of the load strut so that the load was removed suddenly, and a square pulse obtained. In many cases this prevented total destruction of the beam.

Appendix B

SUMMARY OF TEST DATA

The test data (load, deflection, strain, and rotation measurements) at the principal stages of behavior are summarized for the static tests as follows (data for the cracking stage are omitted):

Table No.	Description
B-1	Yield Stage
B-2	Crushing Stage
B-3	Maximum Load
B-4	Ultimate Stage

For the dynamic tests the data are summarized in Tables B-5 to B-8 as follows:

Table No.	Description
B-5	Dynamic Load Data
B-6	Yield Stage
B-7	Crushing Stage
B-8	Maximum Deflection

In the tables, NR indicates that the item noted was recorded but no valid record was obtained because the reading was out of range of the recorder settings or the instrument's capability. In some cases, certain instruments were removed in the latter stages of the test to protect them from damage. This was true for the mechanical rotation gage located at midspan; the data from this instrument are recorded in the tables under θ_m. A double-dash marking in the tables indicates that no measurement was made.

There is a certain degree of error involved in recording or reducing experimental measurements. Reasonable assumptions as to the degree of accuracy of the reduced experimental data for these tests are as follows:

	Accuracy (%)	
Data	Static	Dynamic
Load	3	5
Deflection	3	5
Strain	5	10
Rotation	6	12

Table B-1. Static Test Results - Yield Stage

Beam No.	P_y (lb)	Y_y (in.)	Strain at Midspan (μin./in.)			Rotation (10^{-3} rad)				
			ϵ_s	ϵ_s'	ϵ_c [1]	θ_m	θ_r	θ_ℓ	θ_{E1}	θ_{E2}
C-1	4,380	0.27	1,960	990	1,170	3.0	1.5	2.2	11.0	13.1
C-2	4,570	0.26	2,030	820	1,290	1.7	1.6	1.5	9.6	10.3
C-3	4,360	0.26	2,000	780	1,070	2.0	2.1	1.2	11.0	10.6
C-7	2,240	0.22	2,080	670	1,070	2.7	2.2	1.6	10.9	9.2
C-8	2,860	0.26	2,020	680	930	3.0	1.9	1.9	7.2	9.3
C-11	2,930	0.26	-- [2]	--	1,170	4.2	1.8	1.8	11.4	10.1
4-6	5,540	0.33	1,960	890	1,400	1.6	1.4	0.8	--	--
4-12	5,250	0.35	1,810	820	1,080	2.4	3.0	1.9	NR [3]	11.0
4-13	5,300	0.34	--	--	1,100	2.6	2.9	2.5	11.5	13.7

1/ For "C"-beams, concrete strain is an average of readings from four strain gages (two gages 1-3/4 inches each side of midspan).
2/ Not measured.
3/ No record.

Table B-2. Static Test Results - Crushing Stage

Beam No.	P_c (lb)	Y_c (in.)	Strain at Midspan (μin./in.)			Rotation (10^{-3} rad)				
			ϵ_s	ϵ_s'	ϵ_c [1]	θ_m	θ_r	θ_ℓ	θ_{E1}	θ_{E2}
C-1	4,990	0.97	24,700	1,240	4,740	26.8	1.7	2.6	33.4	35.4
C-2	5,200	0.95	23,100	690	4,800	26.2	3.1	4.5	30.5	30.2
C-3	5,050	1.00	24,000	800	3,880	30.2	3.2	1.5	33.8	32.0
C-7	2,780	1.55	31,400	570	7,620	41.2	9.5	2.3	47.7	48.7
C-8	3,660	1.05	27,500	700	5,600	25.6	2.4	2.4	29.9	29.4
C-11	3,560	1.20	-- [2]	--	3,250	38.4	12.2 [3]	10.0 [3]	37.7	37.7
4-6	6,110	1.90	21,000	1,170	3,650	18.6	24.6	15.6	--	--
4-12	5,420	1.63	22,200	1,030	3,550	23.9	6.6	2.7	NR [4]	44.6
4-13	5,570	1.80	--	--	5,000	27.5	15.0	18.1	58.6	61.6

1/ For "C"-beams, concrete strain is an average of readings from four strain gages (two gages 1-3/4 inches each side of midspan).
2/ Not measured.
3/ Rotation-measuring device was centered 6 inches from midspan rather than 9 inches as in the other static tests on "C"-beams.
4/ No record.

Table B-3. Static Test Results - Maximum Load

Beam No.	P_m (lb)	Y_m (in.)	Strain at Midspan (μin./in.)		Rotation (10^{-3} rad)				
			ϵ_s	ϵ_s'	θ_m	θ_r	θ_ℓ	θ_{E1}	θ_{E2}
C-1	6,320	3.40	73,500	10,650	96.4	19.1	22.3	110	114
C-2	6,430	4.60	NR [1]	15,400	NR	24.3	23.1	147	134
C-3	6,300	4.60	NR	20,600	NR	27.8	25.5	145	139
C-7	3,370	5.20	NR	14,500	137.0	39.2	24.5	144	155
C-8	4,760	4.20	NR	13,000	NR	22.8	23.8	114	110
C-11	4,580	4.60	-- [2]	--	NR	51.9 [3]	54.6 [3]	133	140
4-6 [4]	6,520	2.80	27,500	1,650	26.9	41.1	16.7	--	--
4-12	5,660	2.43	27,600	1,300	28.4	17.3	8.7	NR	70.5
4-13	5,670	2.24	--	--	29.6	28.3	24.4	73.3	74.0

1/ No record.
2/ Not measured.
3/ Rotation-measuring device was centered 6 inches from midspan rather than 9 inches as in the other static tests on "C"-beams.
4/ Data given are minimum values; test was not carried beyond deflection noted.

Table B-4. Static Test Results - Ultimate Stage

Beam No.	P_u (lb)	Y_u (in.)	Mode of Failure[1]	Strain at Midspan (μin./in.)		Rotation (10^{-3} rad)				
				ϵ_s	ϵ_s'	θ_m	θ_r	θ_l	θ_{E1}	θ_{E2}
C-1	5,920	4.80	B	NR[3]	27,300	NR	18.1	24.6	150	151
C-2	6,260	5.20	T	NR	18,000	NR	24.8	23.8	165	152
C-3	6,300	4.60	T	NR	20,600	NR	27.8	25.5	145	159
C-7	3,230	6.20	T	NR	16,800	NR	45.9	25.1	168	173
C-8	4,640	4.60	T	NR	15,000	NR	23.0	24.2	121	118
C-11	4,100	5.80	B	--	--	NR	NR	NR	173	164
4-6	NR	NR	--[2]	NR	NR	NR	NR	NR	--	--
4-12	5,660	2.43	C	27,600	1,304	28.4	17.3	8.7	NR	70.5
4-13	5,480	2.40	C	--	--	31.3	29.3	25.5	79.6	79.2

1/ B = Compression reinforcement bars buckled, C = Concrete in compression failed, T = Tension reinforcement broke.
2/ Not measured.
3/ No record.

Table B-5. Dynamic Load Data

Beam No.	Test	P (lb)	t_r (msec)	t_d (msec)	t_z (msec)	Y_{md} (in.)	t_m (msec)	Y_p (in.)
C-4	1	6,020	2.0	170	200	1.66	38	1.35
	2	6,020	2.5	186	218	1.52	30	1.07
C-5	1	5,850	2.0	>500	NR	1.82	36	2.14
C-6	1	6,180	2.0	>500	NR	1.92	37	2.32
C-9	1	4,450	2.0	32	33	4.56	40	4.00
C-10	1	5,420	2.0	28	29	4.50	35	3.94
C-12	1	5,540	3.0	30	31	4.39	34	3.85
C-13	1	4,760	2.0	30	31	4.66	38	4.24
C-14	1	5,250	2.0	118	149	2.41	46	2.11
	2	5,250	2.0	120	152	2.19	38	1.84
C-15	1	6,860	2.0	31	32	3.96	34	3.42
4-7	1	5,460	2.0	738	766	0.92	23	0.62
	2	5,380	2.0	710	736	1.09	27	0.73
	3	5,460	2.5	712	741	1.14	27	0.70
4-8	1	5,850	3.0	595	621	1.23	33	1.05
	2	5,460	3.0	610	634	1.38	32	1.01
4-9	1	5,810	2.0	633	665	1.26	30	0.90
	2	5,790	2.5	396	432	1.23	28	0.79
	3	5,810	3.0	636	670	1.46	30	1.01
4-10	1	6,280	2.5	588	633	1.55	35	1.18
	2	6,400	3.0	594	644	1.32	29	0.87
4-11	1	6,260	1.5	150	241	1.72	34	1.22
	2	6,180	2.0	202	227	1.55	29	1.02
4-14	1	7,370	1.5	30	31	>4.40	NR	NR
4-15	1	7,000	2.0	29	31	>4.06	NR	NR
4-16	1	NR [1]	NR	NR	NR	2.09	29	1.68
	2	6,980	1.5	2.5	58	2.04	29	1.54

1/ No record.

Table B-6. Dynamic Test Results - Yield Stage

Beam No.	Test[1]	Y_y (in.)	t_y (msec)	Strain at Midspan (μin./in.)			Rotation (10^{-3} rad)				
				ϵ_s	ϵ_s'	ϵ_c[2]	θ_m	θ_r	θ_ℓ	θ_{E1}	θ_{E2}
C-4	1	0.40	7.7	2,950	900	2,610	4.0	3.3	3.0	13	11
	2I	0.45	8.5	3,940	2,160	NR[4]	8.1	3.4	2.4	18	10
	2C	1.80	--[3]	43,200	2,830	NR	49.2	4.2	2.7	56	46
C-5	1	0.42	7.7	2,990	1,120	2,080	5.0	3.1	3.1	16	14
C-6	1	0.35	7.0	2,920	880	1,330	4.1	2.5	2.9	11	12
C-9	1	0.31	7.0	2,860	780	1,300	3.5	0.7	0.8	NR	20
C-10	1	0.36	6.8	2,520	1,020	1,600	6.2	3.3	3.0	10	14
C-12	1	0.33	7.0	--	--	1,120	6.0	1.8	3.1	16	12
C-13	1	0.37	7.2	--	--	1,600	3.2	4.8	3.6	13	14
C-14	1	0.36	7.7	--	--	2,020	3.9	3.4	5.6	15	12
	2I	0.43	7.8	--	--	NR	6.9	4.4	5.1	15	17
	2C	2.54	--	--	--	NR	74.0	28.1	33.3	81	76
C-15	1	0.41	6.8	2,850	1,360	1,930	4.3	5.4	4.2	17	14
4-7	1	0.43	9.5	2,590	1,160	1,590	2.7	2.9	4.0	--	--
	2I	0.38	8.4	2,670	1,280	1,770	2.1	1.5	3.3	--	--
	2C	1.00	--	28,200	1,080	3,390	16.2	3.8	12.4	--	--
	3I	0.39	9.0	2,260	1,410	NR	2.1	1.7	3.2	--	--
	3C	1.74	--	30,000	1,350	NR	23.0	9.9	22.2	--	--
4-8	1	0.41	10.4	2,400	1,090	1,600	4.9	3.5	2.1	--	--
	2I	0.41	8.3	2,690	1,830	NR	3.8	3.6	2.7	--	--
	2C	1.46	--	21,000	1,750	NR	26.9	14.3	5.5	--	--
4-9	1	0.42	8.8	2,450	1,030	1,590	4.3	3.9	4.1	--	--
	2I	0.37	8.4	2,650	1,280	1,620	3.0	4.1	4.5	--	--
	2C	1.27	--	24,900	1,460	3,480	16.8	8.0	17.6	--	--
	3I	0.38	7.7	NR	1,360	NR	1.9	3.1	2.9	--	--
	3C	2.07	--	NR	1,780	NR	23.6	11.4	26.2	--	--
4-10	1	0.42	8.5	2,670	1,000	1,520	5.7	3.2	4.4	--	--
	2I	0.46	9.2	NR	1,210	1,760	4.2	0.6	4.6	--	--
	2C	1.64	--	NR	750	3,730	21.8	18.8	22.8	--	--
4-11	1	0.48	8.5	2,830	940	1,690	7.1	6.5	2.9	21.0	14.0
	2I	0.45	8.3	NR	1,240	1,860	2.5	6.7	2.3	20.0	16.0
	2C	1.67	--	NR	1,000	4,660	31.4	26.9	5.7	62.0	49.0
4-14	1	0.46	7.0	--	--	1,530	2.6	3.0	3.9	20.0	17.0
4-15	1	0.40	7.0	--	--	1,400	2.0	3.8	2.6	17	16
4-16	1	0.42	7.0	--	--	NR	NR	1.8	3.6	NR	NR
	2I	0.44	7.2	--	--	NR	2.5	3.1	3.2	19	20
	2C	2.12	--	--	--	NR	27.5	18.6	24.8	70	66

1/ C = Cumulative value, I = Incremental value.
2/ For "C"-beams, concrete strain is an average of readings from four strain gages (two gages 1-3/4 inches each side of midspan).
3/ Not measured.
4/ No record.

Table B-7. Dynamic Test Results - Crushing Stage

Beam No.	Test[1]	Y_c (in.)	Strain at Midspan (μin./in.)			Rotation (10^{-3} rad)				
			ϵ_s	ϵ_s'	ϵ_c[2]	θ_m	θ_r	θ_ℓ	θ_{E1}	θ_{E2}
C-4	1	0.82	39,800	600	4,280	25.6	3.1	2.7	24	17
C-5	1	0.84	40,500	1,150	4,770	29.2	2.7	3.0	27	22
C-6	1	0.84	45,700	100	3,390	28.8	4.8	3.9	22	19
C-9	1	1.22	NR[3]	60	5,220	48.4	1.9	2.8	22	27
C-10	1	0.88	NR	460	3,250	26.7	8.1	4.6	22	31
C-12	1	1.00	--[4]	--	4,580	30.4	10.3	5.3	34	27
C-13	1	1.14	--	--	3,680	43.1	10.3	7.6	26	22
C-14	1	0.79	--	--	4,380	23.6	3.6	11.3	28	21
C-15	1	0.79	30,000	1,380	4,640	21.0	5.4	4.9	30	22
4-7	2I	0.43	3,080	1,412	2,020	3.3	2.3	4.5	--	--
	2C	1.05	28,500	1,210	3,640	17.4	4.6	13.6	--	--
4-8	1	1.02	3,380	1,360	3,760	19.2	9.5	2.9	--	--
4-9	2I	0.45	3,060	1,410	1,830	4.2	4.9	5.7	--	--
	2C	1.35	45,300	1,590	3,700	18.0	8.8	18.8	--	--
4-10	2I	0.42	NR	1,130	1,640	3.6	0.6	4.1	--	--
	2C	1.60	NR	670	3,610	21.2	18.8	22.3	--	--
4-11	2I	0.82	NR	1,650	2,360	8.5	17.7	3.3	33	24
	2C	2.04	NR	1,410	5,160	37.4	37.9	6.7	75	57
4-14	1	1.40	--	--	3,400	14.3	13.9	9.8	50	37
4-15	1	1.66	--	--	3,650	11.3	17.8	14.3	55	50
4-16	1	1.49	--	--	NR	NR	14.9	21.6	NR	NR

1/ C = Cumulative value, I = Incremental value.

2/ For "C"-beams, concrete strain is an average of readings from four strain gages (two gages 1-3/4 inches each side of midspan).

3/ No record.

4/ Not measured.

Table B-8. Dynamic Test Results - Maximum Deflection

Beam No.	Test[1]	Y_{md} (in.)	Strain at Midspan (μin./in.)		Rotation (10^{-3} rad)				
			ϵ_s	ϵ_s'	θ_m	θ_r	θ_ℓ	θ_{E1}	θ_{E2}
C-4	1	1.66	42,900	2,210	47.5	2.4	2.5	44	40
	2I	1.52	23,500	7,680	39.7	10.2	10.0	39	31
	2C	2.87	62,800	8,350	80.8	11.0	10.3	77	67
C-5	1	1.82	47,400	3,160	59.6	2.3	3.7	52	46
C-6	1	1.92	NR[3]	1,320	65.4	3.4	5.8	48	48
C-9	1	4.56	NR	12,500	127	5	15	NR	125
C-10	1	4.50	NR	22,200	147	51	52	129	122
C-12	1	4.39	--[4]	--	115	50	54	129	124
C-13	1	4.66	--	--	138	62	46	134	135
C-14	1	2.41	--	--	73	26	30	76	68
	2I	2.19	--	--	49	36	31	62	65
	2C	4.30	--	--	139	60	59	128	123
C-15	1	3.96	NR	NR	112	56	56	109	115
4-7	1	0.92	28,100	1,080	17.5	3.7	12.5	--	--
	2I	1.09	5,340	1,520	10.9	8.4	13.4	--	--
	2C	1.71	30,700	1,320	25.0	10.7	22.6	--	--
	3I	1.14	5,340	2,170	7.7	4.1	8.7	--	--
	3C	2.49	33,200	2,110	28.6	12.3	27.6	--	--
4-8	1	1.23	NR	1,570	25.0	12.3	4.0	--	--
	2I	1.38	9,930	3,090	26.4	10.3	7.0	--	--
	2C	2.43	28,200	3,010	49.5	21.0	9.8	--	--
4-9	1	1.26	24,900	1,020	17.0	7.9	15.9	--	--
	2I	1.23	NR	1,760	11.7	8.9	14.9	--	--
	2C	2.13	NR	1,940	25.5	12.8	28.0	--	--
	3I	1.46	NR	1,360	7.5	9.3	11.7	--	--
	3C	3.15	NR	1,780	29.2	17.6	35.0	--	--
4-10	1	1.55	NR	650	20.9	21.7	22.0	--	--
	2I	1.32	NR	1,360	11.0	19.0	16.4	--	--
	2C	2.50	NR	900	28.6	37.2	34.6	--	--
4-11	1	1.72	NR	1,010	34.1	24.8	5.0	55	34
	2I	1.55	NR	2,500	13.9	28.6	6.0	51	40
	2C	2.67	NR	2,260	42.8	48.8	9.4	93	73
4-14	1	3.90[2]	--	--	57	58	30	106	116
4-15	1	4.10[2]	--	--	58	42	43	112	122
4-16	1	2.09	--	--	NR	19	25	NR	NR
	2I	2.04	--	--	28	12	16	68	59
	2C	3.72	--	--	53	14	20	119	105

1/ C = Cumulative value, I = Incremental value.
2/ Most readings were out of range at deflections greater than those shown. Collapse occurred at a deflection greater than that listed.
3/ No record.
4/ Not measured.

REFERENCES

1. International Symposium on Flexural Mechanics of Reinforced Concrete, Miami, Florida, Nov. 10-12, 1964, Proceedings. New York, American Society of Civil Engineers, 1965.

2. A. L. L. Baker and A. M. N. Amarakone. "Inelastic hyperstatic frames analysis," in International Symposium on Flexural Mechanics of Reinforced Concrete, Miami, Florida, Nov. 10-12, 1964, Proceedings. New York, American Society of Civil Engineers, 1965, pp. 85-142.

3. A. H. Mattock. "Rotational capacity of hinging regions in reinforced concrete beams," in International Symposium on Flexural Mechanics of Reinforced Concrete, Miami, Florida, Nov. 10-12, 1964, Proceedings. New York, American Society of Civil Engineers, 1965, pp. 143-181.

4. University of Illinois, Department of Civil Engineering. Structural Research Series No. 234: Load-deformation characteristics of beam-column connections in reinforced concrete, by N. H. Burns and C. P. Siess. Urbana, Ill., Jan. 1962.

5. University of Illinois, Department of Civil Engineering. Structural Research Series No. 260: Moment-rotation characteristics of reinforced concrete members subjected to bending, shear, and axial load, by R. Yamashiro and C. P. Siess. Urbana, Ill., Dec. 1962.

6. U.S. Naval Civil Engineering Laboratory. Technical Report R-371: Plastic hinge formation in reinforced concrete beams, by W. J. Nordell. Port Hueneme, Calif., June 1965.

7. University of Illinois, Department of Civil Engineering. Structural Research Series No. 243: Investigation of resistance and behavior of reinforced concrete members subjected to dynamic loading, Part III, by A. Feldman, W. A. Keenan, and C. P. Siess. Urbana, Ill., Feb. 1962. (DASA-1259; Contract DA-49-129-Eng-344)

8. University of Illinois, Department of Civil Engineering. Structural Research Series No. 40: An investigation of the load-deformation characteristics of reinforced concrete beams up to the point of failure, by J. R. Gaston, C. P. Siess, and N. M. Newmark. Urbana, Ill., Dec. 1952. (Contract N6onr-07134)

9. University of Illinois, Engineering Experiment Station. Bulletin Series No. 399: A study of combined bending and axial load in reinforced concrete members, by E. Hognestad. Urbana, Ill., Nov. 1951.

10. U.S. Naval Civil Engineering Laboratory. Technical Note N-775: An improved stepwise regression analysis procedure, by W. L. Wilcoxson and J. R. Wohlever. Port Hueneme, Calif., Dec. 1965.

11. University of Illinois, Department of Civil Engineering. Structural Research Series No. 76: Load-deformation characteristics of simulated beam-column connections in reinforced concrete, by H. M. McCollister, C. P. Siess, and N. M. Newmark. Urbana, Ill., June 1954. (Contract DA-49-129-Eng-248)

12. W. W. L. Chan. "The ultimate strength and deformation of plastic hinges in reinforced concrete frameworks," Magazine of Concrete Research, Vol. 7, No. 21, Nov. 1955, pp. 121-132.

13. University of Illinois, Department of Civil Engineering. Structural Research Series No. 268: A model to simulate the response of concrete to multi-axial loading, by H. E. H. Roy and M. A. Sozen. Urbana, Ill., June 1963.

14. U.S. Naval Civil Engineering Laboratory. Technical Report R-394: Dynamic tests of concrete reinforcing steels, by W. L. Cowell. Port Hueneme, Calif., Sept. 1965.

15. C. H. Norris et al. Structural design for dynamic loads. New York, McGraw-Hill, 1959.

16. J. E. Breen and P. M. Ferguson. "The restrained long concrete column as a part of a rectangular frame," American Concrete Institute Journal, Proceedings, Vol. 61, No. 5, May 1964, pp. 563-587.

17. J. M. Ruzek et al. "Welded portal frames tested to collapse," Welding Journal, Vol. 33, No. 9, Sept. 1954, pp. 469s-480s.

Unclassified
Security Classification

DOCUMENT CONTROL DATA - R&D

(Security classification of title, body of abstract and indexing annotation must be entered when the overall report is classified)

1. ORIGINATING ACTIVITY (Corporate author) U. S. Naval Civil Engineering Laboratory Port Hueneme, California 93041	2a. REPORT SECURITY CLASSIFICATION Unclassified 2b. GROUP

3. REPORT TITLE
HINGING IN STATICALLY AND DYNAMICALLY LOADED REINFORCED CONCRETE BEAMS

4. DESCRIPTIVE NOTES (Type of report and inclusive dates)
Not final; January 1965 to May 1966

5. AUTHOR(S) (Last name, first name, initial)
Nordell, William J., Ph D

6. REPORT DATE	7a. TOTAL NO. OF PAGES	7b. NO. OF REFS
October 1966	106	17

8a. CONTRACT OR GRANT NO.	9a. ORIGINATOR'S REPORT NUMBER(S)
b. PROJECT NO. Y-F011-05-04-001	TR-489
c.	9b. OTHER REPORT NO(S) (Any other numbers that may be assigned this report)
d.	

10. AVAILABILITY/LIMITATION NOTICES
Distribution of this document is unlimited. Copies available at the Clearinghouse (CFSTI) $4.00.

11. SUPPLEMENTARY NOTES	12. SPONSORING MILITARY ACTIVITY
	Naval Facilities Engineering Command

13. ABSTRACT

The objective was to investigate the hinging mechanism in under-reinforced concrete beams subjected to static or dynamic loads. Two test series on simply supported beams with a 6-foot span length were conducted. In one series, 11 beams were subjected to two concentrated loads symmetrically placed 18 inches apart; the primary variable was the magnitude of the step load pulse (1.0 to 1.4 times the static yield load). In the other series, 15 beams were subjected to a concentrated load at midspan; the primary variables were the type of load (static or dynamic), the amount of tension reinforcement ($p = 0.9$, 1.3, and 2.0; $p'/p = 0.67$), and the size of the transverse reinforcement (1/8- and 1/4-inch round bars and No. 3 deformed bars).

Hinge development was similar in the statically and dynamically loaded beams and resulted from the formation and propagation of a yielded zone or zones in the tension reinforcement. Strain hardening of the tension reinforcement increased the static resistance above the yield value; the increase ranged from 5 to 60 percent.

Although decreasing the amount of tension reinforcement increased the deflection at certain stages, the ultimate rotation capacity was not significantly affected. In addition, the size of the transverse reinforcement had a negligible effect on the ultimate rotation capacity.

DD FORM 1 JAN 64 1473 0101-807-6800

Unclassified
Security Classification

Unclassified
Security Classification

14. KEY WORDS	LINK A		LINK B		LINK C	
	ROLE	WT	ROLE	WT	ROLE	WT
Reinforced concrete						
Beams						
Static loads						
Dynamic loads						
Hinging						
Tension						
Deformation						

INSTRUCTIONS

1. ORIGINATING ACTIVITY: Enter the name and address of the contractor, subcontractor, grantee, Department of Defense activity or other organization *(corporate author)* issuing the report.

2a. REPORT SECURITY CLASSIFICATION: Enter the overall security classification of the report. Indicate whether "Restricted Data" is included. Marking is to be in accordance with appropriate security regulations.

2b. GROUP: Automatic downgrading is specified in DoD Directive 5200.10 and Armed Forces Industrial Manual. Enter the group number. Also, when applicable, show that optional markings have been used for Group 3 and Group 4 as authorized.

3. REPORT TITLE: Enter the complete report title in all capital letters. Titles in all cases should be unclassified. If a meaningful title cannot be selected without classification, show title classification in all capitals in parenthesis immediately following the title.

4. DESCRIPTIVE NOTES: If appropriate, enter the type of report, e.g., interim, progress, summary, annual, or final. Give the inclusive dates when a specific reporting period is covered.

5. AUTHOR(S): Enter the name(s) of author(s) as shown on or in the report. Enter last name, first name, middle initial. If military, show rank and branch of service. The name of the principal author is an absolute minimum requirement.

6. REPORT DATE: Enter the date of the report as day, month, year; or month, year. If more than one date appears on the report, use date of publication.

7a. TOTAL NUMBER OF PAGES: The total page count should follow normal pagination procedures, i.e., enter the number of pages containing information.

7b. NUMBER OF REFERENCES: Enter the total number of references cited in the report.

8a. CONTRACT OR GRANT NUMBER: If appropriate, enter the applicable number of the contract or grant under which the report was written.

8b, 8c, & 8d. PROJECT NUMBER: Enter the appropriate military department identification, such as project number, subproject number, system numbers, task number, etc.

9a. ORIGINATOR'S REPORT NUMBER(S): Enter the official report number by which the document will be identified and controlled by the originating activity. This number must be unique to this report.

9b. OTHER REPORT NUMBER(S): If the report has been assigned any other report numbers *(either by the originator or by the sponsor)*, also enter this number(s).

10. AVAILABILITY/LIMITATION NOTICES: Enter any limitations on further dissemination of the report, other than those imposed by security classification, using standard statements such as:

(1) "Qualified requesters may obtain copies of this report from DDC."

(2) "Foreign announcement and dissemination of this report by DDC is not authorized."

(3) "U. S. Government agencies may obtain copies of this report directly from DDC. Other qualified DDC users shall request through

_____."

(4) "U. S. military agencies may obtain copies of this report directly from DDC. Other qualified users shall request through

_____."

(5) "All distribution of this report is controlled. Qualified DDC users shall request through

_____."

If the report has been furnished to the Office of Technical Services, Department of Commerce, for sale to the public, indicate this fact and enter the price, if known.

11. SUPPLEMENTARY NOTES: Use for additional explanatory notes.

12. SPONSORING MILITARY ACTIVITY: Enter the name of the departmental project office or laboratory sponsoring *(paying for)* the research and development. Include address.

13. ABSTRACT: Enter an abstract giving a brief and factual summary of the document indicative of the report, even though it may also appear elsewhere in the body of the technical report. If additional space is required, a continuation sheet shall be attached.

It is highly desirable that the abstract of classified reports be unclassified. Each paragraph of the abstract shall end with an indication of the military security classification of the information in the paragraph, represented as *(TS), (S), (C), or (U)*

There is no limitation on the length of the abstract. However, the suggested length is from 150 to 225 words.

14. KEY WORDS: Key words are technically meaningful terms or short phrases that characterize a report and may be used as index entries for cataloging the report. Key words must be selected so that no security classification is required. Identifiers, such as equipment model designation, trade name, military project code name, geographic location, may be used as key words but will be followed by an indication of technical context. The assignment of links, roles, and weights is optional.

Unclassified
Security Classification